DYNAMIC MODELING OF ORGANIC RANKINE CYCLE AND ITS EXPERIMENTAL VERIFICATION

by

Ertuğrul Altun

B.S., Mechanical Engineering, Boğaziçi University, 2018

Submitted to the Institute for Graduate Studies in
Science and Engineering in partial fulfilment of
the requirements for the degree of
Master of Science

Graduate Program in Mechanical Engineering
Boğaziçi University
2022

ACKNOWLEDGMENTS

First of all, I would like to thank my thesis advisor Assoc. Prof. Hasan Bedir and co-advisor Prof. Günay Anlaş for their great support during my study. Their encouragement and knowledge allowed me to finish my research.

I would like to thank Alper Buğra Şirin and Murat Ural from Tora Petrol Inc. for their great support on the experimental setup and their time.

I would like to thank my BURET lab mates Alpay Asma, Berkhan Bayraktar and Hasan Eren Bekiloğlu for their great support, friendship, and great memories.

I would like to thank Akın Çağlayan who is my friend, colleague, and ex co-worker for his support on dynamic modelling part of this study. I would like to thank him for spending his time to support me.

I would like to thank Dr.Tolga Nurettin Aynur, Inores Yazılım and Gizem Bilginer for their support on giving free academic Dymola and Thermal Systems Library license to Boğaziçi University. Dymola and Thermal Systems Library are used in this study.

I got sick because of Covid19 pandemic while I was writing my thesis. I especially want to thank my aunts Dear Saliha Yaylı, Dear Mahire Dinç, and my cousins. They prepared their own houses for my isolation period. They prepared food and healthy beverages every day during my isolation period. They made me feel so comfortable and safe while I was writing my thesis.

Finally, I am a lucky person to have such a family who always supported me without questioning anything, thanks to my mother, father, sister and brother. Also, thanks to my best friend and classmate from undergraduate years Engin Demir for his motivation and encouragement.

ABSTRACT

DYNAMIC MODELING OF ORGANIC RANKINE CYCLE AND ITS EXPERIMENTAL VERIFICATION

Renewable energy technologies and waste heat recovery systems have become more important all around the world because of global warming, global climate change, and countries' tendency to decrease fossil fuel consumption. Organic Rankine Cycle is one of the most popular research topics on waste heat recovery systems. In this thesis, a dynamic model of a lab scale Organic Rankine Cycle (ORC) is developed. The main objective of this thesis is to create a dynamic model for ORC system at Bogazici University Renewable Energy Technologies (BURET) laboratory including heat loses and pressure losses in pipes and to validate the model by comparing the simulation results with experiments done at BURET laboratory. The cycle parameters such as temperature and pressure are calculated transiently in the dynamic model. The model is obtained using Modelica language and Dymola program which is an object-oriented modeling software. After the dynamic model testers for each cycle component are created, component models' simulation results are verified by using experimental data taken from ORC setup at BURET laboratory. Once the component models are verified, whole dynamic ORC model is created. Experimental studies are conducted using the ORC setup at BURET laboratory and the results are compared to those of the dynamic model built in this study. It is found that temperature and pressure values for each component's inlet and outlet are accurately simulated by the dynamic model created in this study.

ÖZET

ORGANİK RANKİNE ÇEVRİMİNİN DİNAMİK MODELLEMESİ VE MODELİN DENEYSEL VERİLERLE DOĞRULANMASI

Küresel ısınma, küresel iklim değişikliği ve ülkelerin fosil yakıtların tüketimini azaltma eğilimleri nedeniyle yenilenebilir enerji teknolojileri ve atık ısı geri kazanım sistemlerinin önemi tüm dünyada artmaktadır. Organik Rankine Çevrimi, atık ısı geri kazanım sistemleri üzerine en popüler araştırma konularından biridir. Bu tezde, bir Organik Rankine Çevriminin (ORC) dinamik bir modeli geliştirilmiştir. Bu tezin temel amacı, Boğaziçi Üniversitesi Yenilenebilir Enerji Teknolojileri (BURET) laboratuvarındaki ORC sistemi için borulardaki ısı ve basınç kayıplarını içeren dinamik bir model oluşturmak ve simülasyon sonuçlarını BÜRET laboratuvarında yapılan deneylerle karşılaştırarak modeli doğrulamaktır. Sıcaklık ve basınç gibi çevrim parametreleri dinamik modelde anlık olarak hesaplanmıştır. Model, Modelica dili ve nesne bazlı bir modelleme yazılımı olan Dymola programı kullanılarak elde edilmiştir. Çevrimdeki her bir eleman için ayrı ayrı dinamik model oluşturulduktan sonra BURET laboratuvarı ORC düzeneğinden alınan deneysel veriler kullanılarak simülasyon sonuçları doğrulanmıştır. Tekil eleman modelleri doğrulandıktan sonra elemanlar birleştirilmiş ve bütüncül ORC çevrimi modeli oluşturulmuştur. Daha sonra ise BURET Laboratuvarı'ndaki ORC düzeneği kullanılarak deneysel çalışmalar yapılmış ve sonuçlar bu çalışmada oluşturulan dinamik modelin sonuçlarıyla karşılaştırılmıştır. Bu çalışmada oluşturulan dinamik model ile her bir bileşenin (evaporator, kondenser, kısılma valfi, pompa ve borular) giriş ve çıkışı için sıcaklık ve basınç değerleri doğru bir şekilde simüle edilmiştir.

TABLE OF CONTENTS

LIST OF FIGURES

LIST OF SYMBOLS

A	Area, (m^2)
Amb	(Subscript) Ambient
Ave	(Subscript) Average
b	Height of the corrugation (m)
c	Specific heat, (kj/kgK)
cb	(Subscript) Convective boiling
cond	(Subscript) Conduction
conv	(Subscript) Convection
D	Diameter, (m)
eff	(Subscript) Effective
eq	(Subscript) Equivalent
f	Friction coefficient
fc	(Subscript) Forced convection
g	Gravitational constant, (m/s^2)
G	(Subscript) Vapor phase
gr	(Subscript) Gravity dominated
h	Heat transfer coefficient, (W/m^2K)
htf	(Subscript) Heat transfer fluid
k	Thermal conductivity, (W/mK)
l	(Subscript) Liquid phase
lat	(Subscript) Latent
lg	(Subscript) Liquid gas phase change
max	(Subscript) Maximum
min	(Subscript) Minimum
nb	(Subscript) Nucleate boiling
Nu	Nusselt number
p	Pressure, (Pa)
Pr	Prandtl number
r	(Subscript) Refrigerant

Ra	Rayleigh number
Re	Reynolds number
Re_{eq}	Equivalent Reynolds number
s.ph	Single phase
sat	(Subscript) Saturated vapor
sup	(Subscript) Super-heated vapor
T	Temperature, (K)
th	(Subscript) Thermal
U_L	Overall heat loss coefficient
v	(Subscript) Vapor
W	Width of the plate, (m)
wall	(Subscript) Plate wall
X	Vapor quality
α	Heat transfer coefficient
β	Inclination angle of the corrugation
ΔJ_{lg}	Latent heat of condensation, ($J\ kg^{-1}$)
η	Efficiency
Φ	Enlargement factor
λ	Thermal conductivity, ($W\ m^{-1}\ K^{-1}$)
μ	Dynamic viscosity ($kg\ m^{-1}\ s^{-1}$)
ν	Kinematic viscosity (m^2/s)
ρ	Density, ($kg\ m^{-3}$)

LIST OF ABBREVIETIONS AND ACRONYMS

ASHRAE	American Society of Heating, Refrigerating and Air-Conditioning Engineers
BURET	Bogazici University Renewable Energy Technologies
CHP	Combined Heat and Power
EU	European Union
HTF	Heat Transfer Fluid
IEA	International Energy Agency
IRENA	International Renewable Energy Agency
NREL	National Renewable Energy Laboratory
ORC	Organic Rankine Cycle
PCM	Phase Change Material
P&ID	Piping and Instrumentation Diagram
R&D	Research and Development
TES	Thermal Energy Storage
TEG	Thermoelectric Generator
US	United States
WHR	Waste Heat Recovery

1. INTRODUCTION

Global energy demand is expected to increase by 70% until the year 2050 according to a report of International Energy Agency (IEA); also, by 2050 the global average temperature is expected to increase by 6°C [1]. Such rise in energy use and in the average temperature would no doubt result in climate change, which could be catastrophic. As a result, today the primary source in electricity generation are fossil fuels such as coal, oil and natural gas. The share of fossil fuels in electricity generation is about 70% [2]. Strict emission regulations are mandated by the Kyoto Protocol. Studies are carried out to secure a sustainable future and to limit the consequences of pollutant emissions such as global warming and ozone depletion, and several protocols have been signed in recent years. A scenario proposed by the IEA in 2017 predicted that limiting the average temperature increase to 2°C by 2100 is possible only in collaboration with industry leaders and policy makers [3]. In this context, the Paris Protocol on global climate change was one of the recent EU policy decisions aimed to reduce greenhouse gases by 40% and to increase renewable energy by 27% until 2030 [4].

Obtaining electricity from other energy sources has become very important and, a great emphasis has been put by many researchers in recent years on waste heat recovery (WHR), on concentrated solar power, and on geothermal.

Combined heat and power (CHP) generation is one of the ways to convert waste heat into electricity. Heat sources with temperatures below 350 °C have potential for use in waste heat recovery (WHR) applications [5]. Significant fuel savings can be achieved by using WHR systems, minimizing thermal energy losses and reducing emissions [6]. Three main technologies for waste heat recovery applications are listed in the literature: Thermoelectric Generator (TEG), Phase Change Material (PCM) and Organic Rankine Cycle (ORC) [7].

ORC units are suitable candidates for converting low-grade heat into electricity. ORC, which is similar to the Steam Rankine cycle, uses other working fluids that have higher molecular weight and lower boiling point (like refrigerants) compared to water. These properties make ORC units preferable to convert heat into electricity at low temperatures from 60 ℃ to 350 ℃. Although limited to low thermodynamic efficiencies of up to 20%, their flexibility and success in partial load conditions make them an excellent choice in low and medium grade heat conversion systems [8].

An ORC consists of a pump, an expander (turbine), an evaporator and a condenser. The process starts with a pump that delivers the working fluid to the evaporator, where it changes its phase from liquid to vapor. Subsequently, the pressurized organic fluid flows into an expander where it expands and loses its enthalpy, and consequently power is generated. Finally, the low pressure vapor at the expander outlet passes through the condenser and returns to pump in liquid phase [9]. A regenerative cycle can be used to increase the thermal efficiency of the cycle and reduce the duty of the evaporator. Unlike simple ORC, the vapor at the expander outlet goes to a heat exchanger unit called the recuperator, where it transfers its enthalpy to the cold working fluid from the discharge section of the pump. The schemes representing regenerative ORC and simple ORC are shown in Figure 1.1 and Figure 1.2.

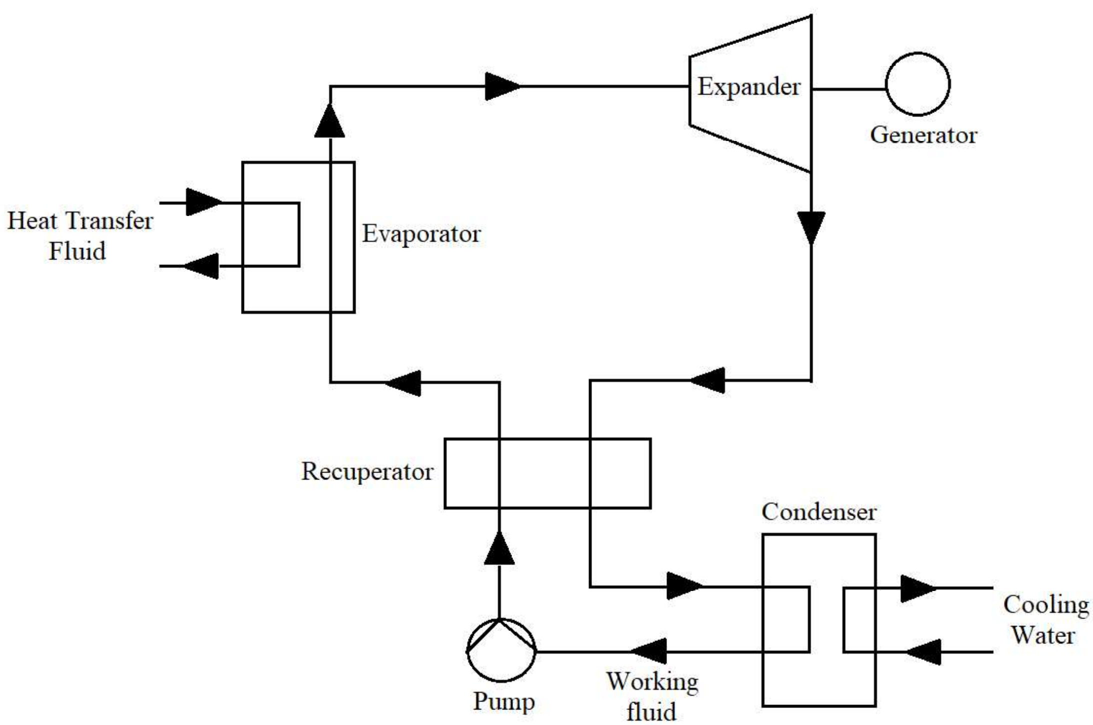

Figure 1.1. Regenerative ORC system.

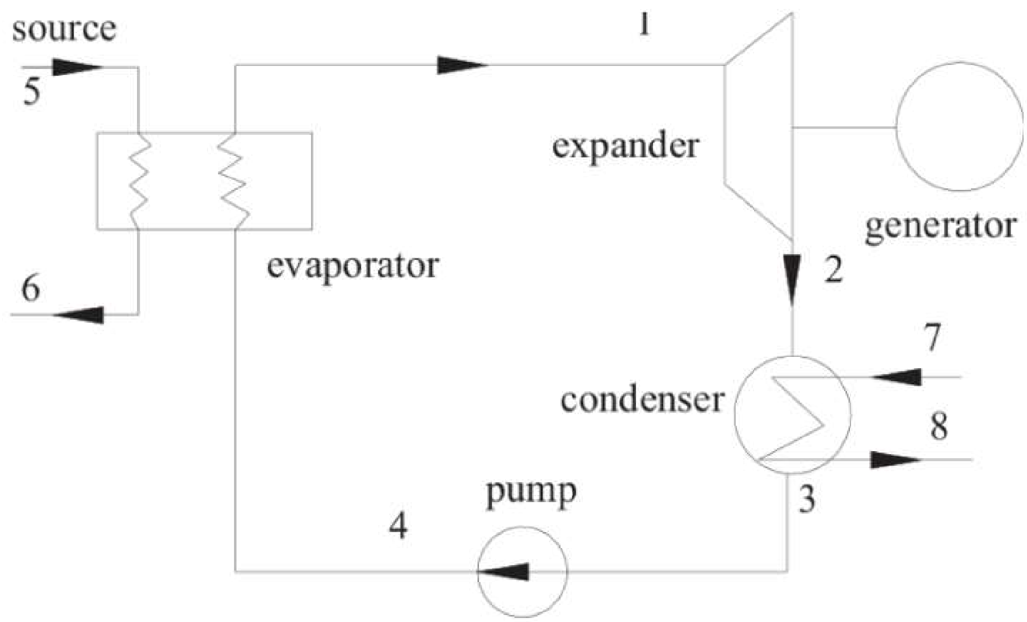

Figure 1.2. Simple ORC system [10].

TS diagram for a simple ORC shown in Figure 1.2 is shown in Figure 1.3.

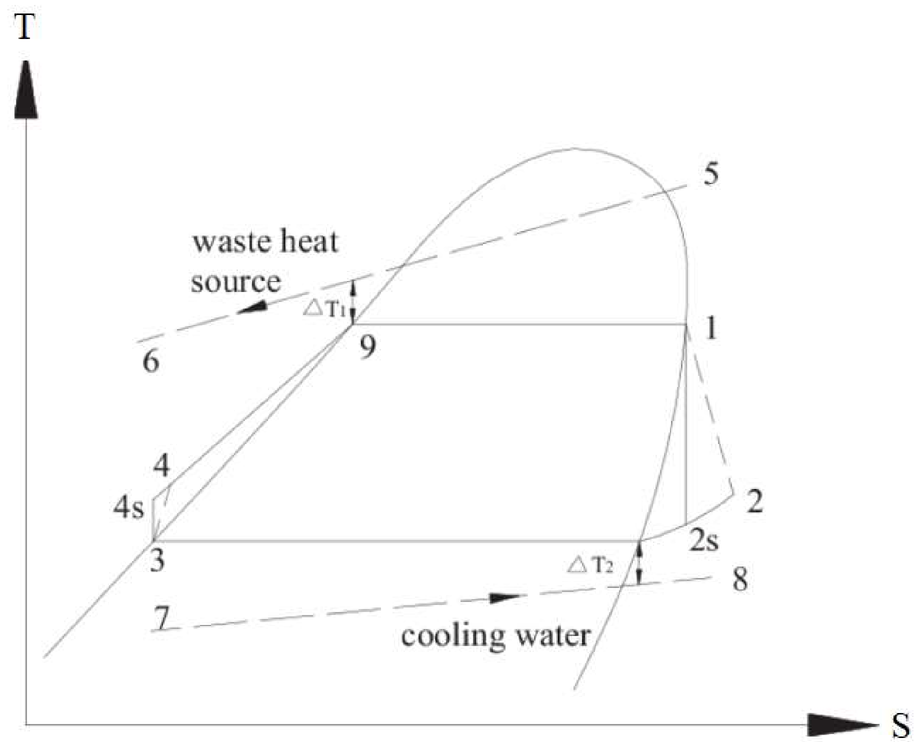

Figure 1.3. TS diagram for a simple ORC [10].

ORC systems have been proposed for many years for utilization of low temperature heat sources. Experimental ORC set-ups are needed to develop and test ORC components. Cost of the test set-up, components and refrigerants are high, so doing efficient experiments is not easy for many researchers. As a result, accurate dynamic models are important. If an accurate dynamic model is created for an ORC system, researchers may easily change system parameters, refrigerant type, observe the effects of these changes, and number of experiments required will decrease, cost of doing experiments will become less. In addition, an accurate dynamic model will simulate an experiment in minutes. Even a proper experiment takes hours, researcher can simulate certain conditions in minutes by using accurate dynamic model.

1.1. Literature Review

There are some important articles about dynamic ORC modeling published in reputable journals. In this chapter, some studies about dynamic ORC modeling are mentioned.

Marchionni et al [11], carried out a study on dynamic modeling of ORC and optimization of some components such as turbine and heat exchangers. In this study, GT-Suite is used as 1D computer aided modeling software. This paper focuses on especially kW scale ORC systems instead of MW scale ones. This study aims to model ORC systems which have power output between 34.5 kW and 55.5 kW. Sub-models for pump, turbine and heat exchangers are created. Radial turbine modeling, design and optimization is done for R245fa. Different mass flowrates and inlet temperatures of cooling water and hot oil is examined to observe transient response of the cycle.

Wei et al [12], created a dynamic model for ORC system using Modelica/Dymola. ORC system. Exhaust gas of a power plant is the heat source of the cycle and cooling is done with air. R245fa is used as working fluid. They compared moving boundary (MB) and finite volume (FV) approaches in terms of accuracy, complexity and simulation speeds. Transient analysis results are plotted and compared with experimental data for both cases. As a result, MB approach is found to be faster and less complex than FV approach. However, the FV approach is more accurate than the MB one. Therefore, if the main concern is the simulation time, MB is more suitable than the FV approach, but if simulation time is not so important, using FV approach would be more reasonable.

Carraro et al [13], studied the dynamic modeling of a small scale ORC system. In their study, the main aim is to design a small ORC system which generates power between 3 kW and 4 kW and create the dynamic model of the small ORC. Matlab/Simulink software is used for modelling. In the dynamic model, the inlet temperature of hot oil is changed between 410 K and 435 K. Then the response of the system is investigated. Simulation results are compared to experimental ones to validate the dynamic model. As a result, a small scale ORC system with its dynamic model is obtained. Maximum of 6.6% relative error occurred between the dynamic model and experimental data.

Tong et al [14], study dynamic models of an internal combustion engine (ICE) and ORC together. The ICE is used as the expander in the ORC system. Their main aim is to increase the overall thermal efficiency of the ICE by recovering the waste heat. The dynamic model is created using GT-Suite software. A four cylinder, direct injection, and turbocharged diesel engine is used in the system. First, the dynamic model of the diesel engine is created, and validated with engine’s data. Then the whole ICE-ORC combination is simulated. R245fa is selected as working fluid in the ICE-ORC combination. As a result of the simulation, paper shows that the overall thermal efficiency is increased and the fuel consumption is decreased.

Zhang et al [15], proposed a dynamic model for a kW scale ORC system. They used Modelica/Dymola software; components are modeled first, then the whole system. Simulation results and experimental data are compared. As a conclusion, the dynamic model is in agreement with experiments. The average overshoot for the outlet temperature of cooling source is 0.7℃, the average overshoot for the evaporation pressure is 48 kPa. The simulation results are very close to experimental data; the thermal efficiency of the system is found as 6.94%.

Quolin et al [16], created a dynamic model for simulation of ORC using Modelica/Dymola. For fluid properties calculation, CoolProp is used. A library named ThermoCycle is created for study of power cycles. In the article, two different cases are simulated for R407c and R245fa separately. After the models are prepared, experiments and simulation results are compared. Accurate dynamic models are obtained when compared to experimental data.

In the literature survey it is observed that, dynamic ORC modeling is a topic that is currently studied by researchers. Some modeling softwares such as GT-Suite, Matlab/Simulink, and Modelica/Dymola are generally used. Accurate component models are created neglecting the losses in the connecting elements such as pipes. Assuming a negligible change in the connecting elements is a reasonable assumption for small scale ORC systems. However, for some ORC applications these losses may be significant. As an example, the ORC system at BURET laboratory has long pipes to accommodate measurement devices such as flow meters, temperature and pressure sensors and heat loses from the pipes can be significant and these losses should be taken into account for an accurate model. In this thesis, a dynamic model that considers heat loses in pipes is built for the ORC system at BURET laboratory, simulation results are compared to experimental ones. Secondly, an accurate dynamic model will be helpful to implement advanced control systems on ORC setup at BURET laboratory.

1.2. Objectives

The main objective of this thesis is to build an accurate dynamic model of an ORC and to validate the dynamic model with experimental data. For that purpose, after validation of the model for each component in ORC, a detailed ORC model that includes heat and pressure losses in pipes is studied to obtain a model of the ORC in BURET laboratory. Then, experiments are conducted at BURET laboratory and the results are compared to those of the dynamic model.

2. MODELING TOOL AND LANGUAGE

In this chapter, modeling tool and modeling language used in this thesis study is introduced.

2.1. Introduction to Modelica

Modelica software language was used to model the Organic Rankine Cycle and each component of the experimental setup at BURET laboratory. There are many programs available for system modeling using the Modelica language. Dymola program was used to carry out this study.

Modelica is an object-oriented and equation-based software language designed to appropriately model complex physical systems (mechanical, electrical, electronic, hydraulic, thermal, control, etc.). In Modelica, models can be defined with differential, algebraic, and discretized equations. It has a structure that allows non-causal modeling without considering the order of equations. In Figure 2.1, an object-based component and equation structure prepared in Modelica language can be seen.

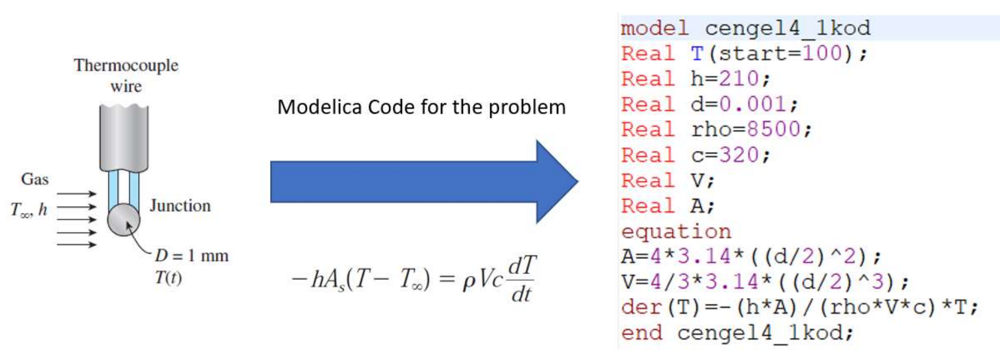

Figure 2.1. Object and equation-based structure in Modelica.

The aim to use Modelica language is to create models close to the real life systems. When the studies in literature are investigated, the advantages of using Modelica language in a system modeling will be seen. Some advantageous features of Modelica are hierarchical structuring, reuse and development of large complex models, and special graphical formatting.

2.2. Introduction to Dymola

In order to analyze a mathematical model prepared using the Modelica language, it is necessary to convert it to a fixed causal differential algebraic equation (DAE) system. Thus, to have equations that can be integrated with standard methods transformation algorithms are needed to transform the equations. These transformation algorithms and solvers can be used in various programs, open source and commercial ones are available to perform these operations. In this study, the Dymola program of Dassault Systems, which is one of the most widely used programs in the world is used.

2.2.1. Introduction to Dymola Program, Solution Logic and Libraries

Dymola is a Modelica language based commercial program to create dynamic model of real life systems [17]. Dymola is a very useful program as it supports system modeling with various libraries and carry and drop method. Some features of Dymola are listed below:

- Capable to handle large, complex multiple engineering models.
- It has faster modeling capability with graphical model composition.
- Faster simulation.
- Open for user-defined model components.
- It has an interface structure open to other programs.
- It can perform real-time simulation.

In the Dymola program, there are various open source and commercial libraries specially made for various engineering fields.

A commercial library written in Modelica was used to model the ORC and its components. This library was prepared by TLK-Thermo company. The name of the library is Thermal Systems Library. In order to model various systems in the Thermal Systems

Library, different components have been modeled on object and equation basis. Figure 2.2 shows the Thermal Systems Library structure.

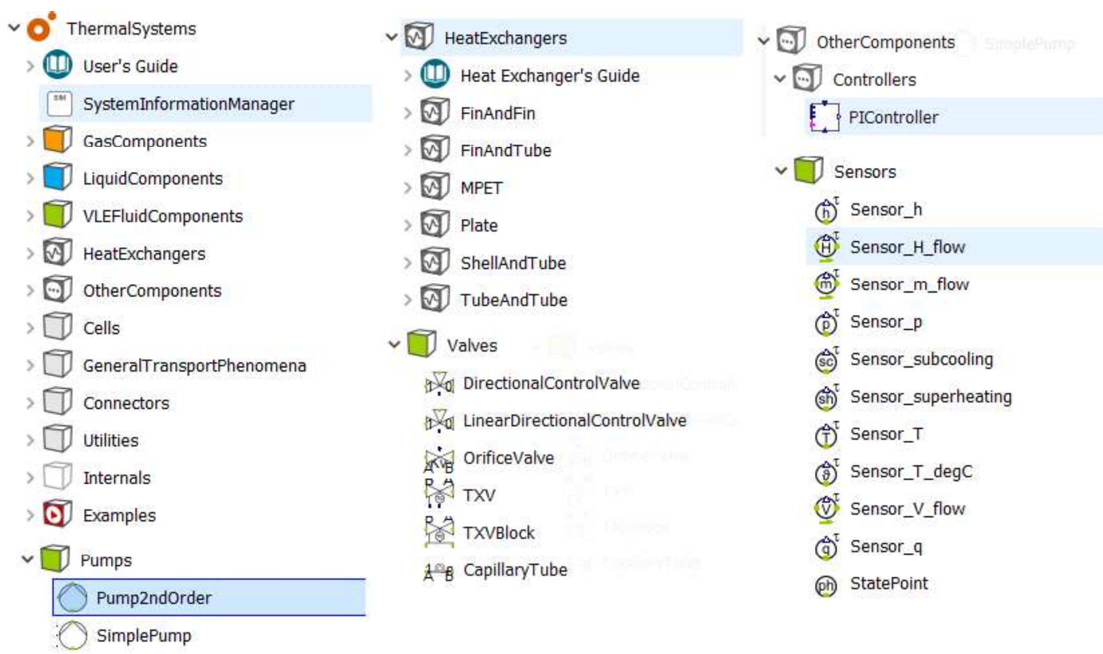

Figure 2.2. Thermal Systems Library structure and some modeled components.

Using the components in the Thermal Systems Library, different thermodynamic systems can be modeled and simulated. In Figure 2.3, a simple automobile air conditioner cycle that is modeled with the components in the library is given as an example.

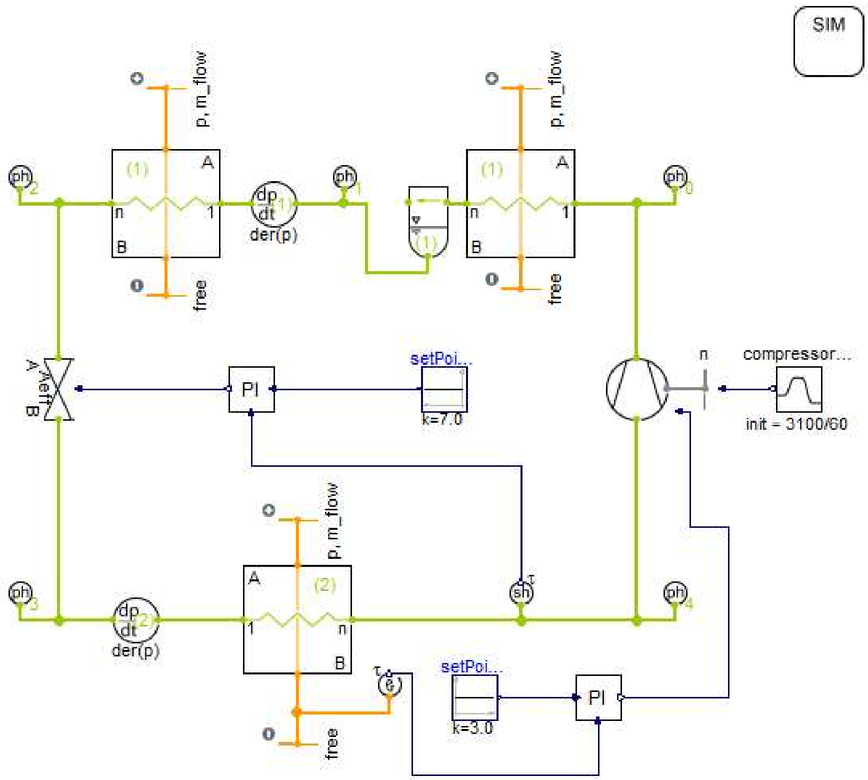

Figure 2.3. A simple automobile AC cycle modeled using the Thermal Systems Library.

Components in the library are not sufficient to model whole ORC in BURET laboratory. Model for throttle valve and pipes in the ORC setup are created in accordance with Modelica language. Pump and plate type heat exchanger already exist in the library, but some modifications were made.

Various methods are available for solving models in Dymola. Generally, DASSL developed by Petzold [18] is preferred among these methods. DASSL is used as an integrator designed to solve differential algebraic equations. Numerical solution with DASSL is very reliable and efficient.

3. EXPERIMENTS

3.1. Experimental Setup at BURET Laboratory

BURET was founded in 2015 at Bogazici University Saritepe Campus by Günay Anlaş and Hasan Bedir with financial support from Bogazici University and ISTKA. This laboratory focuses on renewable energy technologies. An ORC setup as a power cycle to generate electricity from a low temperature heat source is placed at BURET laboratory. In Figure 3.1, BURET laboratory is shown.

Figure 3.1. External view of BURET laboratory.

During this thesis study, some modifications are made to this experimental setup. Aim was to correct the errors in the setup and do improved experiments. To describe the changes and advantages of these changes, first the experimental setup is explained. Then changes are described, and latest version of the experimental setup is described.

3.2. The ORC Setup and Its Components

The experimental setup consists of a working fluid pump, a refrigerant filter, an evaporator, a throttle valve, a condenser, a liquid collector, a bypass line, temperature sensors at different locations, pressure sensors at different locations, ball type valves, globe type valves, a check valve, a needle valve, flow meters at different locations, a filling station to fill working fluid into the setup, a chiller unit to provide cold water, an oil pump, and a heater unit to provide hot heat transfer oil. The working fluid is R134a, the cooling source is cold water from chiller unit, and the heating source is a heat transfer oil heated by the heater unit. In Figure 3.2, ORC setup at BURET laboratory is shown.

Figure 3.2. ORC setup at BURET laboratory.

Figure 3.3. Working fluid pump.

In Figure 3.3, the working fluid pump is shown. Working fluid pump is a product of Speck Pump firm, it is a side channel pump. The model name is SK2007-LL side channel pump. Maximum operating pressure is 25.2 bars. Speed of the pump can be controlled by a frequency converter, and the maximum working speed is 1450 rpm. A minimum working speed of 1000 rpm is necessary due to internal flow for cooling and bearing lubrication. Below 1000 rpm pump temperature increases and it cuts the electric current to protect the pump. In Figure 3.4, working fluid pump frequency converter is shown.

Figure 3.4. Working fluid pump frequency converter.

The working fluid pump circulates the working fluid through the ORC cycle which is liquid at pump suction line. R134a exits the pump at higher pressure and temperature than inlet conditions. The working fluid then enters the evaporator and evaporates with the heat transferred from the heat transfer oil. Working fluid exits evaporator as a superheated vapor. In Figure 3.5, evaporator is shown.

Figure 3.5. Evaporator.

The evaporator used is a plate type heat exchanger, its geometry is shown in the Figure 3.6.

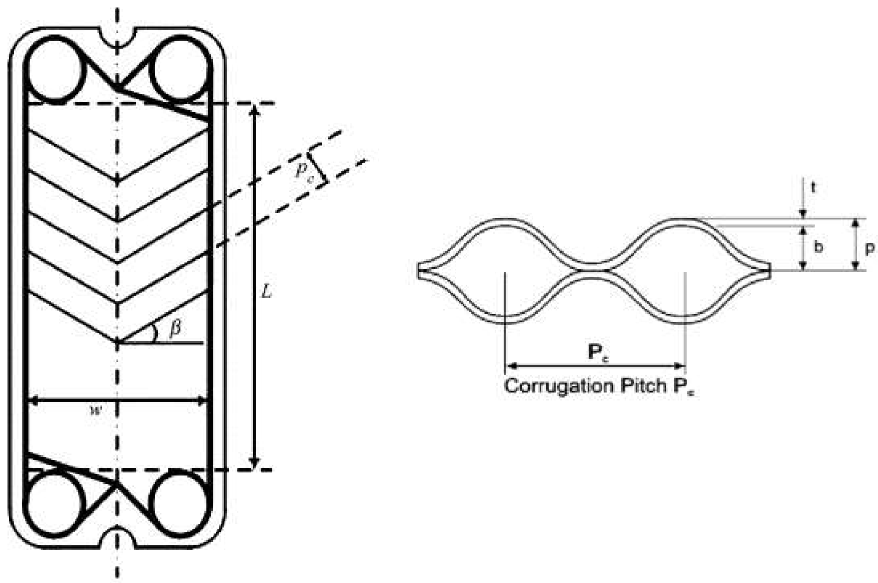

Figure 3.6. Geometric structure of a plate type heat exchanger [19].

L is the plate length, w is the plate depth, β is the chevron angle, p is the corrugation depth, and the P_c is the corrugation pitch. There are N number of plates in the evaporator. These parameters are used in evaporator model. For the evaporator used in the BURET laboratory, the geometrical parameters are given in Table 3.1.

Table 3.1. Geometrical parameters for evaporator.

Geometrical Parameter	Value and Unit
b	1 mm
t	0.4 mm
p	1.4 mm
P_c	6.58 mm
N	80
Heat Transfer Area	7.4 m^2

As the refrigerant flows in the channels of the evaporator its phase will change from liquid to vapor. Provided that there is sufficient rate of heat transfer from the hot thermal oil, the evaporator can be divided into three regions during the operation by looking at the phase of the refrigerant. The boundaries of these divisions are not fixed at a certain place in the evaporator but may move with an increase or decrease in heat transfer from the hot thermal oil. The first one is sub-cooled liquid region, the second one is two phase region and the third one is superheated vapor region. Working fluid R134a enters to evaporator as a sub-cooled liquid. R134a temperature increases and when it reaches the saturation temperature at the operating pressure it starts to evaporate. As the evaporation continues along the flow channel of the evaporator quality of the two phase mixture increases. After the refrigerant is fully vaporized its temperature may increase in the superheated vapor portion of the evaporator and it exits the evaporator as superheated vapor.

The oil heater unit heats the heat transfer oil to the desired temperature. The temperature level can be controlled by a control panel. In Figure 3.7, the oil heater is shown.

Figure 3.7. Oil heater.

Maximum oil temperature is limited to 160 °C and the thermal capacity of oil heater is 107 kW. Hot oil is circulated by an oil pump. In Figure 3.8, oil pump is shown.

Figure 3.8. Oil pump.

King G3C model oil pump is used in system. Oil pump speed can be controlled by a frequency converter used in the system. The maximum frequency used for the oil pump is 50 Hz, and the maximum flowrate is 5.7 m^3/h. In Figure 3.9, oil pump frequency converter is shown.

Figure 3.9. Oil pump frequency convertor.

An ORC has a turbine to generate electricity but the test setup in BURET has a turbine simulator in addition to a turbine. The simulator is modelled in this thesis. Decrease of pressure in the turbine is generated with a throttle valve in the simulator. In Figure 3.10, throttle valve is shown. R134a enters the throttle valve after it exits from the evaporator.

Figure 3.10. Throttle valve.

The throttle valve decreases the working fluid's pressure. It is a SAMSON Type 41-23 product. There is a setting screw on the valve, the exit pressure can be adjusted by using setting screw. Outlet pressure range is 4.5 bar-10 bar. Due to limited heat transfer area the change in enthalpy from the inlet to the exit of the throttle valve is negligible. Outlet pressure is adjusted by the user in an experiment. As the pressure decrease and enthalpy remains constant the outlet temperature is different than the inlet temperature of the throttle valve.

Figure 3.11. Condenser.

After the working fluid exits the throttle valve, it enters the condenser shown in Figure 3.11. The condenser used is also a plate type heat exchanger. The only difference between the condenser and the evaporator is the number of plates. The evaporator has 80 plates, whereas the condenser has 66 plates. For the condenser used, the geometrical parameters are given in Table 3.2.

Table 3.2. Geometrical parameters for condenser.

Geometrical Parameter	Value and Unit
b	1 mm
t	0.4 mm
p	1.4 mm
P_c	6.58 mm
N	66
Heat Transfer Area	6.1 m^2

Similar to the evaporator the condenser can be divided to three regions which are superheated vapor region, two phase region, and sub-cooled liquid region. Working fluid coming from throttle valve enters the condenser as superheated vapor. Cold water coming from the chiller unit cools and condenses the refrigerant vapor and then decreases the temperature of the liquid refrigerant. Thus, R134a exits the condenser as sub-cooled liquid.

After condenser outlet, working fluid passes through a refrigerant filter. Refrigerant filter's aim is to prevent dirt in the cycle. In Figure 3.12, refrigerant filter is shown.

Figure 3.12. Refrigerant filter.

After the refrigerant filter, working fluid returns the working fluid pump and cycle repeats. Working fluid is filled to ORC setup by using a filling device. In Figure 3.13, working fluid filling device is shown.

Figure 3.13. Working fluid filling device.

Filling station is ELCİ AB93 model product. It has a 22 kg tank capacity of R134a. User can add R134a to the ORC setup. Amount of R134a can be adjusted easily. In case needed, user can also draw R134a back from the ORC setup and fills the tank. Amount of R134a filled is 20 kg in the ORC experiments.

Amount of R134a needed in ORC setup at BURET laboratory is determined by calculating the volume of liquid region (from condenser's half to evaporator's half) and multiplying the value with the known density of working fluid. Thus, mass of working fluid needed is calculated.

There are temperature and pressure sensors installed on the ORC cycle test setup. Temperature sensors are ABB TSP121 model product. In Figure 3.14, a temperature sensor is shown. Measurement range is 0-250 °C. Measurement sensitivity of temperature sensor is ±0.5 °C.

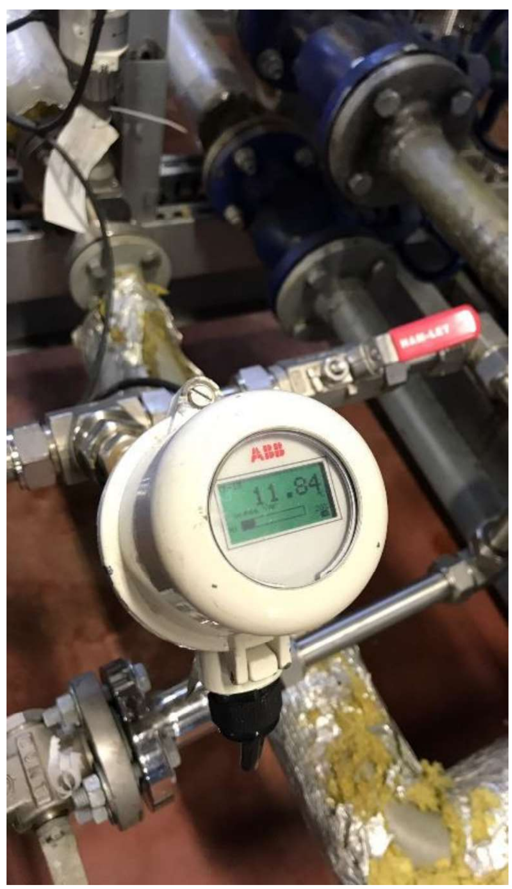

Figure 3.14. Temperature sensor.

Pressure sensors are ABB 261GN model product. In Figure 3.15, pressure sensor is shown. Measurement sensitivity of pressure sensor is ±0.15%.

Figure 3.15. Pressure sensor.

There are three types of flow meters used in ORC setup, coriolis flow meter, vortex flow meter and electromagnetic flow meter. Coriolis flow meter is used to measure working fluid’s mass flowrate. This device can also measure density. Vortex flow meters measure only volumetric flowrate. There is one electromagnetic flow meter and one vortex flow meter used in ORC setup. Electromagnetic flow meter is at chiller unit cold water line and it measures cold water’s flowrate. Vortex flow meter is placed on hot oil line. It is placed after King oil pump, and it measures hot oil’s flowrate.

In Figure 3.16, coriolis flow meter is shown. Coriolis flow meter is ABB FCB330 model product. Measurement sensitivity is ±0.1%. Maximum flowrate is 18 m^3/h.

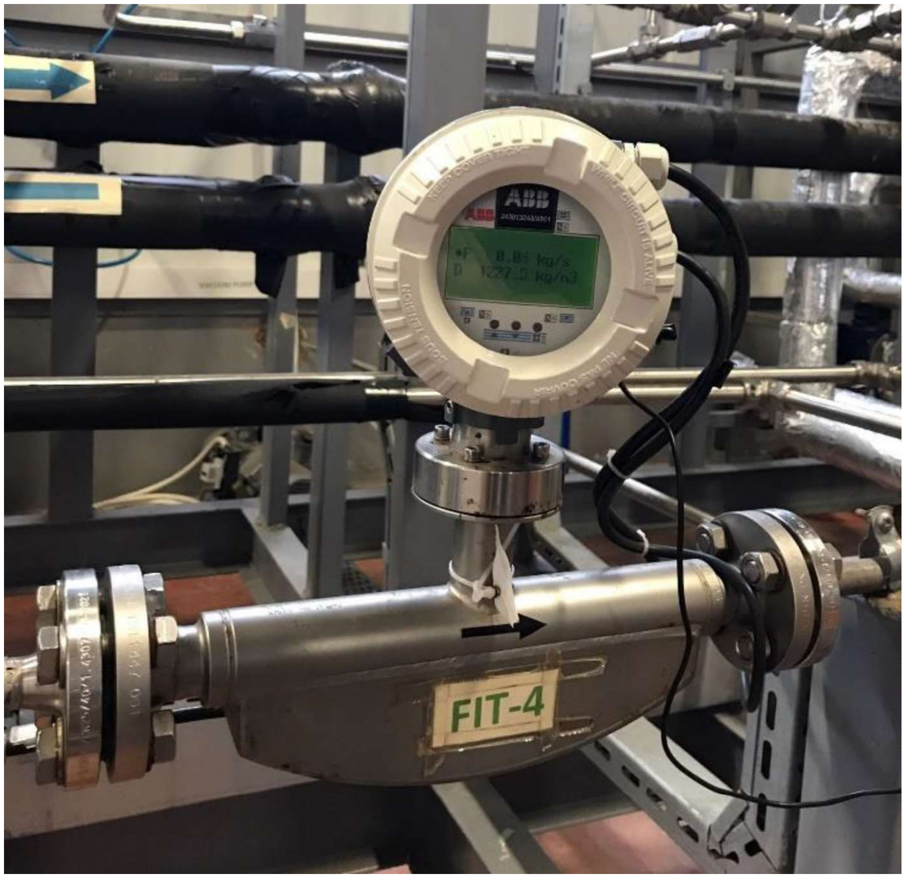

Figure 3.16. Coriolis flow meter.

In Figure 3.17, electromagnetic flow meter used on cold water line is shown. Electromagnetic flow meter used on cold water line is ABB FEW111 model product. Measurement sensitivity is ±0.4%. Maximum flowrate is 24 m^3/h.

Figure 3.17. Electromagnetic flow meter on cold water line.

In Figure 3.18, vortex flow meter used on hot oil line is shown. This vortex flow meter is ABB FSV430 model product. Measurement sensitivity is ±0.65%. Maximum flowrate is 18 m^3/h.

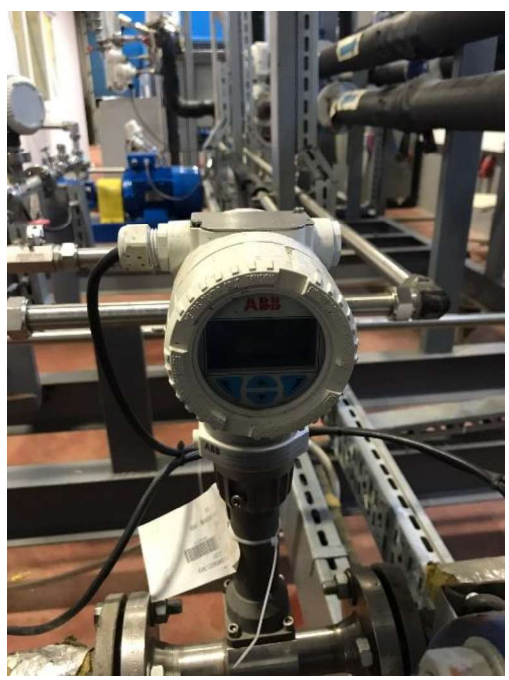

Figure 3.18. Vortex flow meter on hot oil line.

There are many ball type valves in the ORC setup. All ball type valves are placed on R134a route of the setup. Flow route is determined by opening/closing ball type valves. If researcher does not want working fluid to go some region of ORC setup, he/she closes the ball type valve on the line that reaches unwanted region. In Figure 3.19, a ball type valve is shown.

Figure 3.19. Ball type valve.

There are globe type valves on chiller unit water line and oil heater oil line. The aim of globe valves is adjusting the flowrates in these lines. In Figure 3.20, a globe type valve is shown.

Figure 3.20. Globe type valve.

There is a check valve placed after the working fluid pump. The aim is to prevent back flow. Back flow causes problems for the pump. Check valves allow only one way flow. In Figure 3.21, the check valve is shown.

Figure 3.21. Check valve.

There is a needle valve placed just after the check valve. The aim is to decrease pump exit pressure if needed. There is a setting screw to adjust pressure level. In Figure 3.22, needle valve is shown.

Figure 3.22. Needle valve.

Total pipe length of the ORC setup is nearly 27 m. Outer radius pipe is 25.4 mm, thickness of pipe is 2.1 mm. Material is 316 AISI steel. In Figure 3.23, a pipe section is shown.

Figure 3.23. Pipe.

Elbow elements are used in the ORC setup when R134a flow direction change of 90° is wanted. An elbow element is shown in Figure 3.24.

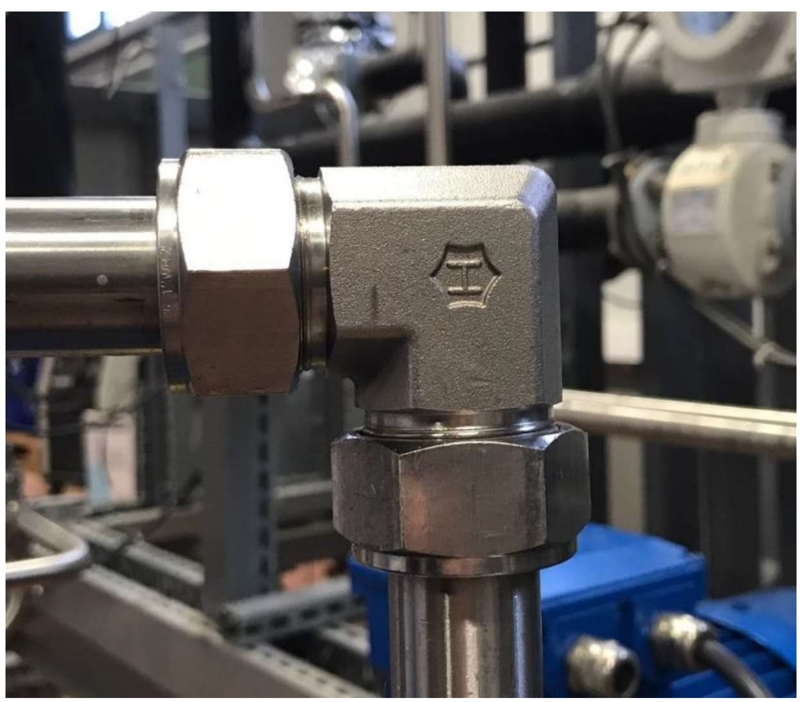

Figure 3.24. Elbow element.

T elements are used in the ORC setup where R134a flow separates in two different directions. A T element is shown in Figure 3.25.

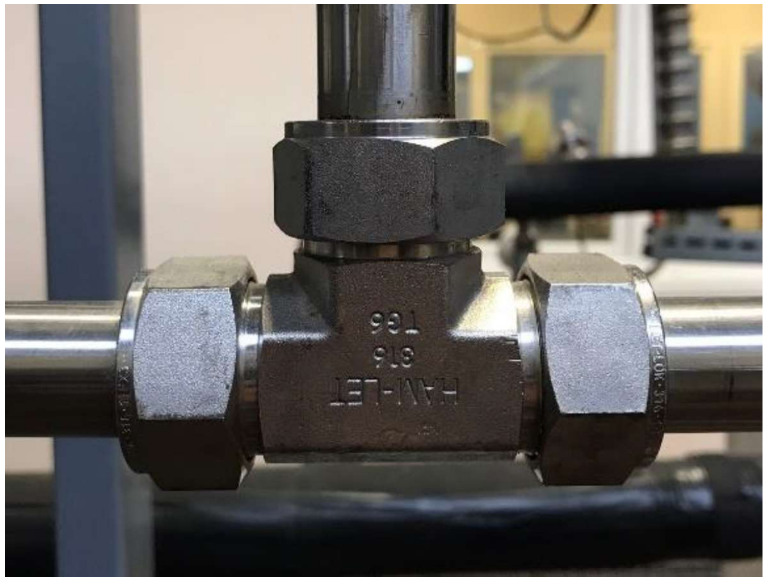

Figure 3.25. T element.

Pipes are connected to ball valves, needle valve, check valve, elbow elements, T elements, etc. by Let-Lok fittings. Let-Lok fittings are very safe against leakage. There is a ferrule set inside. A ferrule set consists of back and front ferrules. Ferrule set is shown in Figure 3.26.

Figure 3.26. Back and front ferrule set [20].

First, ferrule set is placed and touched to target connections inner surface. Then nut is tightened by a proper wrench. In Figure 3.27, an example for Let-Lok fitting between pipe and elbow is shown.

Figure 3.27. Let-Lok fitting between pipe and elbow [21].

There was a liquid collector between condenser exit and refrigerant filter inlet in the ORC setup. However, liquid collector was removed. The reason is that outer radius and outer surface area of the liquid collector is too high and liquid collector acts like a heat sink. Heat coming from environment to the liquid collector leads temperature increase in R134a. This temperature increase causes bubble formation at pump suction line. Therefore, circulation stops. To prevent bubble formation, liquid collector was removed. In Figure 3.28, liquid collector is shown.

Figure 3.28. Liquid collector.

There was a bypass line between pump exit and condenser exit in the ORC setup. However, bypass line was removed. The reason is that pipes of bypass line acts like a heat sink just like the liquid collector. Working fluid's temperature increase causes bubble formation at pump suction line. Therefore, circulation stops. To prevent bubble formation, bypass line was removed. In Figure 3.29, bypass line is shown.

Figure 3.29. Bypass line [22].

When bypass line was removed, a direction of the T element on the pipeline became useless. Fitting plugs are used to close this direction. The fitting plug is shown in Figure 3.30.

Figure 3.30. Fitting plug.

There are two level indicators in the cycle. One level indicator is used for the evaporator and the other is used for the condenser. The aim to use level indicators is to see liquid level in the evaporator or the condenser. These level indicators show where condensation or evaporation occurs. Level indicators are Valftek-Bonetti BR23-G11 model products. In Figure 3.31, a level indicator is shown.

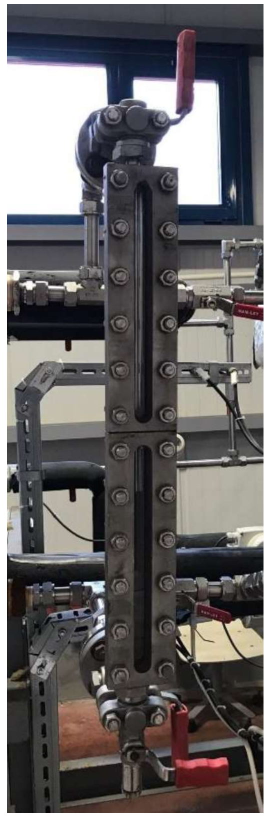

Figure 3.31. Level switch.

There is a data acquisition system to collect signals from sensors and convert these signals to measurement data. IPETRONIC 2016 Professional Edition is used as data acquisition software. In Figure 3.32, data acquisition system is shown.

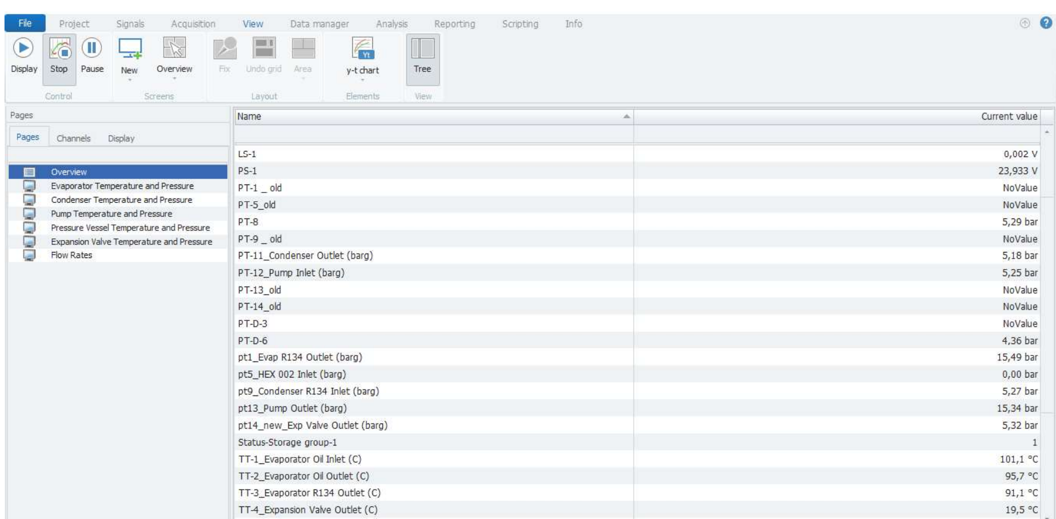

Figure 3.32. Data acquisition system.

3.3. Changes Made on the ORC Setup

One of the most important problems on the ORC setup was refrigerant leakage problem, there were many points in the setup that leaked. To detect leakage locations, pressurized air at nearly 7 bar is filled to the system. System is divided into four parts by using ball type valves. The aim was to monitor the pressure values in these four setup segments separately. Pressure values for each pressure sensor were recorded at the beginning. A table that includes time and pressure values for different locations to follow pressure values vs time was formed. After a pressure drop was determined, leakage fixing procedure was started. If the leaking connection was Let-Lok type fitting, fixing was easy. Connection was tightened using a wrench.

If the leaking part was not a Let-Lok fitting, the connection was removed firstly. All contact surfaces were cleaned, and a liquid seal was applied to contact surfaces. Then the connection was tightened by a wrench. There were some connections where the leakage was not stopped with this procedure due to the quality of the material. In those cases, proper parts were purchased, and the connections were replaced. For example, the leakage at evaporator exit connection could not be solved by a using liquid seal, and a new connection was manufactured then mounted to the setup.

Sensor connections were also possible leakage locations. To prevent leakage from sensor connections, all sensors removed from the system. Contact surfaces of connections were cleaned. Liquid seal is applied to contact surfaces. Then connections were tightened by a wrench.

After leakage fixing procedure was applied to all connections of the setup, final leakage tests were done. One final leakage test was done by filling the system with 7 bar air. And the second final leakage test was done by filling the system with 15 bar N_2. Higher pressure level makes finding leakages easier. After last leakage tests, it was seen that leakage problem was solved.

Long pipes and many elbows on pipes created temperature and pressure losses especially in some parts of the ORC setup. The most problematic part being the line from the throttle valve exit to the condenser inlet. Lower pressure level side of the ORC setup is from the throttle valve exit to the pump inlet. The pressure drop between the throttle valve and the condenser inlet was about 1.4 bar. This value was very high when compared to the saturation pressure value. Pressure losses are more important on this side; the system is cooled by cold water and cold water inlet temperature is about 5 ℃, and working fluid outlet temperature cannot be less than cold water inlet temperature. The saturation pressure at 5 ℃ of R134a is 3.5 bar which means that the condenser inlet pressure must be greater than 3.5 bar to have condensation in the condenser. If there is a large pressure drop between the throttle valve outlet and the condenser inlet, the throttle valve outlet pressure value should be adjusted to a higher value to prevent lower pressure level at the condenser inlet than the saturation pressure at the condensation temperature. Also, having higher throttle valve outlet pressure decreases the pressure ratio and efficiency of the cycle.

Piping between throttle valve and condenser inlet was changed. Not only pipe length between the throttle valve and condenser is shortened, but also five elbows are removed from the cycle. These changes decreased temperature and pressure drop greatly. The pressure drop reduced to about 0.3 bar.

Modifications in the piping between the throttle valve and the condenser also prevented the bubble formation at the inlet of the working fluid pump. When the pressure and temperature values were too close to saturation values, even a small temperature increase of R134a due to a heat input from the environment to pipes led to bubble formation. The working fluid pump is a liquid pump, so the inlet fluid should be liquid, when bubbles occur in the pump inlet, pump does not pressurize the working fluid and the cycle is not completed. Changes in the piping resulted in a lower pressure drop and higher condenser inlet pressures that are higher than the saturation values and therefore prevented bubble formation. Thus, a temperature increase due to stray heat transfer from the environment to the pipe did not lead bubble formation.

There was a liquid collector placed between the condenser and the pump which is shown in Figure 3.28, liquid collector was shown. Main aim was to send only liquid to the pump. However, due to its high outer surface, heat income from environment to liquid collector led to bubble formation. Temperature increases of nearly 3°C through the liquid collector were measured. When the temperature of R134a increases, it becomes vapor and when bubble came to the pump suction circulation stopped. Therefore, the liquid collector was removed, and a straight pipe was installed in the place of the liquid collector.

An escape valve is added just before the working fluid pump. The aim was to discharge any bubble at pump suction line if necessary. In Figure 3.33, the escape valve is shown.

Figure 3.33. Escape valve for bubble.

There are also improvements made on data acquisition system: The calibration for each sensor was made by using calibration data given in sensor's catalogue, instantaneous data tracking windows were created. With these windows on the software the user can follow data at different locations of the setup easily. For example, there is a window named 'Pump Pressures and Temperatures'. In this window, the user can see the pump inlet and outlet pressures, the pump inlet and outlet temperatures vs time graphs. Other windows are

'Evaporator Pressures and Temperatures', 'Throttle Valve Pressures and Temperatures', 'Condenser Pressures and Temperatures', and 'Flowrates'. In Figure 3.34, 'Pump Pressures and Temperatures' window is shown.

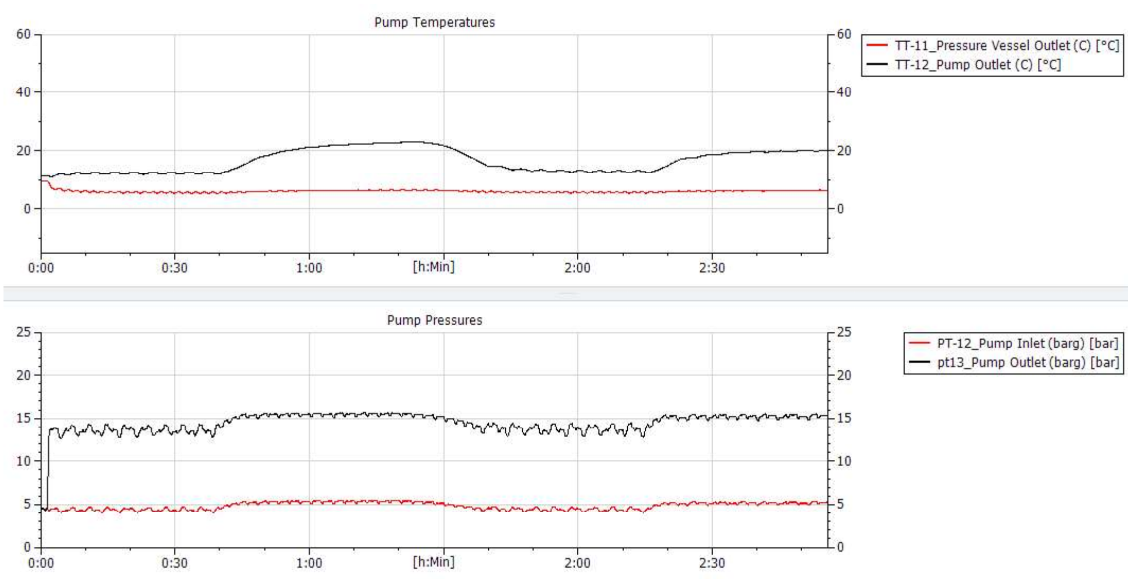

Figure 3.34. Tracking window for pump pressures and temperatures.

Data acquisition system's data collecting frequency is 1 Hz, it records one data per second for each sensor. After an experiment is completed, the user can get experimental data as an excel file and use data easily.

A summary of all components after modifications made to the ORC setup, components and elements used in the setup is tabulated in Table 3.3.

Table 3.3. List of table for ORC components.

Component/Element Name	Unit	Amount
Side Channel Pump (Speck)	piece	1
Evaporator	piece	1
Throttle Valve	piece	1
Condenser	piece	1
Chiller Unit	piece	1
Oil Heater Unit	piece	1
Oil Pump (King)	piece	1
Pipe (current)	m	27 (latest)
Elbow	piece	14
T Element	piece	15
Ball Type Valve	piece	17
Globe Type Valve	piece	3
Check Valve	piece	1
Needle Valve	piece	1
Coriolis Flowmeter	piece	1
Vortex Flowmeter	piece	2
Temperature Sensor	piece	10
Pressure Sensor	piece	6
Escape Valve	piece	1
Refrigerant Filter	piece	1

After the modifications are completed, the experiments are carried out under the following inputs:

- Chiller unit cold water temperature set value
- Cold water flowrate
- Oil heater unit hot oil temperature set value
- Oil pump speed
- Throttle valve exit pressure set value
- Working fluid pump speed

These parameters can be controlled by the researcher. The outputs of experiments are the followings:

- Evaporator R134a outlet and inlet temperature
- Evaporator hot oil outlet temperature
- Throttle valve outlet and inlet temperature
- Condenser R134a outlet and inlet temperature
- Condenser cold water outlet temperature
- Evaporator R134a outlet and inlet pressures
- Condenser R134a outlet and inlet pressures.
- R134a mass flowrate

All data are recorded using the data acquisition system. The outputs of the experiments and the dynamic model are then compared. The Dynamic model is explained in the following chapter and the comparison of results of the dynamic model and experiments is presented in Results and Conclusion chapter.
Ambient Conditions

4. THE DYNAMIC MODEL OF THE ORC

A simple ORC has mainly five components which are a working fluid pump, an evaporator, a turbine, a condenser, and piping. In BURET, a scroll turbine is present however it is not installed in the ORC setup yet. Therefore, a throttle valve is used to provide pressure drop in the turbine. Therefore, five separate components are modeled on Dymola.

The components used on this thesis are a working fluid pump, an evaporator, a throttle valve, a condenser and piping. This chapter explains the dynamic model for each component. A tester for each component is created and simulated. Testers are verified by experimental data. After verified model testers for all components are prepared, components are integrated to create whole ORC model.

Refrigerant properties such as density, specific heat, enthalpy etc. are calculated by using REFPROP program.

4.1. Evaporator

A plate type heat exchanger is used as evaporator in the ORC setup at BURET laboratory. There are two flow channels in the evaporator. The first one is for working fluid and the second one is for the heat transfer fluid. Heat is transferred from heat transfer oil to the working fluid.

In experiments, R134a is used as working fluid and AKPET ATHERMA M32 is used as heat transfer fluid. Temperature and mass flowrate of heat transfer oil can be adjusted by a heater controller panel easily. These are input values for the evaporator. General view of a plate type heat exchanger is shown in Figure 4.1.

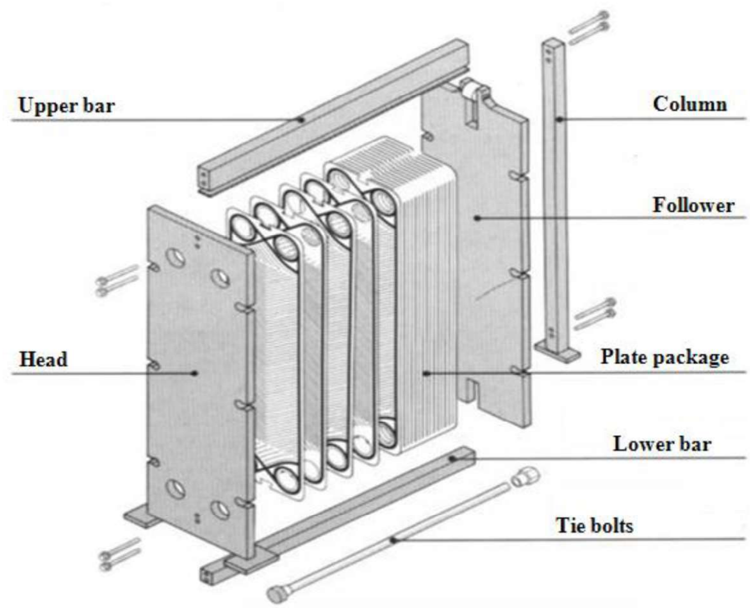

Figure 4.1. General view for a plate type heat exchanger [23].

A plate type heat exchanger geometry in Dymola is shown in Figure 4.2.

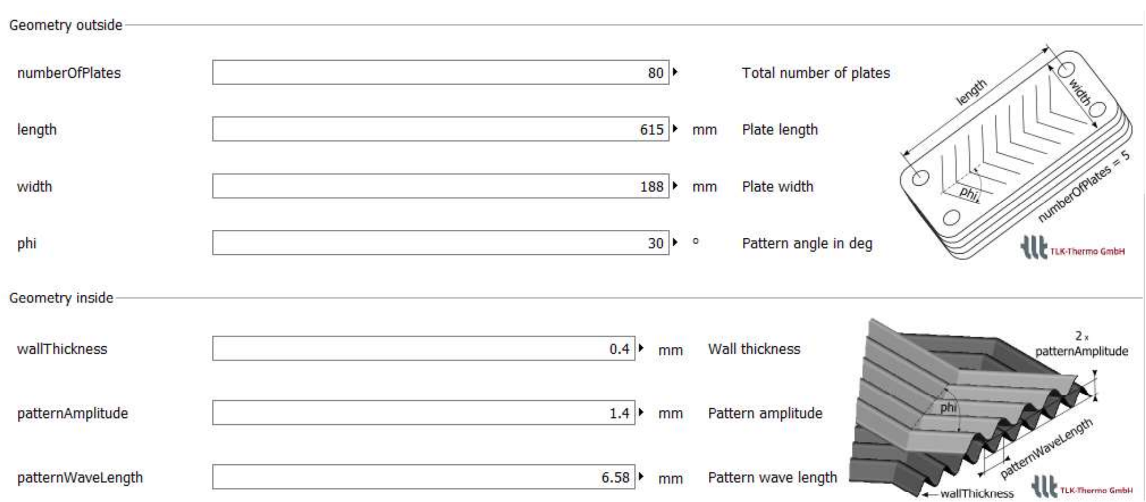

Figure 4.2. Geometry for a plate type heat exchanger.

As shown in the Figure 3.6, L is the plate length, w is the plate depth, β is the chevron angle, p is the corrugation depth, and the P_c is the corrugation pitch. There is also a parameter named N which shows number of plates in the evaporator. These parameters are used in evaporator model. For the evaporator used at BURET laboratory, geometrical parameters are given in Table 3.1.

There are three regions in an evaporator. The first one is sub-cooled liquid region, the second one is two phase region and the third one is superheated vapor region. Different convective heat transfer correlations are available for these regions, such as Shah-Chen, Longo, etc. in the literature. In this thesis, Longo [24] correlations are used to simulate evaporation phenomena.

R134a enters the evaporator as sub-cooled liquid. Therefore, following correlation by Longo for sub-cooled liquid is used

$$Nu = 0.2267 Re^{0.631} Pr^{1/3} \tag{4.1}$$

where Nusselt number is

$$Nu = \frac{h d_h}{\lambda_l} \tag{4.2}$$

and Reynolds number is

$$Re = \frac{\rho V d_h}{\mu} \tag{4.3}$$

and Prandtl number is

$$Pr_l = \frac{\mu_l c_{p,l}}{\lambda_l}. \tag{4.4}$$

Sub-cooled R134a is heated by hot oil and when the temperature reaches the saturation temperature two phase region calculation starts.

There are two types of boiling. The first one is nucleate boiling and the second one is convective boiling. Boiling number, Bo is defined as

$$Bo = \frac{q}{G\left(h_l - h_g\right)} \tag{4.5}$$

and X_{tt} is Martinelli parameter is defined as

$$X_{tt} = [(1 - X_m)/X_m]^{0.9} \left(\rho_g/\rho_l\right)^{0.5} \left(\mu_l/\mu_g\right)^{0.1} . \quad (4.6)$$

If Bo.X_{tt} > 0.00015, the boiling type is nucleate boiling. If Bo.X_{tt} < 0.00015 it is convective boiling.

For convective boiling, following correlations are used

$$\alpha_{cb} = 0.122\Phi(\lambda_l/d_h){Re_{eq}}^{0.8}{Pr_l}^{1/3} \quad (4.7)$$

where Φ is enlargement factor which is the ratio of the actual and the projected area of the plates. Equivalent Reynolds number is defined as follows

$$Re_{eq} = \frac{G\left[(1 - X) + X\left(\rho_l/\rho_g\right)^{1/2}\right] d_h}{\mu_l} \quad (4.8)$$

where X is assumed to be the average vapor quality X_m between inlet and outlet. Therefore, X_m is 0.5 for the ORC setup at BURET laboratory.

For nucleate boiling, following correlations are used

$$\alpha_{nb} = 0.58\Phi\alpha_0 C_{Ra} F(p^*) \left(\frac{q}{20000\ Wm^{-2}}\right)^{0.467} \quad (4.9)$$

$F(p^*)$ is defined as following

$$F(p^*) = 1.2{p^*}^{0.27} + [2.5 + 1/(1 - p^*)]p^* \quad (4.10)$$

where p^* is reduced pressure and it is equal to following

$$p^* = \frac{P}{P_{critical}} . \quad (4.11)$$

In the superheated region heat transfer coefficient is calculated by the following correlation

$$Nu = 0.277Re^{0.766}Pr^{1/3}\,. \tag{4.12}$$

To validate the evaporator model, an experiment is done. For this experiment input parameters are heat transfer oil inlet temperature, heat transfer oil mass flowrate, R134a inlet temperature, and R134a mass flowrate. Outputs are heat transfer oil outlet temperature and R134a outlet temperature. Simulation and experiment results are compared.

Evaporator tester model includes two paths. The first path is for R134a and it is indicated with green color. The second path is for heat transfer oil and it is highlighted with red and blue color. General structure for the evaporator tester is shown in Figure 4.3. SIM icon in Figure 4.3 and other figures means System Information Manager. User defines working fluid, water, and heat transfer oil from this icon.

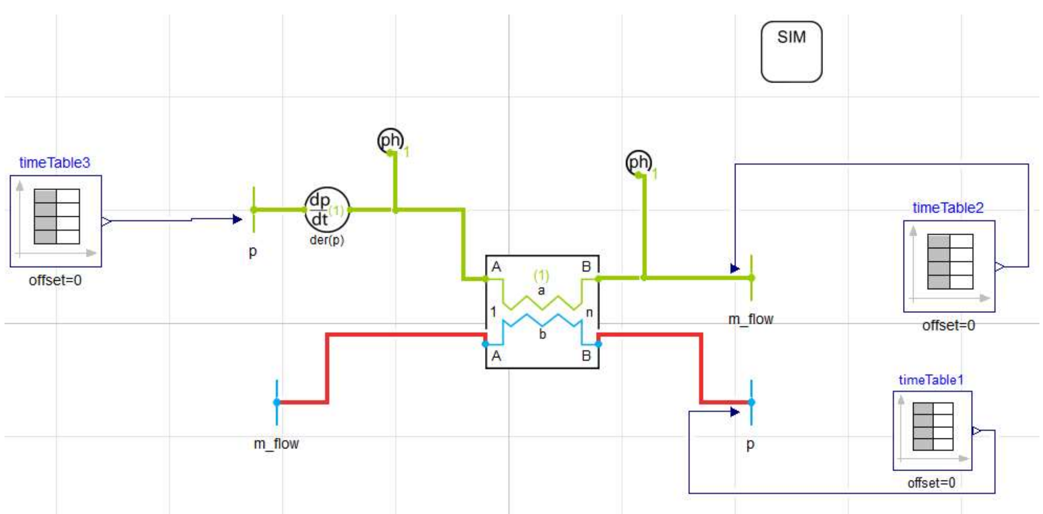

Figure 4.3. Evaporator tester.

Heat transfer oil inlet temperature is like a sinus wave. Figure 4.4 shows the experimentally measured evaporator oil inlet temperature.

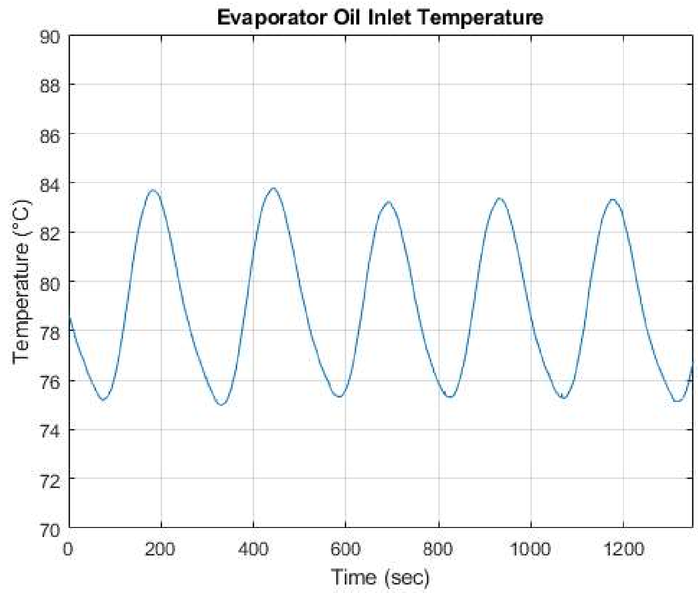

Figure 4.4. Evaporator oil input temperature.

Heat transfer oil flowrate is almost constant. Flowrate is 4.6 m^3/h. Figure 4.5 shows the experimentally measured heat transfer oil flowrate.

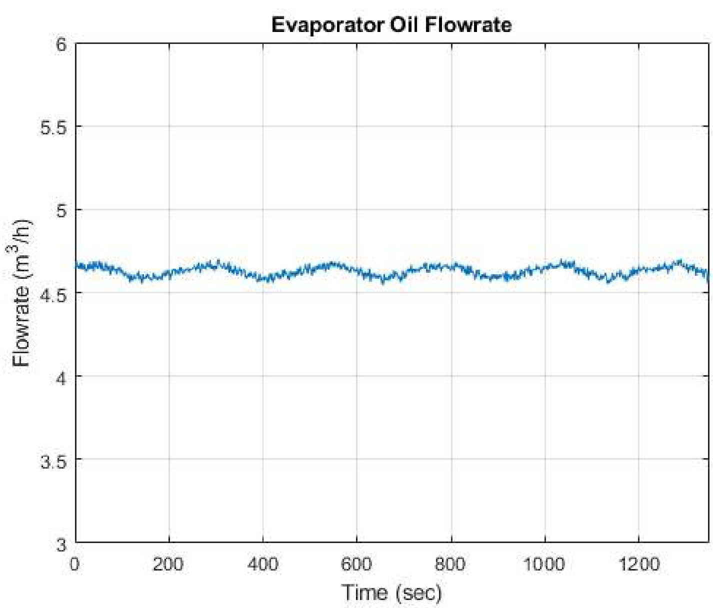

Figure 4.5. Evaporator oil flowrate.

Experimentally measured inlet temperature data for R134a is used as input for the model. The data are shown in Figure 4.6.

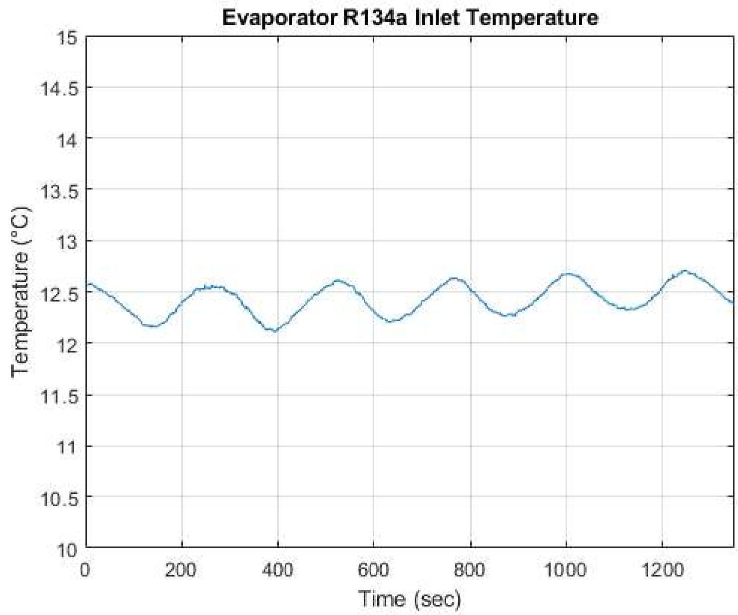

Figure 4.6. Evaporator R134a inlet temperature.

Experimentally measured R134a mass flowrate input data are shown in Figure 4.7.

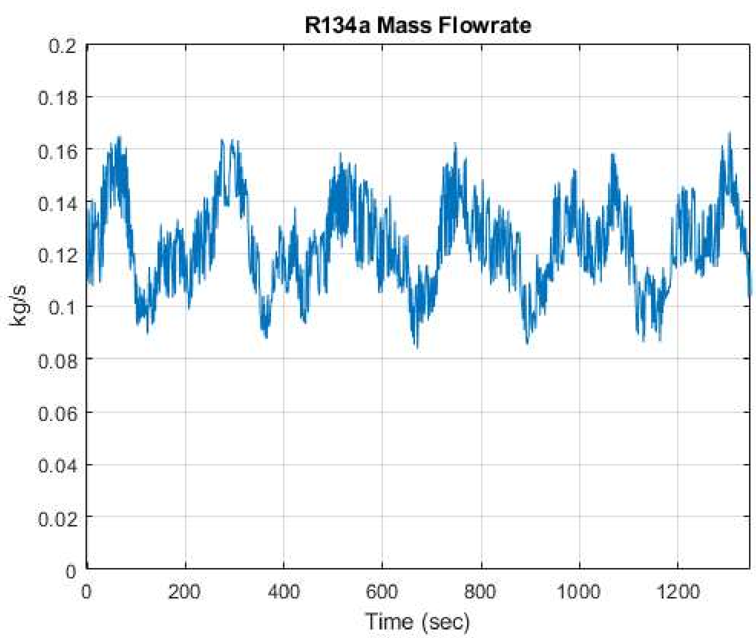

Figure 4.7. Evaporator R134a mass flowrate.

There are two outputs of the dynamic simulation. The first output is the evaporator R134a outlet temperature, and the second output is the heat transfer oil outlet temperature.

In Figure 4.8 and Figure 4.9, these outputs are shown. In Figure 4.8, evaporator R134a outlet temperature for both model and experiment are compared, and in Figure 4.9, evaporator oil outlet temperature for both model and experiment are shown.

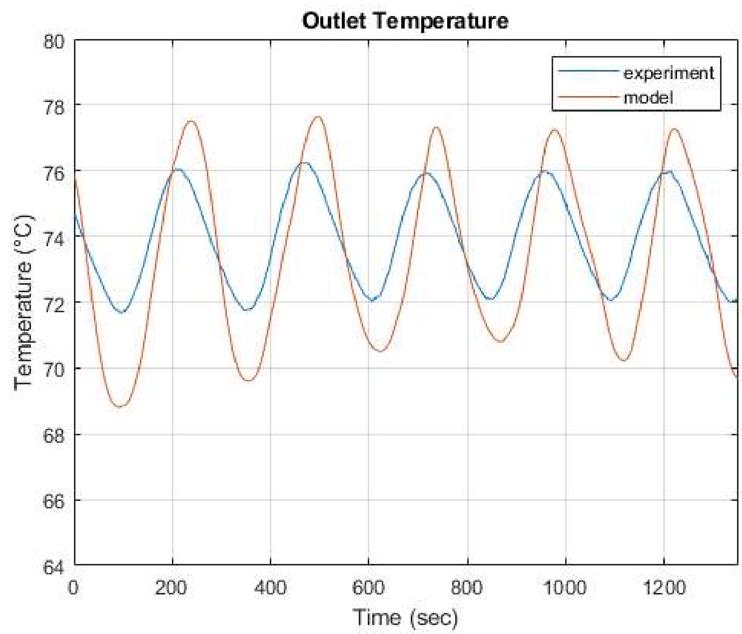

Figure 4.8. Evaporator R134a outlet temperature.

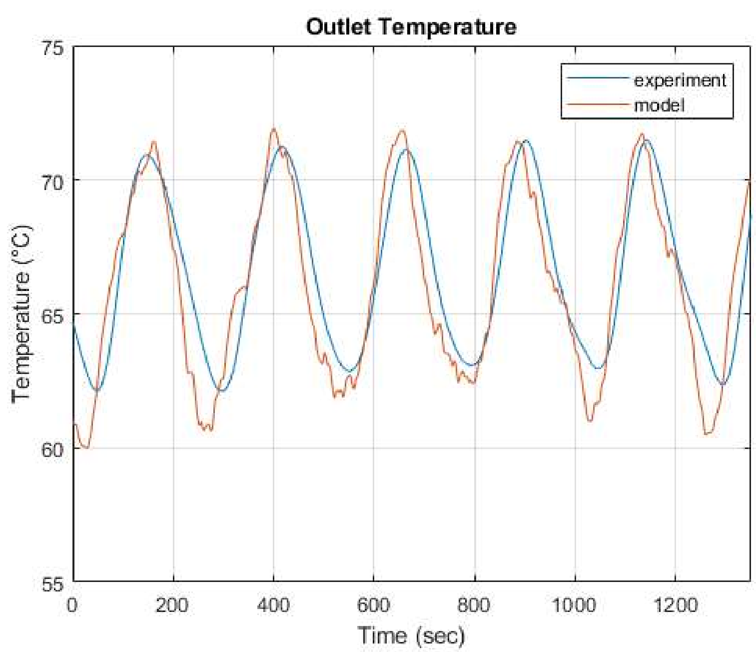

Figure 4.9. Evaporator oil outlet temperature.

Output results for simulation and experiment are very close to each other and the temporal behavior is captured accurately. Maximum temperature difference is less than 3°C. It is concluded that the evaporator tester is working correctly. Thus, dynamic evaporator model can be used in dynamic ORC model safely.

4.2. Throttle Valve

As it is mentioned in the beginning of the chapter, ORC test setup at BURET Laboratory has a turbine simulator. A throttle valve is used to provide pressure drop in the cycle while the enthalpy remains almost constant, since the heat transfer rate is low due to small heat exchange area and there is no accumulation of energy within the throttle valve. Inlet pressure and temperature to the throttle valve is determined by the evaporator outlet of the cycle. Outlet pressure of the throttle valve can be set to a desired value by a adjusting the setting screw. Therefore, outlet pressure is a parameter that can be controlled. The outlet temperature of the throttle valve is obtained from the energy balance which dictates that at the inlet and outlet of the throttle valve is equal

$$h_{in,tv} = h_{out,tv} \,. \tag{4.13}$$

Since the enthalpy is a function of pressure and temperature, equation 3.13 can be expressed as follows

$$h(P_{in,tv}, T_{in,tv}) = h(P_{out,tv}, T_{out,tv}) \tag{4.14}$$

where $P_{in,tv}, T_{in,tv}, and\ P_{out,tv}$ are known parameters for the tester. Therefore, there is only one unknown parameter which is $T_{out,tv}$ (throttle valve outlet temperature) and one equation. This is solvable. Enthalpy values are calculated by REFPROP software.

In Figure 4.10, general structure of the tester of throttle valve in Dymola is shown. There is a PI controller used in the tester. The aim is to take the set value for valve outlet pressure from user.

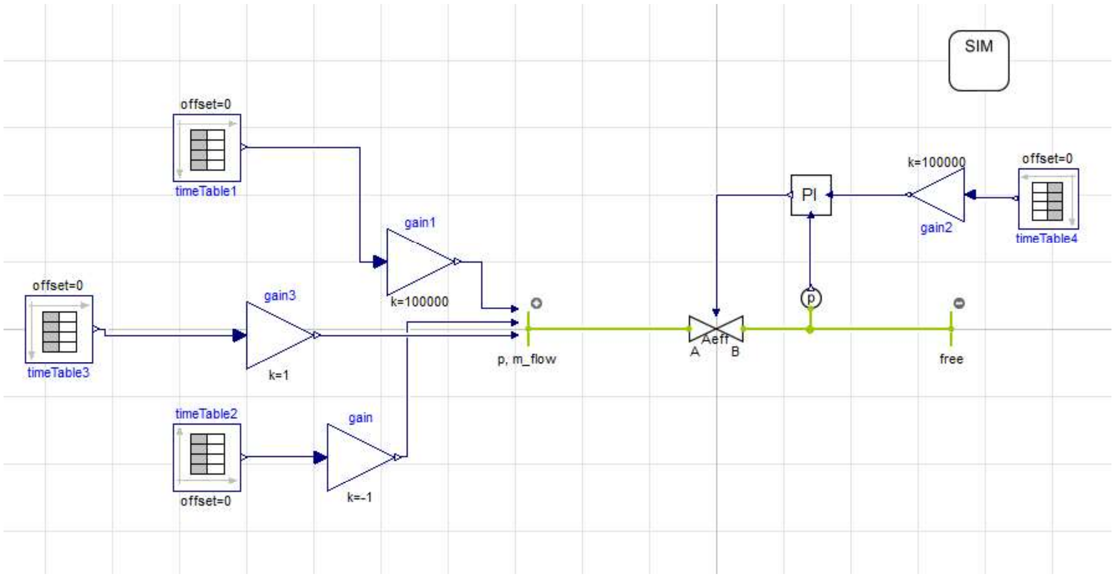

Figure 4.10. General structure of throttle valve tester.

Thermal systems library has an 'orifice valve' components. It takes effective flow area from user. However, user can not set output pressure value. Therefore, a PI controller is added. The PI controller arranges the effective flow area to reach desired output pressure value. It is similar SAMSON throttle valve's working principle. It changes the flow area and gives a desired output pressure. Mass flowrate relation used in tester is given below

$$\dot{m} = A_{eff}\sqrt{(P_{in} - P_{out}).2\rho_{in}}\,. \tag{4.15}$$

In Figure 4.11, input window for the throttle valve tester is given. For the tester, inlet pressure and inlet temperature are inputs. Outlet pressure is given by the user. Model calculates the outlet temperature from the energy balance equation. After the correct throttle valve model is validated and added to whole ORC model, input pressure and input temperature will not be manual inputs. These will come from outlet conditions of evaporator.

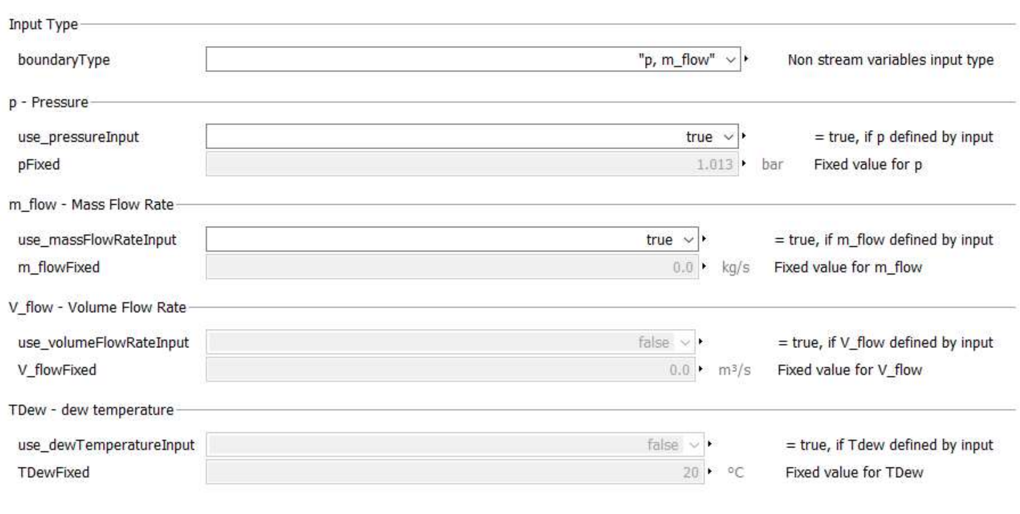

Figure 4.11. Input window for throttle valve tester.

After the tester is created, output results were compared to experimental results. In Figure 4.12, throttle valve outlet temperature is shown.

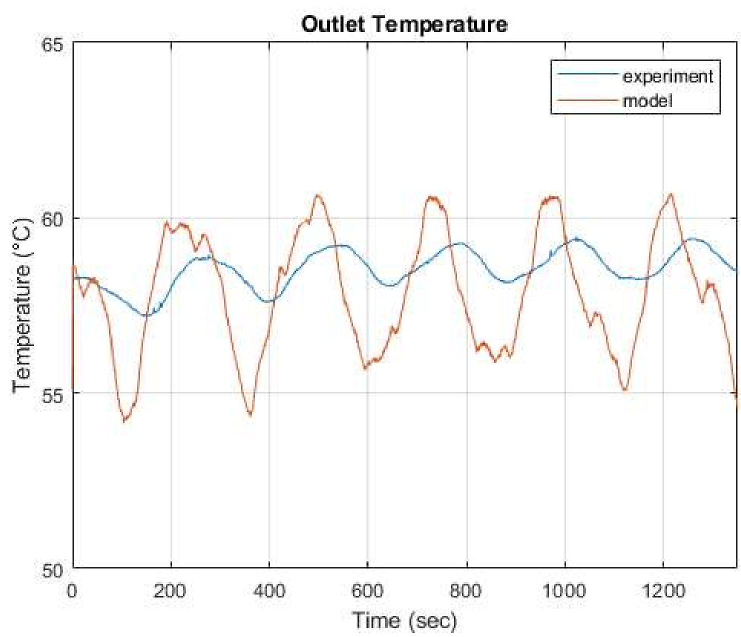

Figure 4.12. Throttle valve outlet temperature.

Maximum temperature difference is less than 3 °C. It is concluded that the throttle valve tester is working correctly. Thus, dynamic throttle valve model can be used in dynamic ORC model safely.

In Figure 4.13, throttle valve outlet pressure is shown. Model and experiment data are the same because throttle valve outlet pressure is set by user. Therefore, experimental data for outlet pressure is given to tester as input.

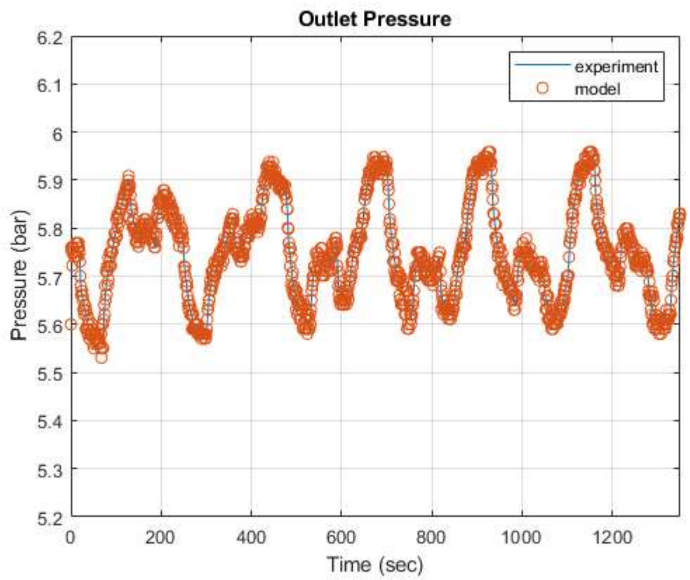

Figure 4.13. Throttle valve outlet pressure.

In Figure 4.14, throttle valve inlet and outlet enthalpy values are shown to see enthalpy equality between inlet and outlet of the valve.

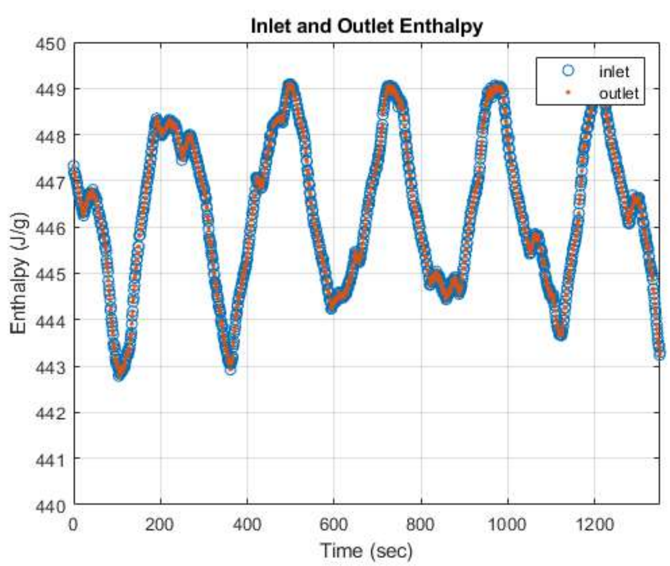

Figure 4.14. Throttle valve tester inlet and outlet enthalpy.

4.3. Condenser

Condenser in the experimental setup at BURET laboratory is also a plate type heat exchanger. Only physical difference between the evaporator and condenser is number of plates. There are 80 plates in evaporator, but there are 66 plates in condenser. For the condenser used in BURET laboratory, geometrical parameters are given in Table 3.2.

Condenser has three regions, superheated vapor region, two phase region, and sub-cooled liquid region. Different convective heat transfer correlations are available for these regions, such as Shah-Chen, Longo, etc. in the literature. In this thesis, Longo [25] correlations are used to simulate condensation phenomena.

R134a enters the condenser as superheated vapor. The heat transfer coefficient is calculated by the following correlations

$$Nu = 0.277 Re^{0.766} Pr^{1/3} \tag{4.16}$$

where Nusselt number is

$$Nu = \frac{h d_h}{\lambda_l} \tag{4.17}$$

and Prandtl number is

$$Pr = \frac{\mu_l c_{p,l}}{\lambda_l}. \tag{4.18}$$

The superheated R134a cools down by cold water flow and when the temperature equals to saturation temperature condensation starts. There are two types of condensation considered in Longo correlation. The first one is gravity dominated condensation and the second one is forced convection condensation. If equivalent Reynolds number is smaller than 1600, tester uses correlation for gravity dominated condensation. If equivalent Reynolds number is greater than 1600, tester uses correlation for forced convection condensation. Following correlations are used

$$Re_{eq} = \frac{G\left[(1-X) + X\left(\rho_l/\rho_g\right)^{1/2}\right] d_h}{\mu_l} \tag{4.19}$$

where X is assumed as averaged vapor quality X_m between inlet and outlet. Therefore, X_m is 0.5 for the ORC setup at BURET laboratory.

If $Re_{eq} < 1600$, then heat transfer coefficient is calculated by

$$\alpha_{gr} = 0.943\Phi\left(\frac{{\lambda_l}^3{\rho_l}^2 g(h_v - h_l)}{\eta_l |T_v - T_{wall}| L_{hx}}\right)^{0.25}. \tag{4.20}$$

If $Re_{eq} > 1600$, then heat transfer coefficient is calculated by

$$\alpha_{fc} = 1.875\Phi\left(\frac{\lambda_l}{d_h}\right) Re^{0.445}{Pr_l}^{1/3} \tag{4.21}$$

where Φ is enlargement factor equal to the ratio between the actual area and the projected area of the plates.

After condensation, subcooled region is considered. Following correlation is used for subcooled region

$$Nu = 0.2267Re^{0.631}Pr^{1/3}. \tag{4.22}$$

Only difference between condenser and evaporator correlations is two phase region calculations. In evaporator, model uses evaporation correlations. In condenser, model uses condensation correlation. Subcooled and superheated region correlations are the same for both condenser and evaporator.

To validate the condenser model, an experiment is made. For this case input parameters are cold water inlet temperature, cold water mass flowrate, R134a inlet temperature, and R134a mass flowrate. Outputs are cold water outlet temperature and R134a outlet temperature. Simulation and experiment results are compared.

Condenser tester includes two paths. The first path is for R134a and it is indicated with green color. The second path is for cold water and it is highlighted with blue color. General structure for the condenser tester is shown in Figure 4.15. Cold water source is a chiller device placed at BURET laboratory. Cold water inlet temperature and cold water flowrate can be controlled by the chiller control panel.

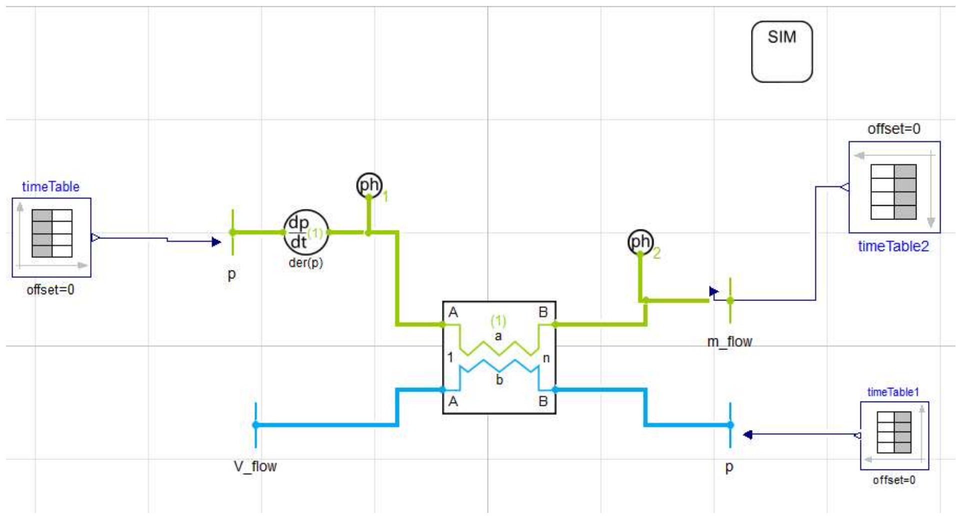

Figure 4.15. Condenser tester.

Cold water inlet temperature data shown below is used as input for tester. Figure 4.16 shows the condenser cold water inlet temperature.

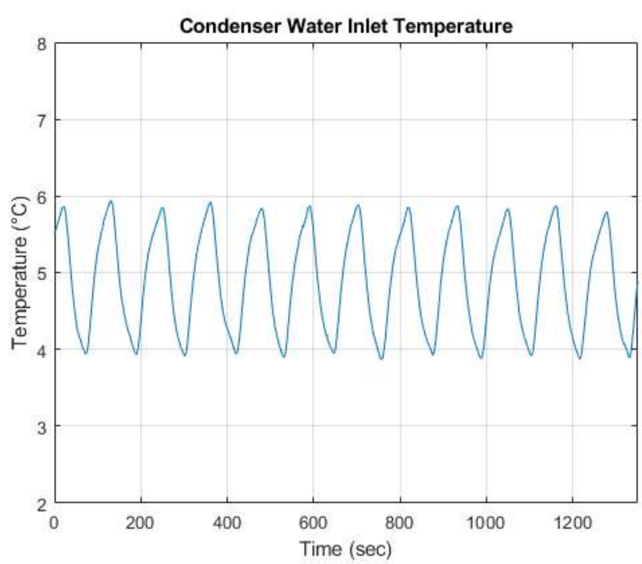

Figure 4.16. Condenser cold water inlet temperature.

Cold water flowrate is almost constant. Flowrate is 8,5 m^3/h. Figure 4.17 shows the cold water flowrate.

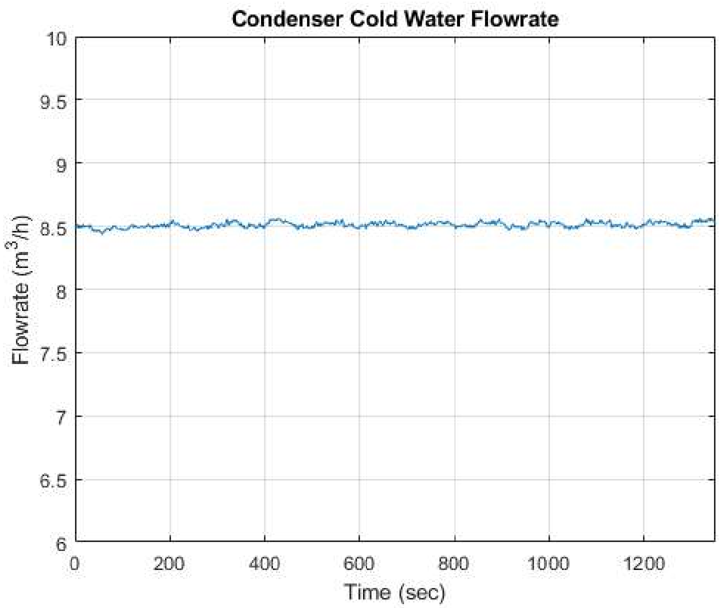

Figure 4.17. Cold water flowrate.

Inlet temperature data for R134a shown below is used as input for tester. Figure 4.18 shows the condenser R134a inlet temperature.

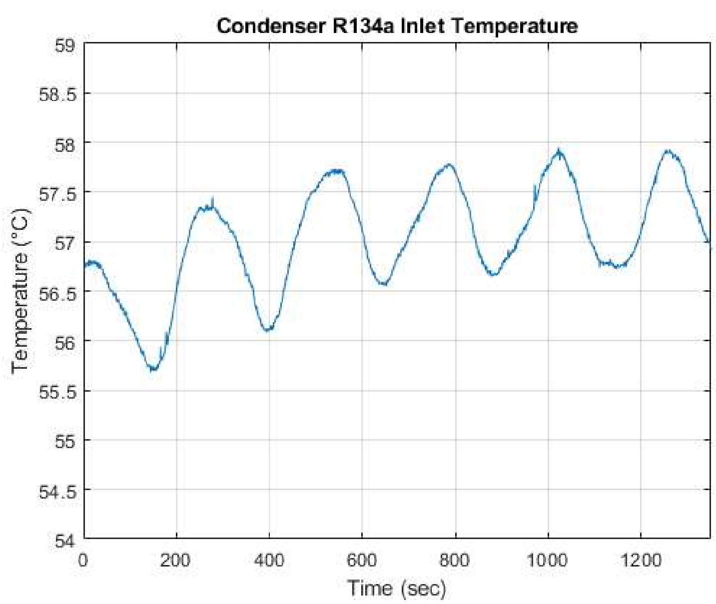

Figure 4.18. Condenser R134a inlet temperature.

R134a mass flowrate input data are shown in Figure 4.19 below. It is same as the evaporator R134a mass flowrate.

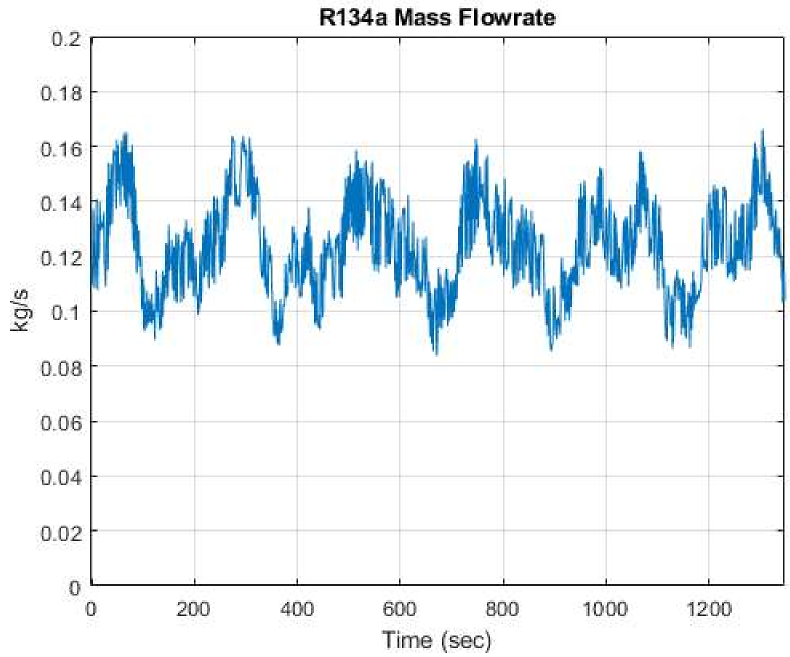

Figure 4.19. Condenser R134a mass flowrate.

After the inputs are added to the evaporator tester, dynamic simulation is made. There are two outputs obtained. The first output is condenser R134a outlet temperature, and the second output is cold water outlet temperature. In Figure 4.20 and Figure 4.21, outputs are shown.

In Figure 4.20, the condenser cold water outlet temperature and in Figure 4.21, the condenser R134a outlet temperature calculated with the model along the measured data are shown.

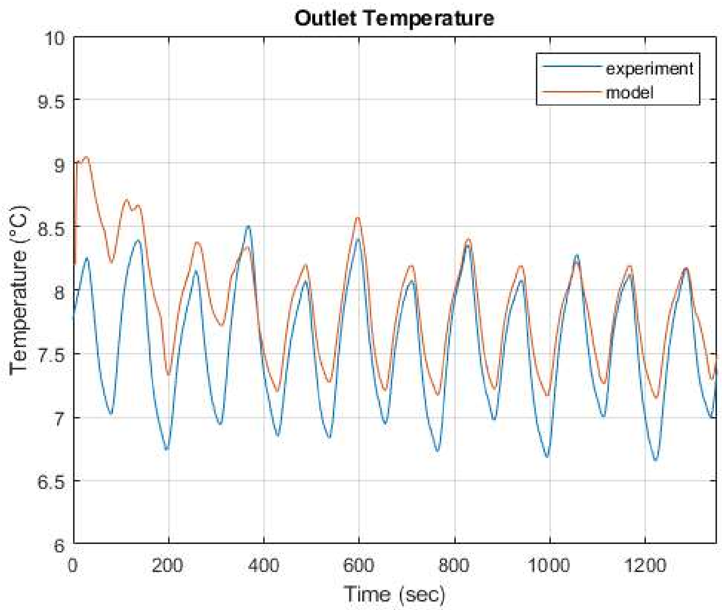

Figure 4.20. Condenser cold water outlet temperature.

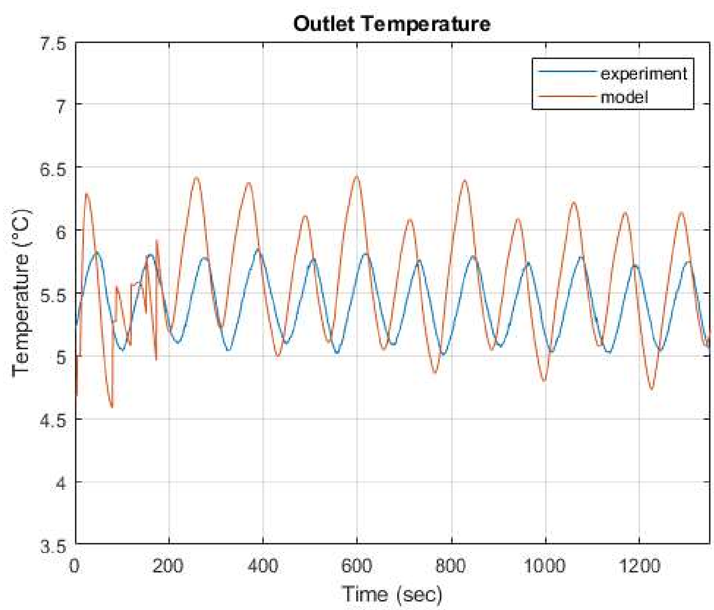

Figure 4.21. Condenser R134a outlet temperature.

Output graphs for simulation and experiment are very close to each other. Maximum difference for both R134a outlet temperature and cold water outlet temperature is smaller than 1 °C. Therefore, condenser model is able to model condenser accurately and it can be used in the dynamic ORC model safely.

4.4. Pipes

In the literature, most of the studies do not include heat or pressure losses in pipes. For example, they assume that throttle the valve inlet temperature is equal to the evaporator outlet temperature; also, they assume that the throttle valve inlet pressure is equal to the evaporator outlet pressure. However, there are temperature and pressure differences between the throttle valve inlet and the evaporator outlet at the ORC setup at BURET laboratory. The reason is that pipes are too long to be neglected. When pipes are long, heat and pressure losses in pipes become considerable. Therefore, to develop an accurate dynamic model, heat and pressure losses in pipes are considered for the ORC setup at BURET laboratory. As it is mentioned in the introduction chapter, considering heat and pressure loss in pipes is the contribution of this study to literature.

In Figure 4.22, the general structure of the pipe model is shown.

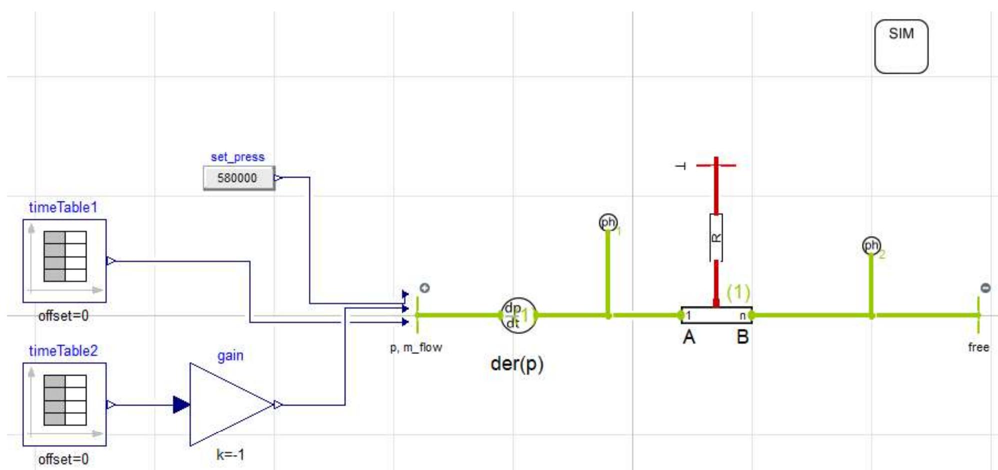

Figure 4.22. General structure of pipe tester.

The tube AB in Figure 4.22 represents the pipe itself. It has an inner radius, an outer radius and length. Thermal resistance shown with ‘R’ is used to consider the convection heat transfer between pipe surface and the environment. Air side convection heat transfer coefficient is taken from the literature. Pipe model also includes conduction and convection inside the pipe. Lastly, the pipe model considers friction inside and model calculates pressure losses.

Inputs for the pipe tester are listed below:

- Inner diameter of the pipe,
- Thickness of the pipe,
- Length of the pipe,
- Ambient temperature,
- R value which is equal to 1/hA where h is convective heat transfer coefficient, between environment and pipe's outer surface and A is pipe's outer surface area,
- Mass flowrate of liquid or gas inside the pipe,
- Inlet temperature of the pipe,
- Inlet pressure of the pipe.

There are two outputs for pipe tester: the first output is the pipe outlet temperature, and the second output is the pipe outlet pressure.

There are two pipe testers: The first one is for pipes which have vapor flow inside and the second one is for pipes that have liquid flow inside. The first tester is named 'gas pipe tester' and the second one is named 'liquid pipe tester'. After testers are created, the calculated values and measured ones in the experiments are compared.

Correlations used in pipe testers are given below

$$\dot{Q}_{flow} = \frac{\Delta T}{R_{th}} \tag{4.23}$$

where R_{th} is the thermal resistance given by

$$R_{th} = \frac{\ln{(D_o/D_i)}}{2\pi\lambda L} + \frac{1}{hA}. \tag{4.24}$$

L is the length of the pipe, λ is heat conductivity, D_o is the outer diameter of the pipe, D_i is the inner diameter of the pipe, A is pipe's outer surface area, and ΔT is temperature difference between the environment, and the fluid flowing inside the pipe.

Figure 4.23 shows the outlet temperature of gas pipe tester. Maximum temperature difference is less than 0.7 ℃.

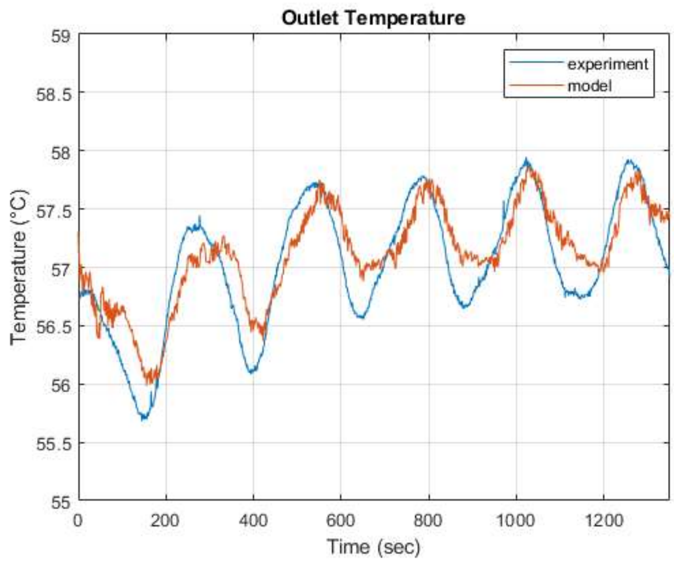

Figure 4.23. Pipe outlet temperature for gas pipe tester.

Konakov correlations [26] are used to model pressure drop in pipes. The correlation is as follows

$$\Delta P = \delta \left(\frac{\rho}{2}\right) v^2 \tag{4.25}$$

where v is velocity of fluid and δ is defined as

$$\delta = \gamma \frac{L}{d_h} \tag{4.26}$$

for laminar flow, Re < 2300

$$\gamma = \frac{64}{Re} \tag{4.27}$$

for turbulent flow, 2300 < Re < 10^7

$$\gamma = (1.8\, ln(Re) - 1.5)^{-2}\,. \tag{4.28}$$

Figure 4.24 shows the comparison of the measured and calculated outlet pressure of gas pipe tester. Maximum pressure difference is less than 10 percent.

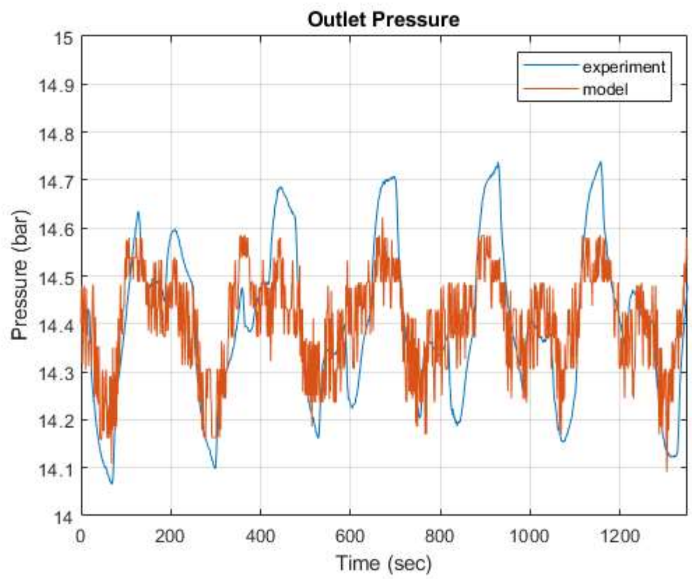

Figure 4.24. Pipe outlet pressure for gas pipe tester.

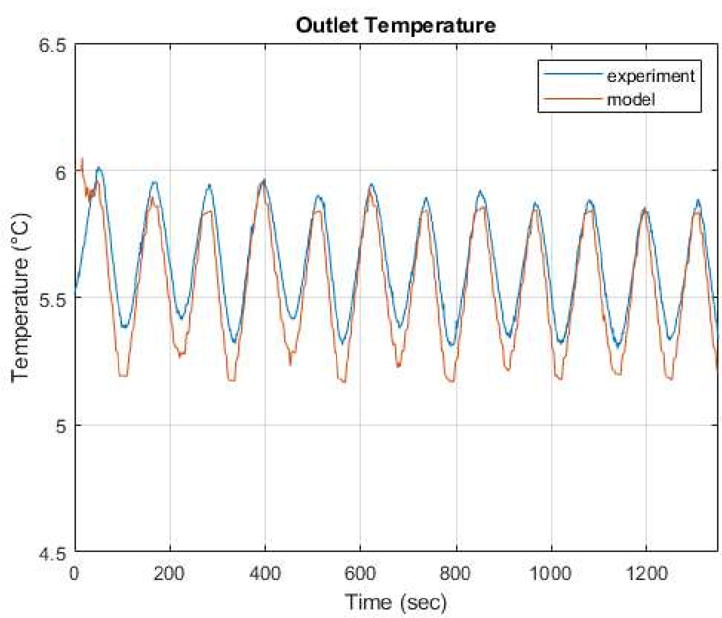

Figure 4.25. Pipe outlet temperature for liquid pipe tester.

Figure 4.25 shows the outlet temperature of liquid pipe tester. Maximum temperature difference is less than 0.3 °C.

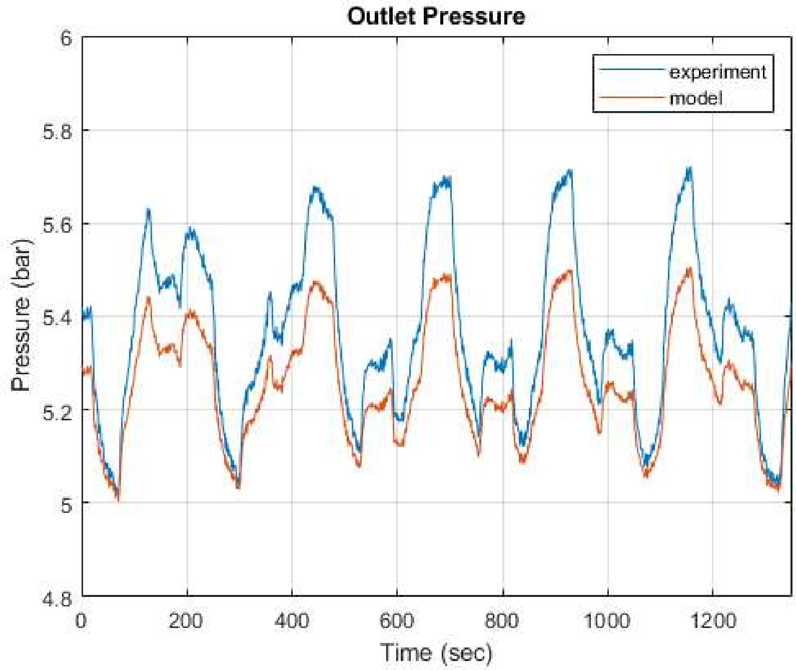

Figure 4.26. Pipe outlet pressure for liquid pipe tester.

Figure 4.26 shows the outlet pressure of liquid pipe tester. Maximum pressure difference is less than 8 percent.

As differences between model and experiment are small enough, both gas pipe model and liquid pipe model can be used in whole ORC model safely.

4.5. Working Fluid Pump

Working fluid of the ORC setup at BURET is R134a. There is a side channel pump to circulate the working fluid. Pump curve is taken from the manufacturer. Pump curve data are used to create a pump model. The aim of pump tester is getting similar pressure and temperature values for pump outlet for certain inlet conditions. General structure of pump tester is shown in Figure 4.27.

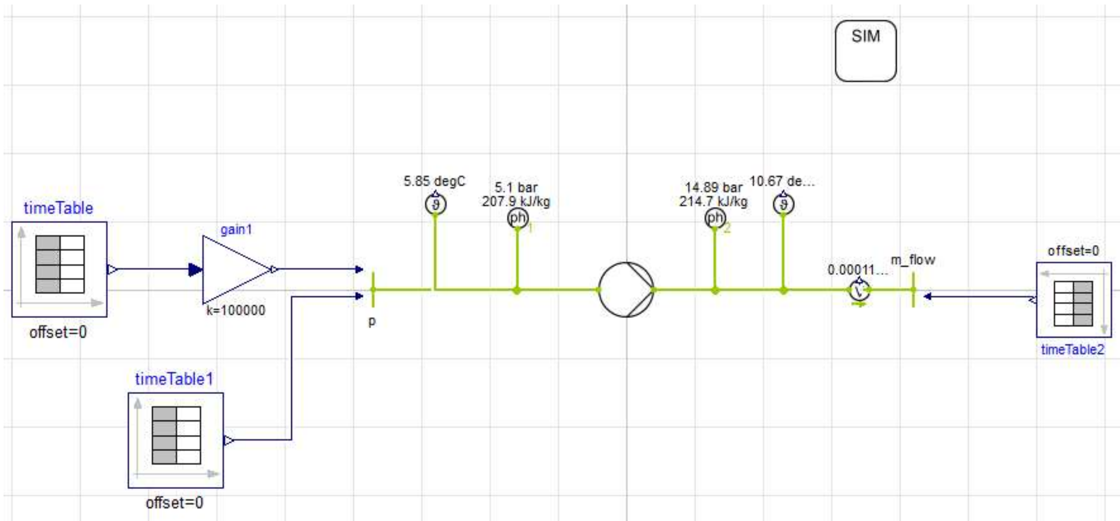

Figure 4.27. General structure of pump tester.

Correlations used in the pump model are given below.

Pump curve is almost a parabola. Therefore, it can be expressed with a second order equation

$$\Delta P = aQ^2 + bQ + c \tag{4.29}$$

where ΔP (bar) is pressure difference between pump outlet and inlet, Q (m^3/h) is the pump flowrate, a, b, and c are constants. These constants are found by a curve fitting process to the pump curve data given by the manufacturer. Pump curve is defined in the Dymola software by the user. In Figure 4.28, the pump curve information input for pump tester is given.

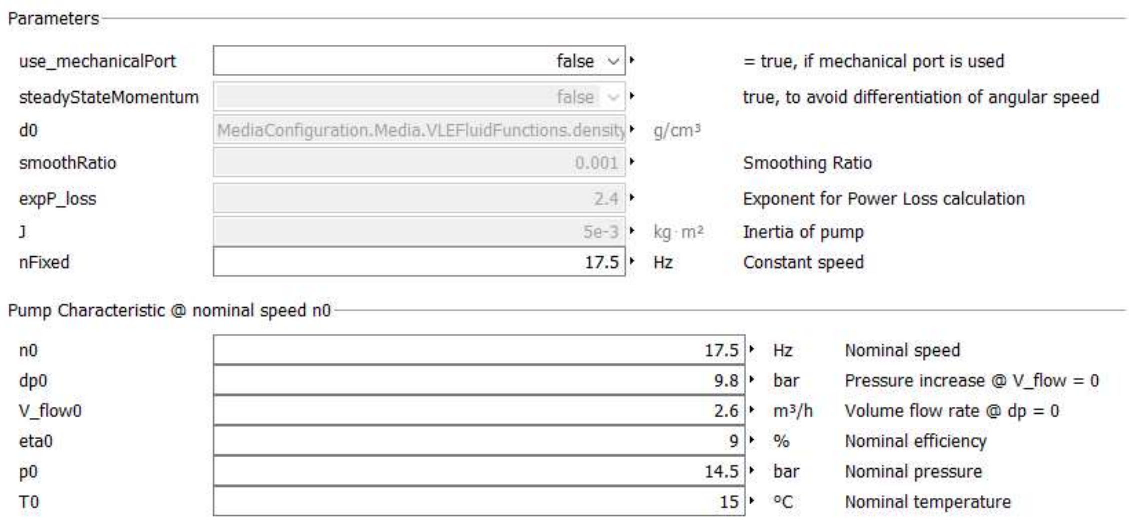

Figure 4.28. User inputs to define pump curve.

- nFixed is pump speed,
- n0 is nominal speed; nominal speed is the speed of pump where pump curve is sketched by manufacturer. To have consistent model results, pump is operated at speeds given in manufacturer's pump curve. Pump speeds for known pump curves are 1050 rpm, 1150 rpm, 1250 rpm, 1350 rpm, and 1450 rpm; the curve for 1050 rpm is used.
- dp0 is pressure increase at zero flowrate on pump curve,
- V_flow0 is volumetric flowrate at zero pressure difference on pump curve,
- p0 is nominal pressure which is working pressure of the pump,
- T0 is nominal temperature.

Temperature difference between the pump outlet and inlet is calculated by using the pump power loss which is given by

$$P_{loss} = \dot{m}_{wf} C_{p,wf} \Delta T \tag{4.30}$$

where ΔT is temperature difference between pump outlet, inlet, $C_{p,wf}$ is specific heat of the working fluid, and $\dot{m}_{wf}$ is mass flowrate of the working fluid. Frictional losses associated with pump calculated with equation 4.29 are observed to be around 1 kW in the experiments. P_{loss} is taken as 1 kW.

An experiment is done to check correctness of the dynamic pump model. In Figure 4.29, pump outlet pressure for model and experiment is shown.

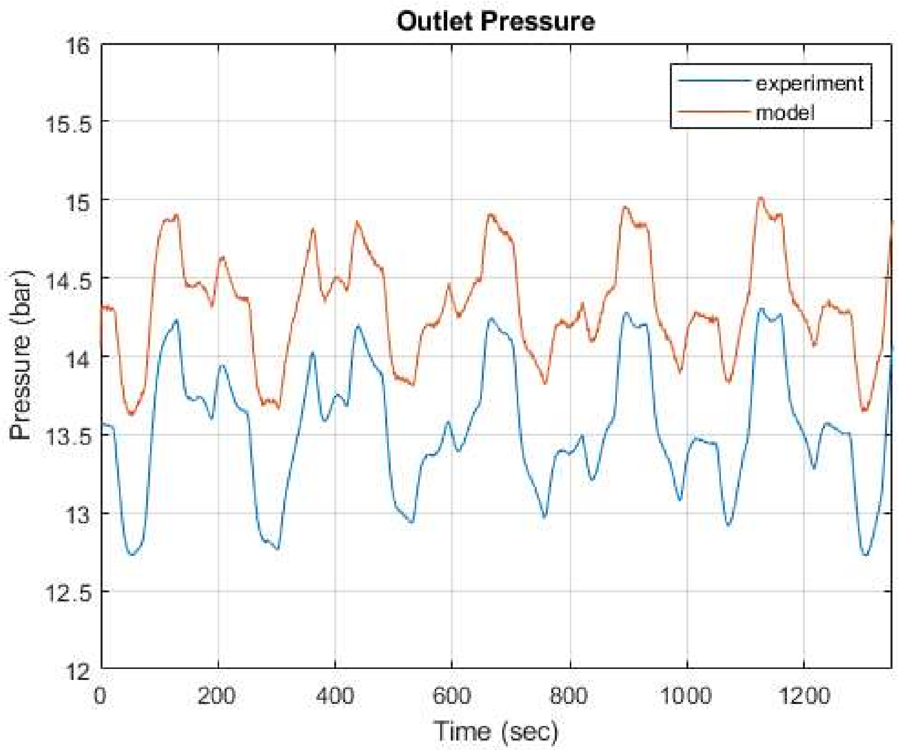

Figure 4.29. Pump outlet pressure.

Pressure difference between model and experiment is below 10 percent. Therefore, pump model is working correctly and can be used in ORC model safely. In Figure 4.30, comparison of calculated and measured pump outlet temperature values is shown.

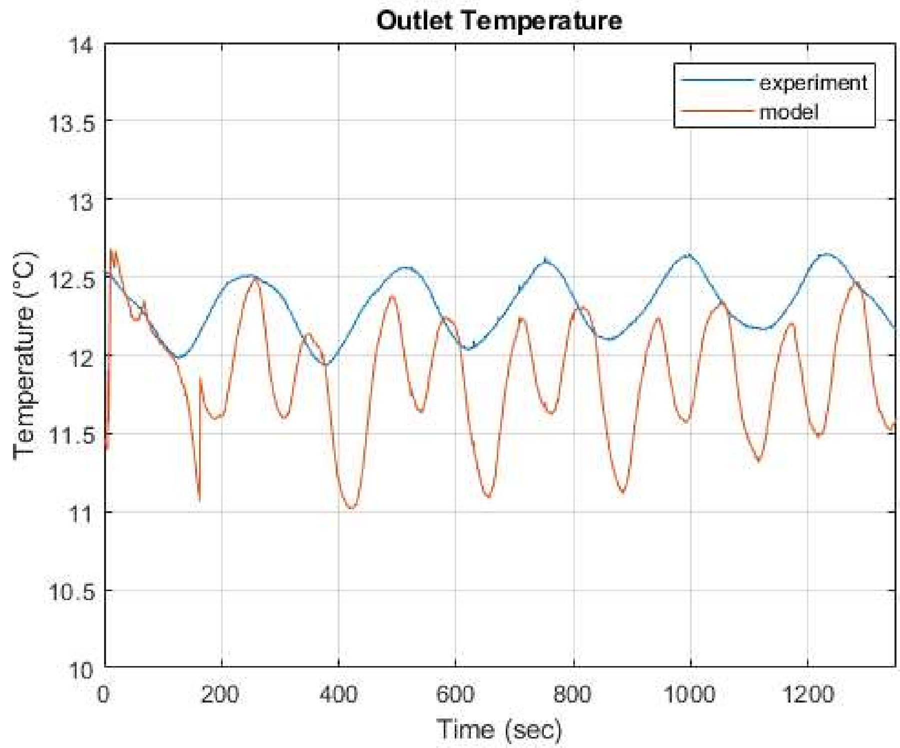

Figure 4.30. Pump outlet temperature.

Temperature difference between model and experiment is below 1.5 °C. Therefore, pump model simulates the real pump accurately. Therefore, pump model can be used in whole ORC model.

There are two peaks in dynamic model but there is one peak in experimental data. The temperature difference between pump outlet and inlet is inversely proportional to mass flowrate when the frictional loss is constant as it is assumed in this thesis based on experimental observations. Mass flowrate has two peaks as shown in Figure 4.19. Therefore, the calculated pump outlet temperature follows the mass flowrate behavior and has two peaks.

4.6. The Complete Model for the ORC

After all component testers are validated with experimental data, components are assembled, and the final ORC model is created. In Figure 4.31, general view of whole ORC model is shown.

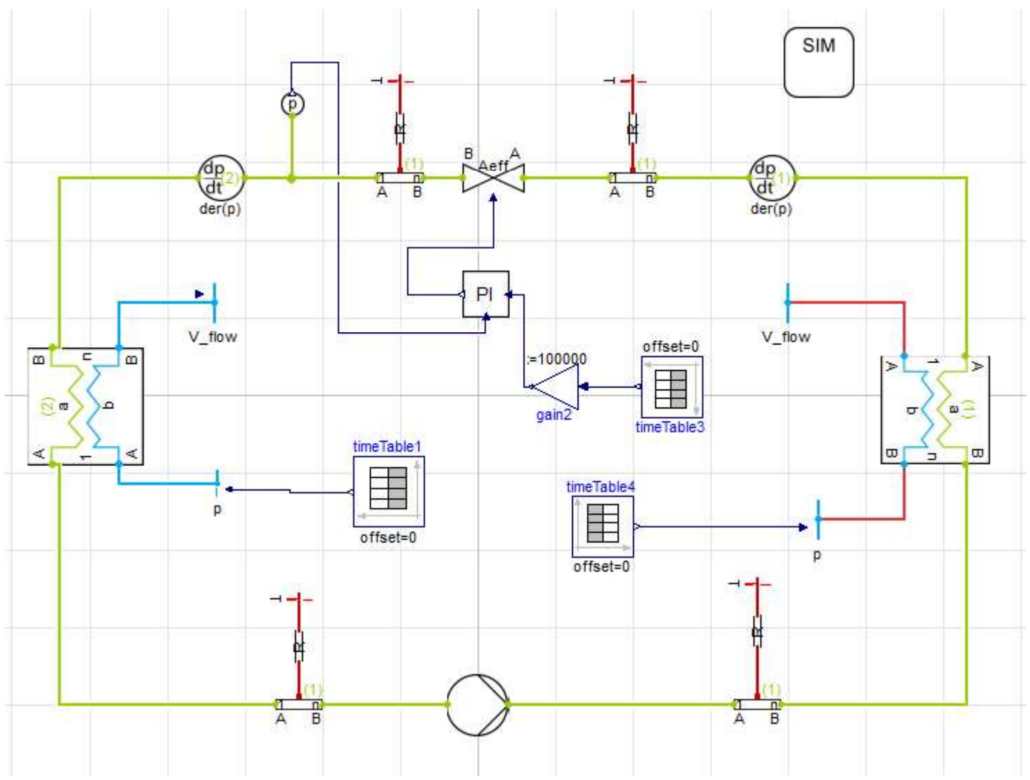

Figure 4.31. General view of whole ORC model.

After the final model is obtained, experiments carried out, and experimental results and simulation results are compared. Comparison results are discussed in the Results and Discussion chapter.

5. RESULTS AND DISCUSSIONS

A transient ORC cycle experiment is carried out to verify the dynamic model as a whole. The ORC is operated for more than 5 hours, to be exact 19000 seconds. During the operation the conditions are changed in seven steps; the conditions that are kept constant are shown in Table 5.1. Only changing experimental input is the evaporator oil set temperature.

Table 5.1. Experimental parameters.

Experiment Parameter	Value and Unit
Working fluid pump speed	1050 rpm
Ambient temperature	15 °C
Hot oil pump speed	40 Hz
Throttle valve outlet pressure set value	5.80 bar
Chiller cold water set value	4 °C
Chiller cold water flowrate	8.6 m^3/h

The throttle valve outlet pressure set value, chiller cold water set value, chiller cold water flowrate values are unchanging inputs for the experiment. However, because they fluctuate a little these fluctuations are considered while giving inputs to the dynamic model.

Flowrate, temperature, and pressure set values change during the experiment. For example, hot oil set temperature is a constant value, but hot oil inlet temperature is not a constant in time it is a dynamic input. It can be seen in Figure 4.4. The reason is the working principle of oil heater unit. When user enters a set value to oil heater unit, oil heater unit heats the oil until it reaches a temperature (T_{max}) little more than set value (T_{set}) and stops. Then hot oil temperature decreases due to heat loss to environment. When hot oil temperature reaches a temperature (T_{min}) value which is little less than set value, oil heater unit starts to heat hot oil to T_{max}, then stops again. Cycle goes on based on this principle. Briefly, hot oil temperature fluctuates between T_{min} and T_{max}. Where $T_{min} < T_{set} < T_{max}$. For example, in Figure 4.4, hot oil set temperature is 80 °C, but oil temperature fluctuates between 83.5 °C and 75.5 °C. In this case, T_{set} is 80 °C, T_{min} is 75.5 °C, and T_{max} is 83.5 °C.

In the first step of experiment, the oil heater is set to 80 °C. Data are recorded for approximately 24 minutes. Then step 2 is started.

In step 2, the oil heater set value is changed to 110 °C. Data are recorded for approximately 40 minutes. Then step 3 is started.

In step 3, the oil heater set value is changed back to 80 °C. The aim is to see the repeatability of the experiment and to determine whether experimental outputs come back to previous values or not. Nearly 15 minutes passed during the cooling time of oil heater from 110 °C to 80 °C because the oil is cooled down by only air. Data are recorded for approximately 54 minutes. Then step 4 is started.

In step 4, the oil heater set value is changed to 100 °C. Data are recorded for approximately 51 minutes. Then step 5 is started.

In step 5, the oil heater set value is changed back to 80 °C. Data are recorded for approximately 58 minutes. Then step 6 is started.

In step 6, the oil heater set value is changed to 90 °C. Data are recorded for approximately 52 minutes. Then step 5 is started.

In step 7, the oil heater set value is changed back to 80 °C. Data are recorded for approximately 38 minutes. Then the experiment is completed.

Changes in hot oil set temperature are shown in Table 5.2. Total experiment time is 317 minutes which is nearly 19000 seconds.

Table 5.2. Change in hot oil set temperature.

Step Number	Hot Oil Set Temperature	Time Interval (minutes)	Duration (minutes)
1	80 °C	0-24	24
2	110 °C	24-64	40
3	80 °C	64-118	54
4	100 °C	118-169	51
5	80 °C	169-227	58
6	90 °C	227-279	52
7	80 °C	279-317	38

The results of the dynamic model and those of the experiment are compared for the following:

- Evaporator R134a outlet and inlet pressures vs time
- Evaporator R134a outlet and inlet temperatures vs time
- Evaporator hot oil outlet temperature vs time
- Condenser R134a outlet and inlet pressures vs time
- Condenser R134a outlet and inlet temperatures vs time
- Condenser cold water outlet temperatures vs time
- Throttle valve outlet and inlet temperatures vs time
- Throttle valve inlet pressure vs time
- Working fluid pump outlet and inlet pressures vs time
- Working fluid pump outlet and inlet temperatures vs time
- R134a mass flowrate vs time

The comparison of model and experiment results is made for a total of 19000 seconds. Therefore, it is not easy to show all details in one plot. Comparison results will be given in 4 separate plots for the following time periods:

- Step 1-2: 0-4200 seconds,
- Step 3-4: 4200-10200 seconds,
- Step 5-6: 10200-16700 seconds,
- Step 6-7: 13700-19000 seconds.

Before the comparisons, inputs of experiment are shown in the figures below. In Figure 5.1, evaporator oil inlet temperature is shown.

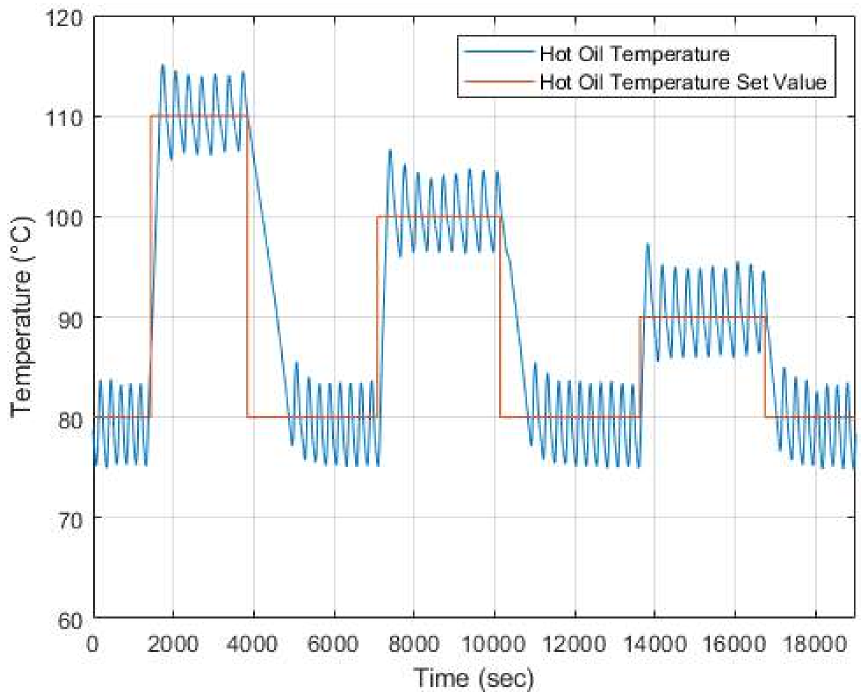

Figure 5.1. Evaporator oil inlet temperature.

Evaporator oil inlet temperature is fluctuating between T_{min} and T_{max} for certain T_{set} values. when T_{set} is 80 °C, temperature fluctuates between 83.5 °C and 75.5 °C, when T_{set} is 90 °C, temperature fluctuates between 95 °C and 87 °C, when T_{set} is 100 °C, temperature fluctuates between 105 °C and 97 °C, when T_{set} is 110 °C, temperature fluctuates between 115 °C and 105 °C. The reason of fluctuation is explained in the beginning of the chapter.

In Figure 5.2, evaporator oil flowrate is shown. Oil flowrate is almost constant, and it is nearly 4.6 m^3/h.

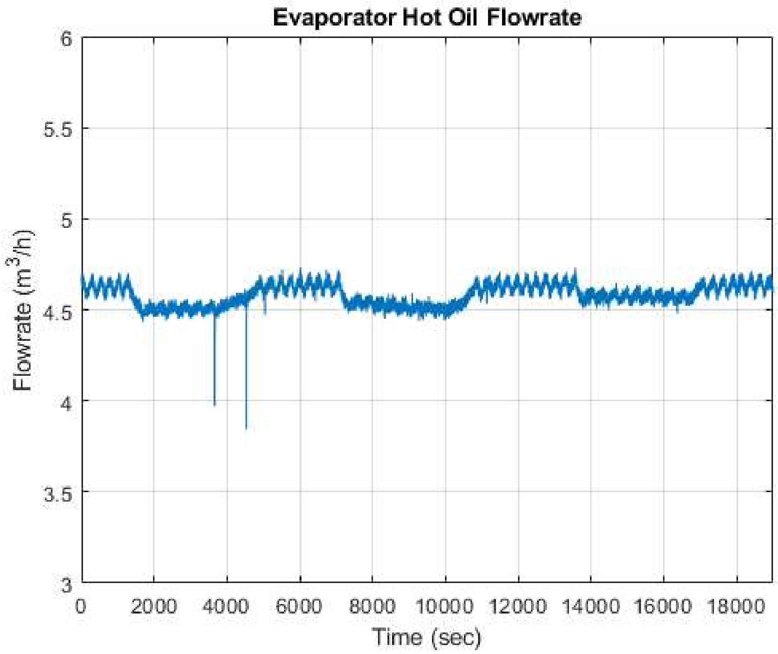

Figure 5.2. Evaporator hot oil flowrate.

In Figure 5.3, condenser water inlet temperature is shown. Water inlet temperature is fluctuating around chiller cold water set value.

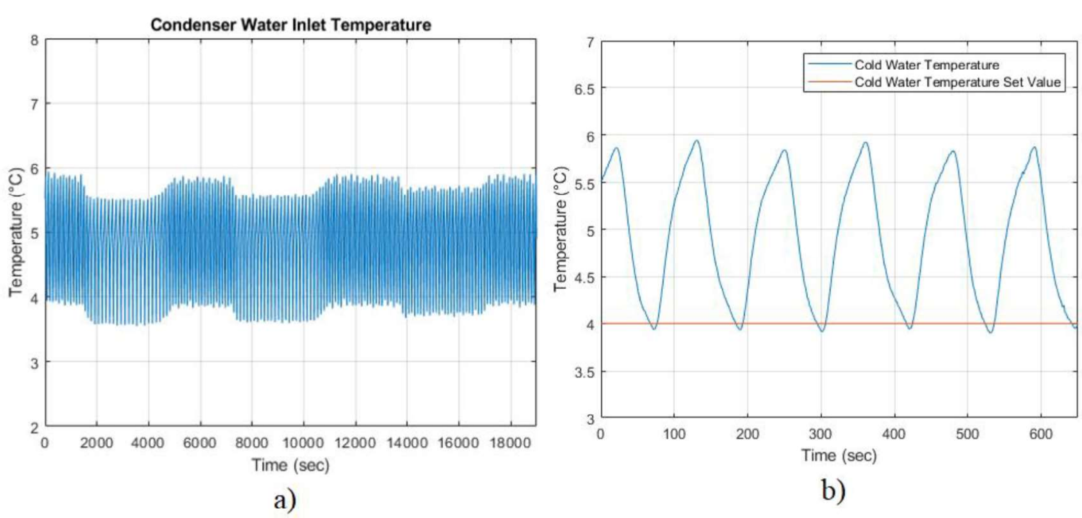

Figure 5.3. Condenser water inlet temperature.

In Figure 5.4, condenser cold water flowrate is shown. Flowrate is almost constant, and it is nearly 8.6 m^3/h.

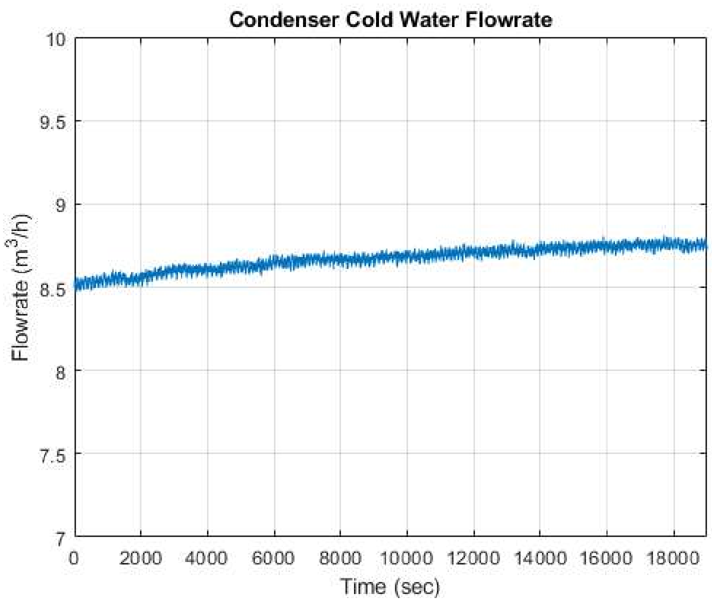

Figure 5.4. Condenser cold water flowrate.

In Figure 5.5, throttle valve outlet pressure is shown. Outlet pressure fluctuates around the throttle valve outlet pressure set value.

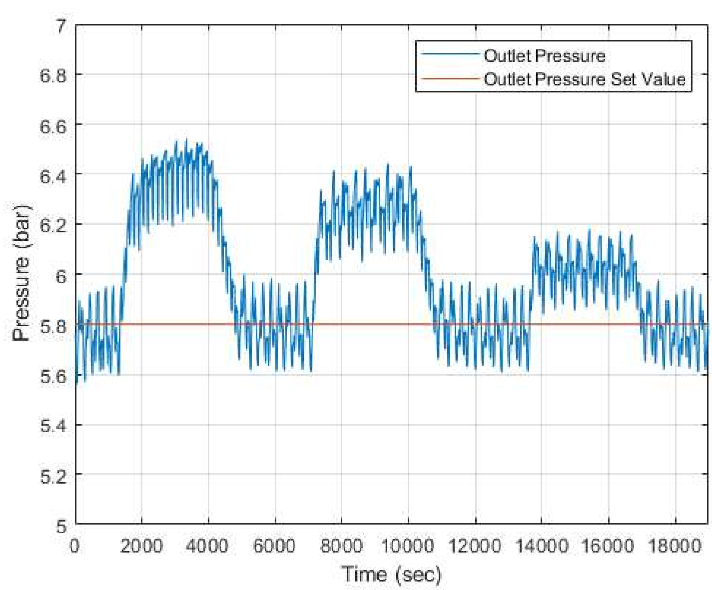

Figure 5.5. Throttle valve outlet pressure.

5.1. Evaporator Results

In this part, the evaporator R134a outlet temperature, the hot oil outlet temperature, R134a inlet temperature, R134a outlet pressure, and R134a inlet pressure values measured in the experiment and calculated with the model are compared.

In Figure 5.6, evaporator R134a outlet temperature for Step 1-2 is shown.

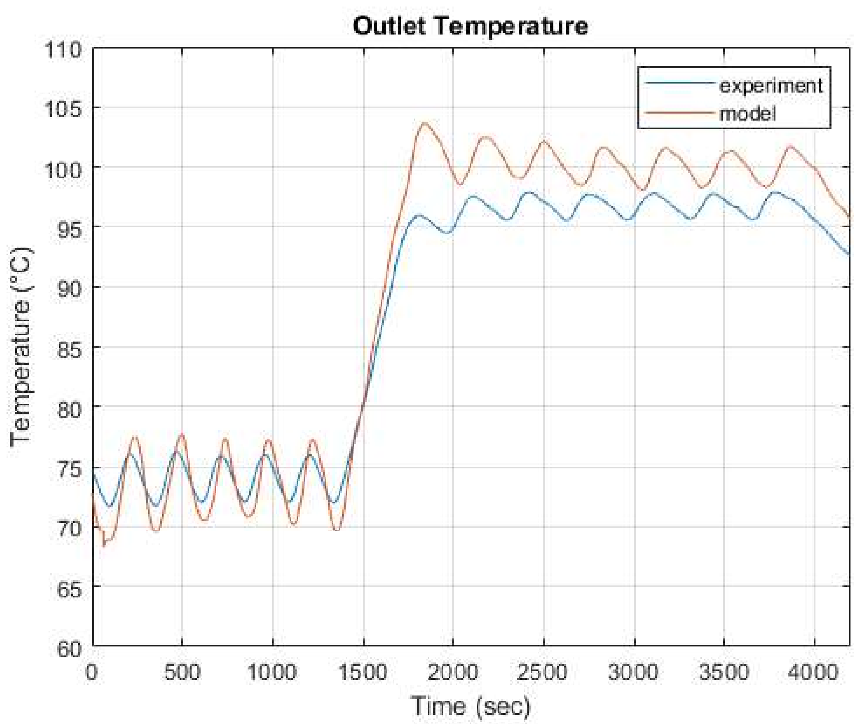

Figure 5.6. Evaporator R134a outlet temperature for Step 1-2.

In Figure 5.7, evaporator R134a outlet temperature for Step 3-4 is shown.

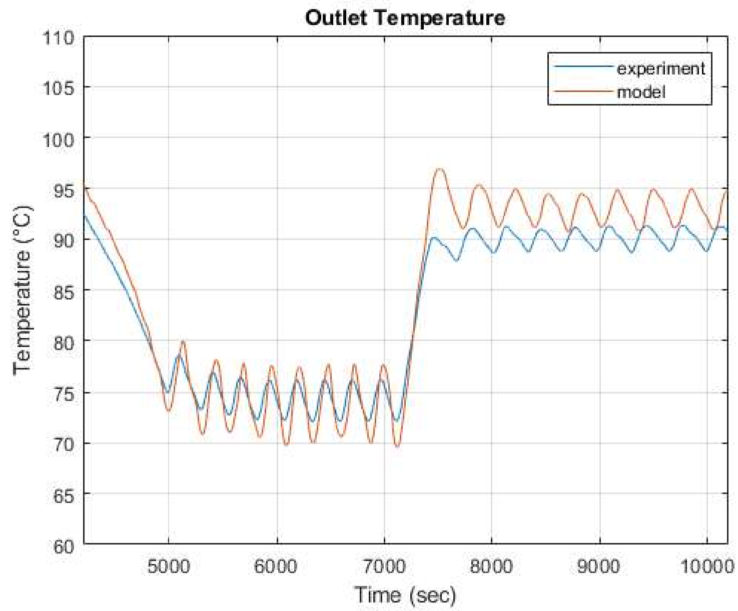

Figure 5.7. Evaporator R134a outlet temperature for Step 3-4.

In Figure 5.8, evaporator R134a outlet temperature for Step 5-6 is shown.

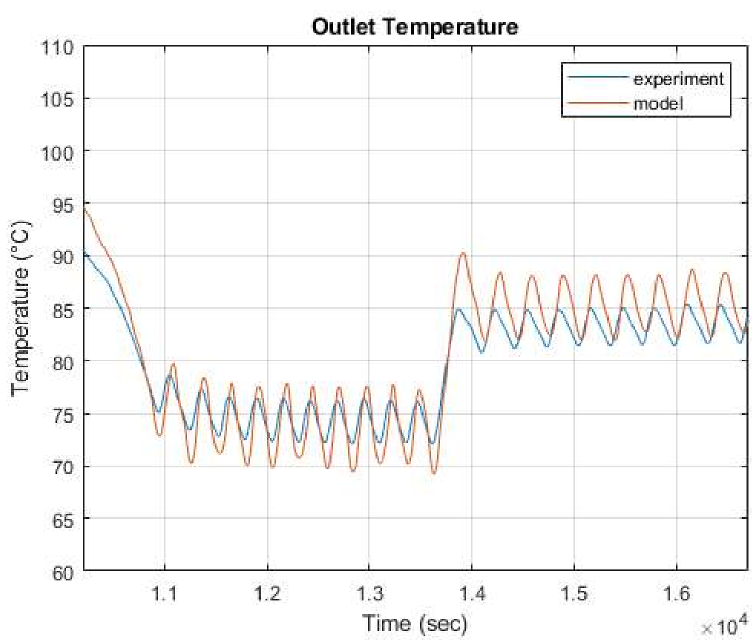

Figure 5.8. Evaporator R134a outlet temperature for Step 5-6.

In Figure 5.9, evaporator R134a outlet temperature for Step 6-7 is shown.

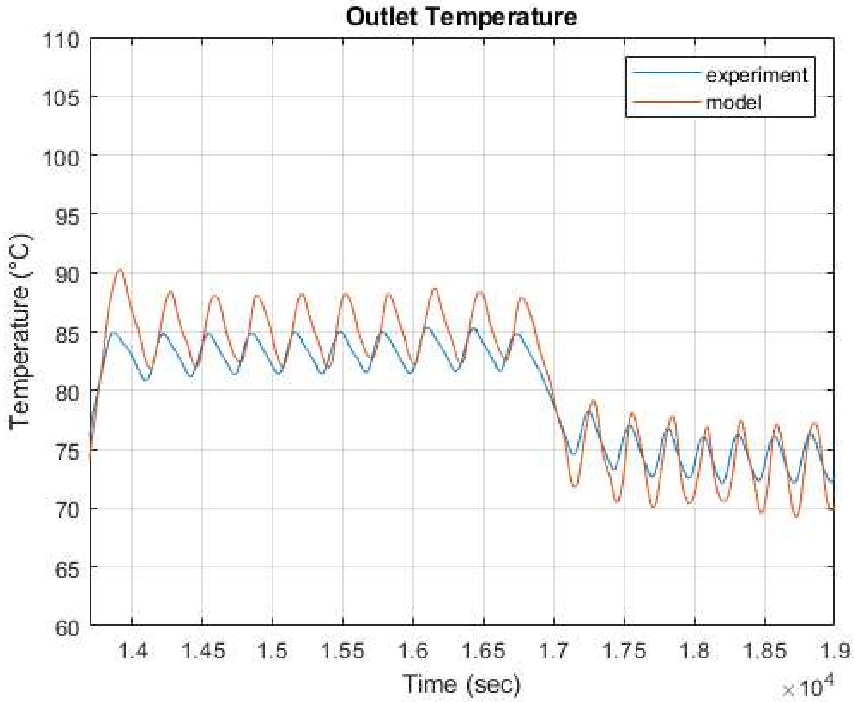

Figure 5.9. Evaporator R134a outlet temperature for Step 6-7.

Figure 5.6. – Figure 5.9. show the evaporator R134a outlet temperature. In these 4 figures, maximum temperature difference for R134a outlet temperature between model and experiment is less than 5.5 °C. Temperature difference increase in steps for which hot oil temperature is increased. When hot oil temperature decreases, difference between model and experiment gets smaller. The reason is that, when hot oil temperature gets higher, system temperature and pressure values increase. Accuracy and sensitivity of correlations used for heat transfer and pressure drop decreases. The other reason is that R134a mass flowrate fluctuations increase when temperature and pressure values increase. However, even difference between model and experiment increases when hot oil temperature increases, the difference between model and experiment is acceptable and better than most of studies in the literature.

In Figure 5.10, evaporator hot oil outlet temperature for Step 1-2 is shown.

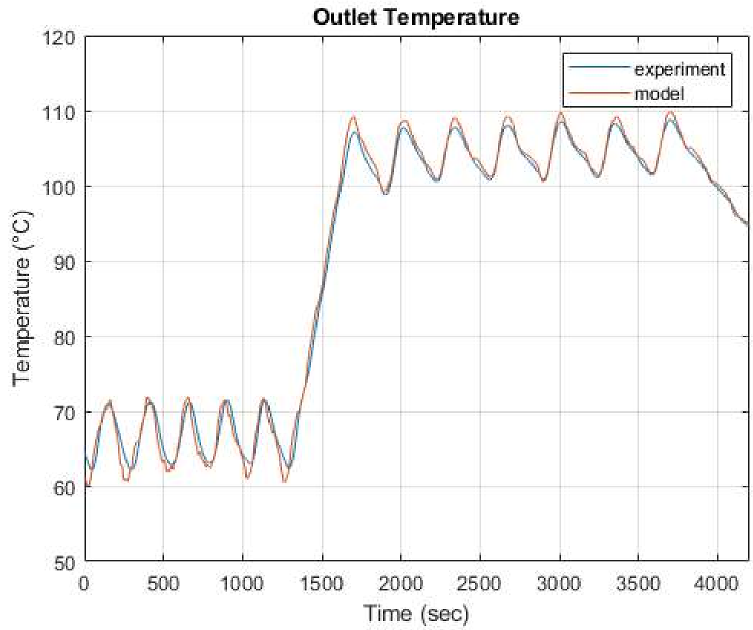

Figure 5.10. Evaporator hot oil outlet temperature for Step 1-2.

In Figure 5.11, evaporator hot oil outlet temperature for Step 3-4 is shown.

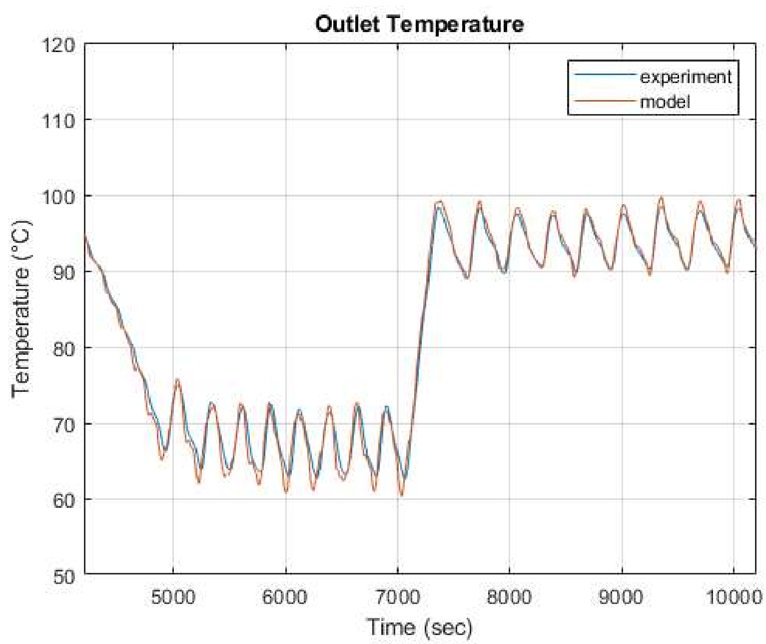

Figure 5.11. Evaporator hot oil outlet temperature for Step 3-4.

In Figure 5.12, evaporator hot oil outlet temperature for Step 5-6 is shown.

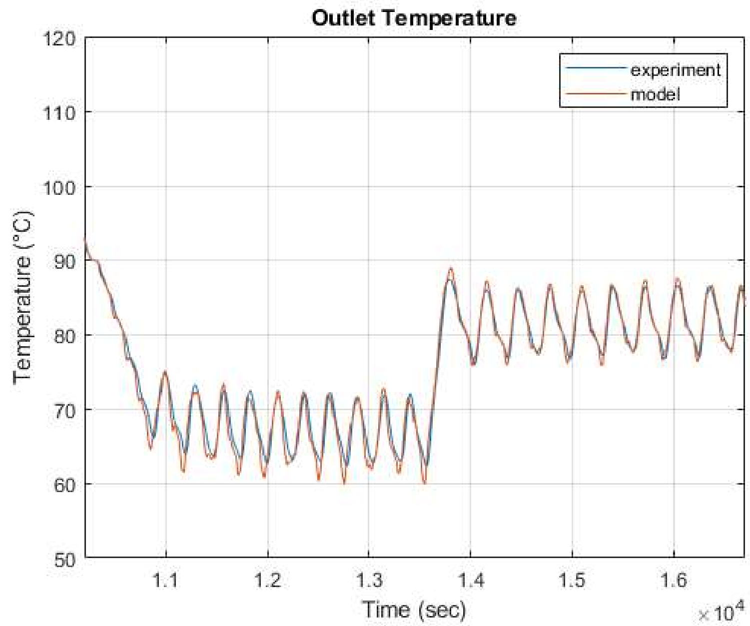

Figure 5.12. Evaporator hot oil outlet temperature for Step 5-6.

In Figure 5.13, evaporator hot oil outlet temperature for Step 6-7 is shown.

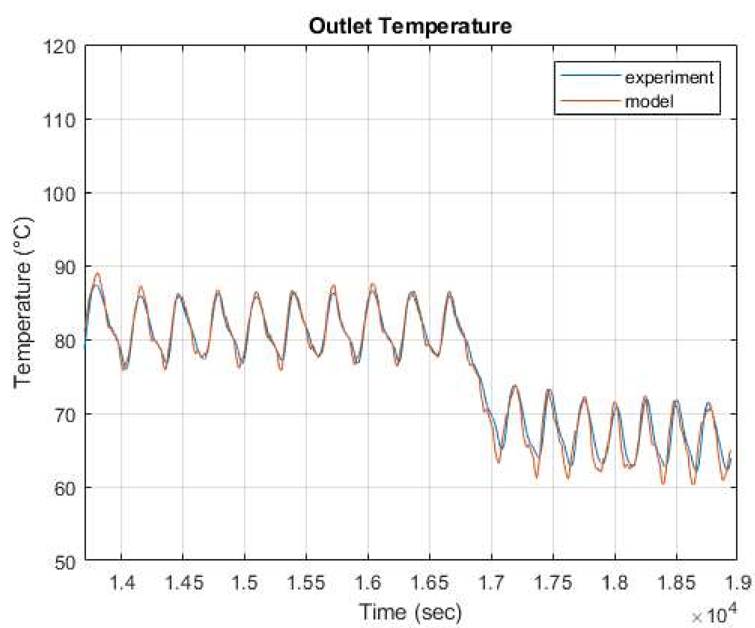

Figure 5.13. Evaporator hot oil outlet temperature for Step 6-7.

Figure 5.10. – Figure 5.13. show the evaporator hot oil outlet temperature. In these 4 figures, maximum difference between the model and the experiment is less than 1 °C. In Figure 5.14, evaporator R134a inlet temperature for Step 1-2 is shown.

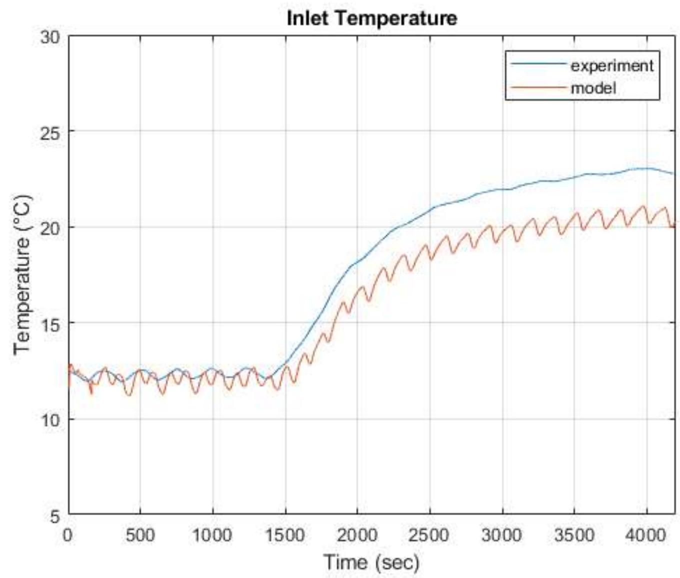

Figure 5.14. Evaporator R134a inlet temperature for Step 1-2.

In Figure 5.15, evaporator R134a inlet temperature for Step 3-4 is shown.

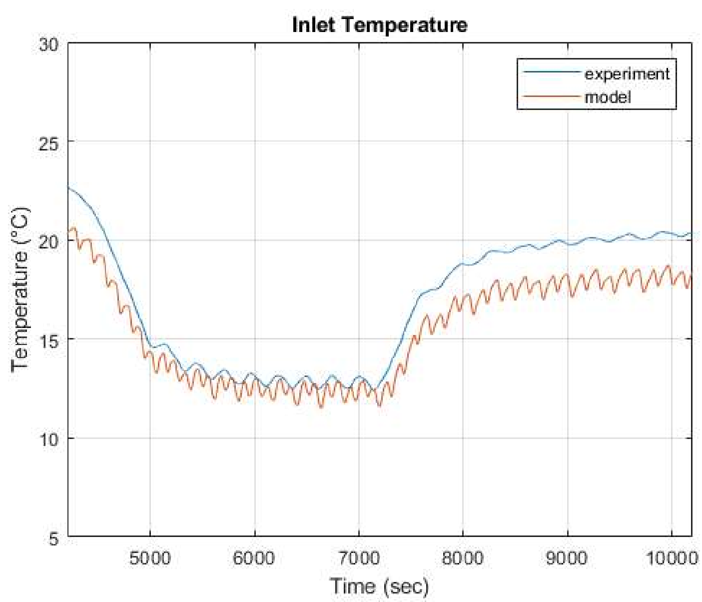

Figure 5.15. Evaporator R134a inlet temperature for Step 3-4.

In Figure 5.16, evaporator R134a inlet temperature for Step 5-6 is shown.

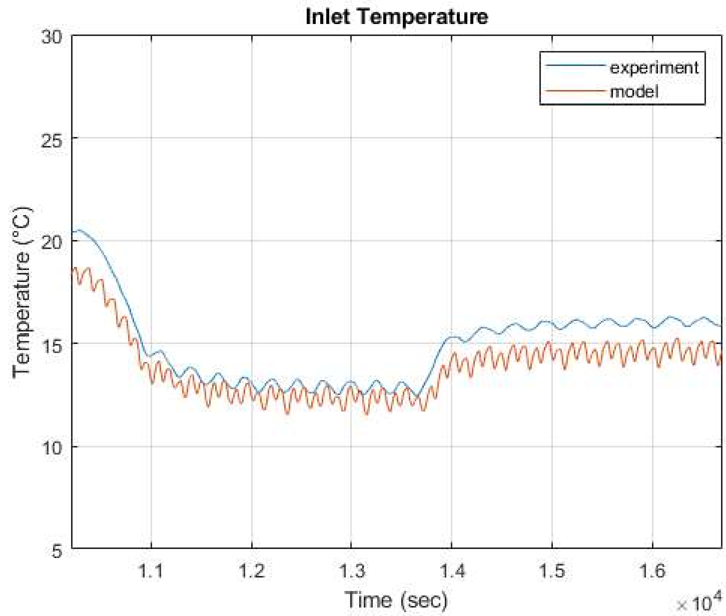

Figure 5.16. Evaporator R134a inlet temperature for Step 5-6.

In Figure 5.17, evaporator R134a inlet temperature for Step 6-7 is shown.

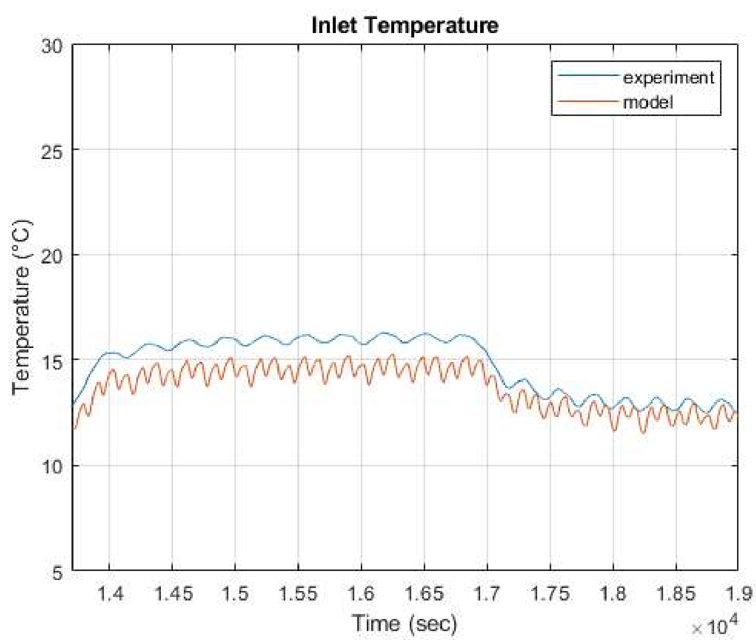

Figure 5.17. Evaporator R134a inlet temperature for Step 6-7.

Figure 5.14. – Figure 5.17. show the evaporator R134a inlet temperature. In these 4 figures, maximum difference between the model and the experiment is less than 3 °C. In Figure 5.18, evaporator R134a outlet pressure for Step 1-2 is shown.

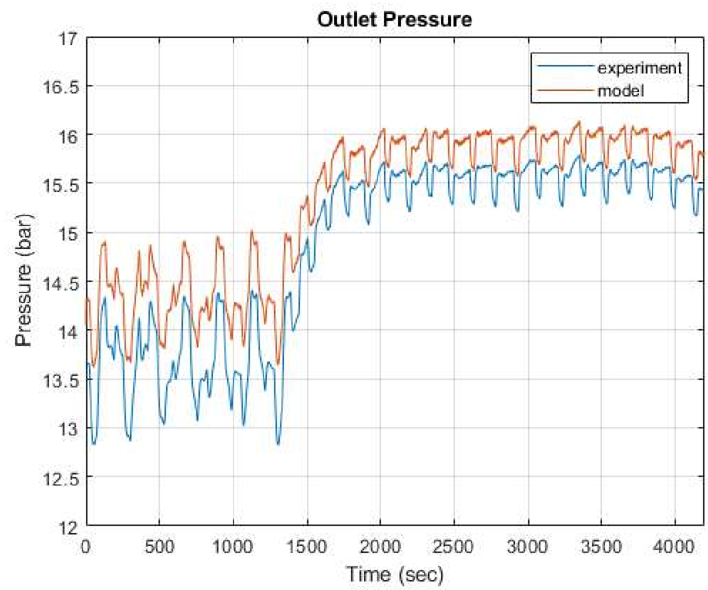

Figure 5.18. Evaporator R134a outlet pressure for Step 1-2.

In Figure 5.19, evaporator R134a outlet pressure for Step 3-4 is shown.

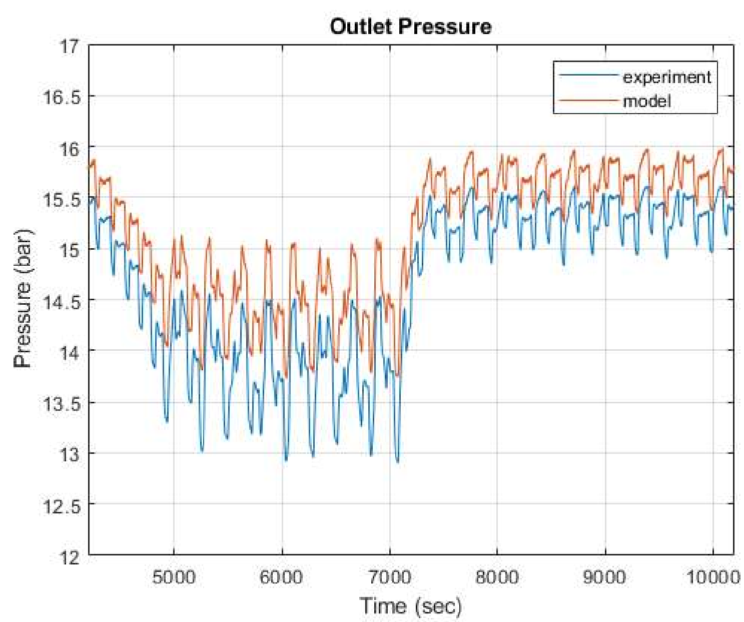

Figure 5.19. Evaporator R134a outlet pressure for Step 3-4.

In Figure 5.20, evaporator R134a outlet pressure for Step 5-6 is shown.

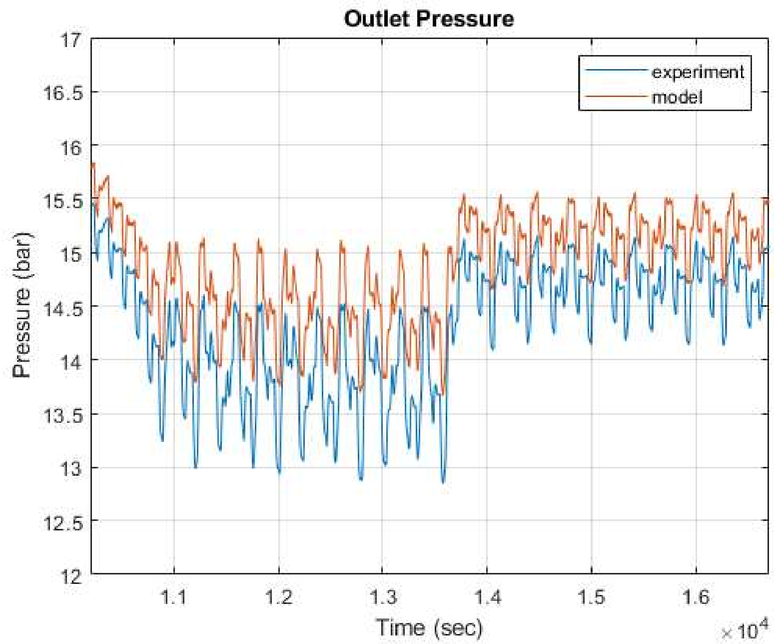

Figure 5.20. Evaporator R134a outlet pressure for Step 5-6.

In Figure 5.21, evaporator R134a outlet pressure for Step 6-7 is shown.

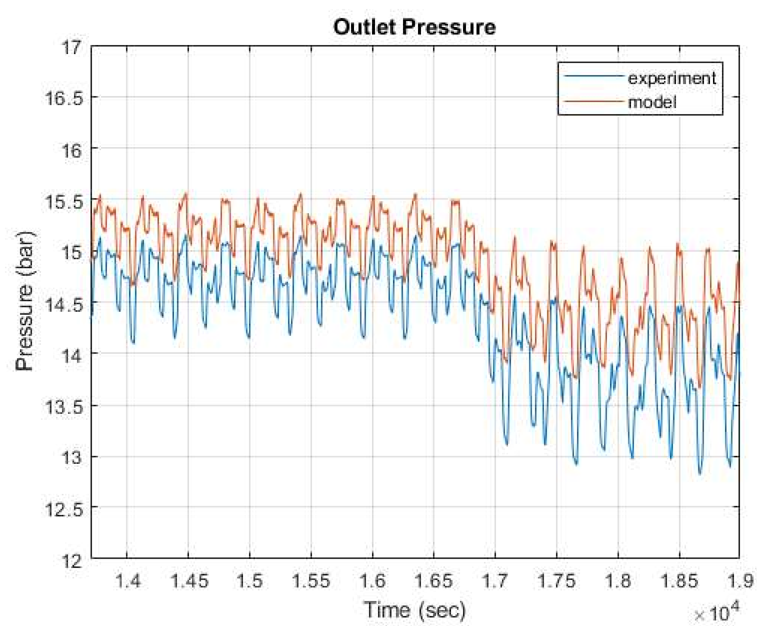

Figure 5.21. Evaporator R134a outlet pressure for Step 6-7.

Figure 5.18. – Figure 5.21. show the evaporator R134a outlet pressure. In these 4 figures, maximum pressure difference between the model and the experiment is less than 10 percent. In Figure 5.22, evaporator R134a inlet pressure for Step 1-2 is shown.

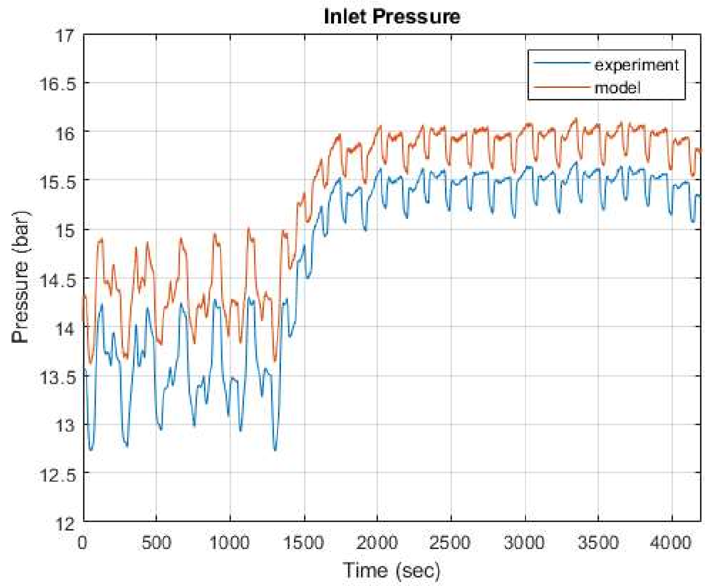

Figure 5.22. Evaporator R134a inlet pressure for Step 1-2.

Figure 5.23, evaporator R134a inlet pressure for Step 3-4 is shown.

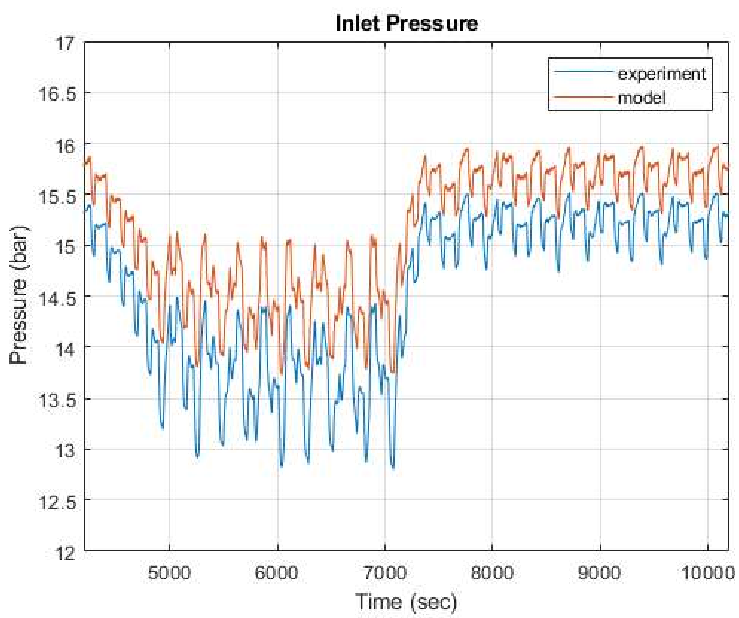

Figure 5.23. Evaporator R134a inlet pressure for Step 3-4.

Figure 5.24, evaporator R134a inlet pressure for Step 5-6 is shown.

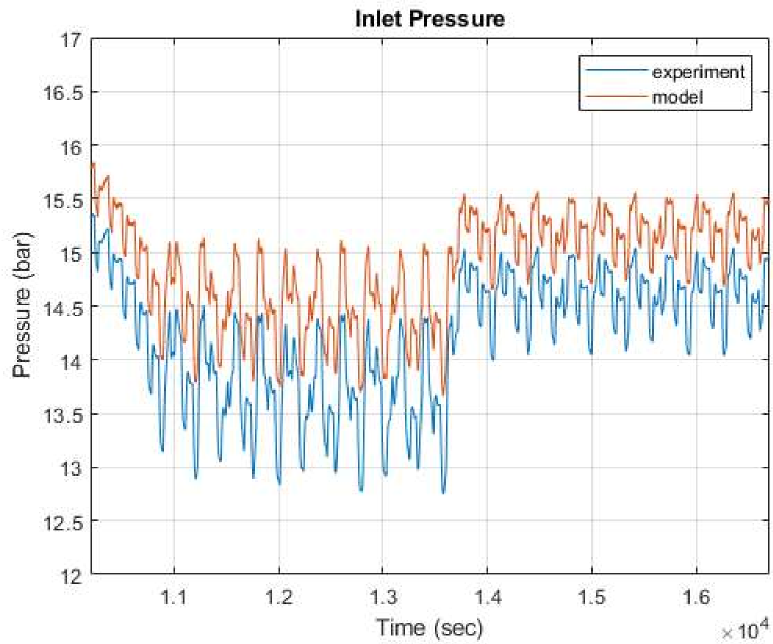

Figure 5.24. Evaporator R134a inlet pressure for Step 5-6.

Figure 5.25, evaporator R134a inlet pressure for Step 6-7 is shown.

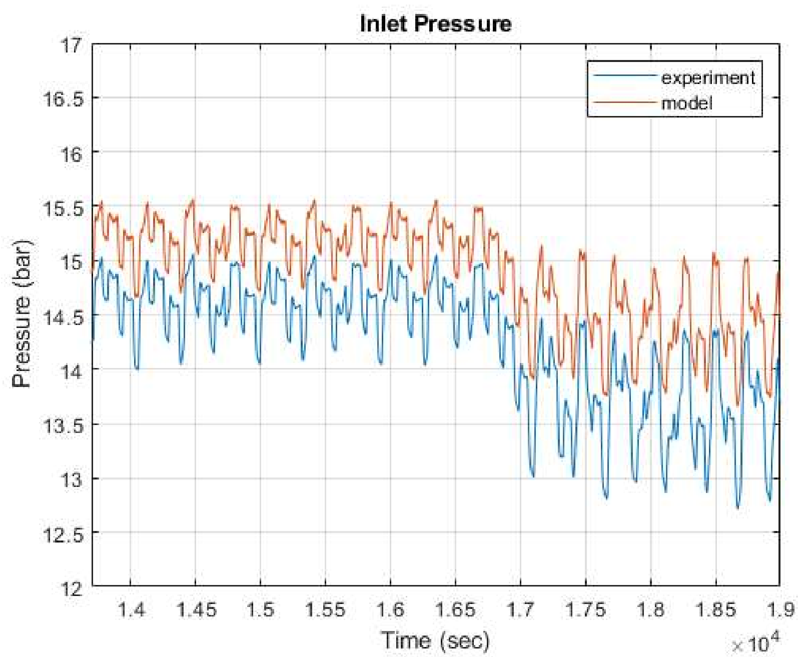

Figure 5.25. Evaporator R134a inlet pressure for Step 6-7.

Figure 5.22. – Figure 5.25. show the evaporator R134a inlet pressure. In these 4 figures, maximum pressure difference between the model and the experiment is less than 10 percent. From figures given above, evaporator inlet and outlet pressure values almost do not show any difference between the model and experiment.

In experiments, it is observed that inlet and outlet temperature for evaporator are almost equal. Pressure difference is about 0.1 bar. Therefore, a pressure drop correlation is not added to evaporator model. The aim is to decrease computational cost and simulation time.

5.2. Condenser Results

In this part, condenser R134a outlet temperature, condenser water outlet temperature, condenser R134a inlet temperature, condenser R134a outlet pressure, and condenser R134a inlet pressure values for both experiment and model are shown. In Figure 5.26, condenser R134a outlet temperature for Step 1-2 is shown.

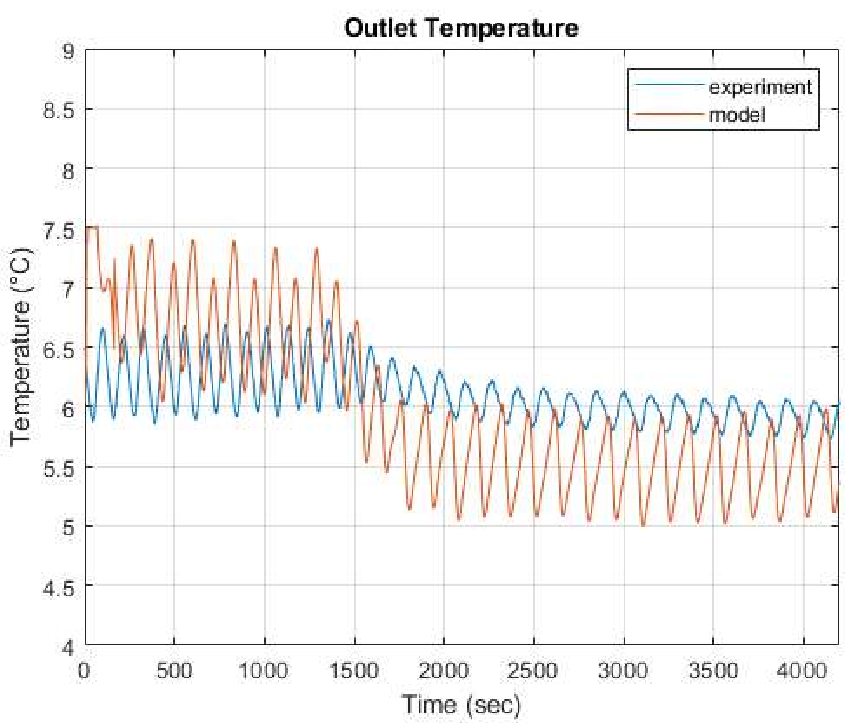

Figure 5.26. Condenser R134a outlet temperature for Step 1-2.

In Figure 5.27, condenser R134a outlet temperature for Step 3-4 is shown.

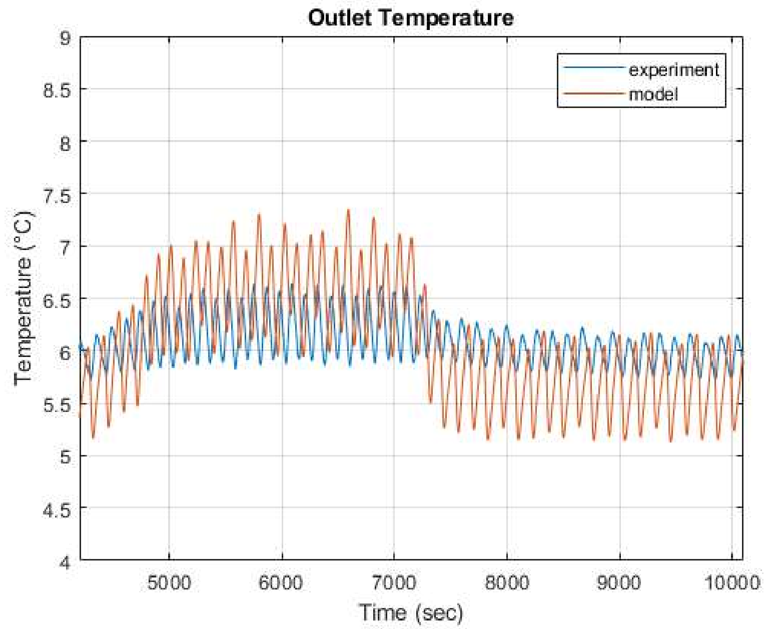

Figure 5.27. Condenser R134a outlet temperature for Step 3-4.

In Figure 5.28, condenser R134a outlet temperature for Step 5-6 is shown.

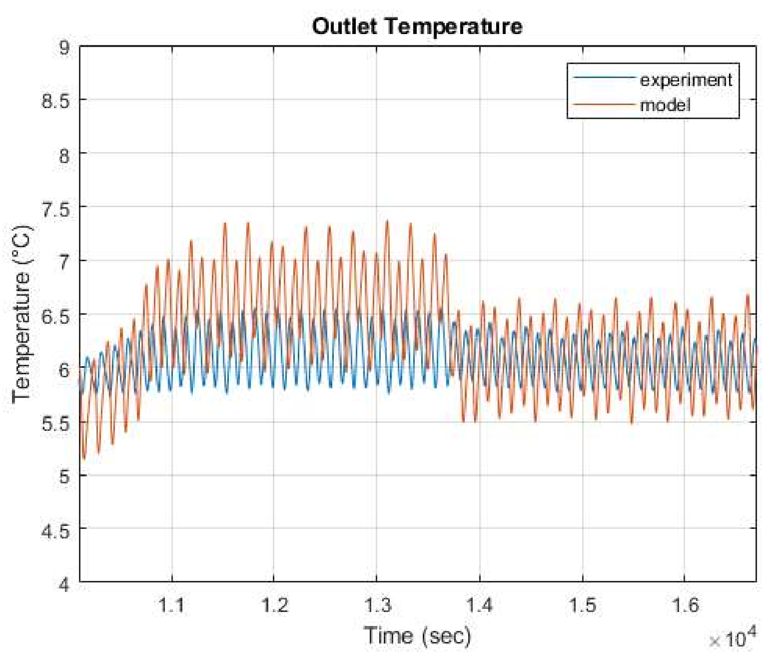

Figure 5.28. Condenser R134a outlet temperature for Step 5-6.

In Figure 5.29, condenser R134a outlet temperature for Step 6-7 is shown.

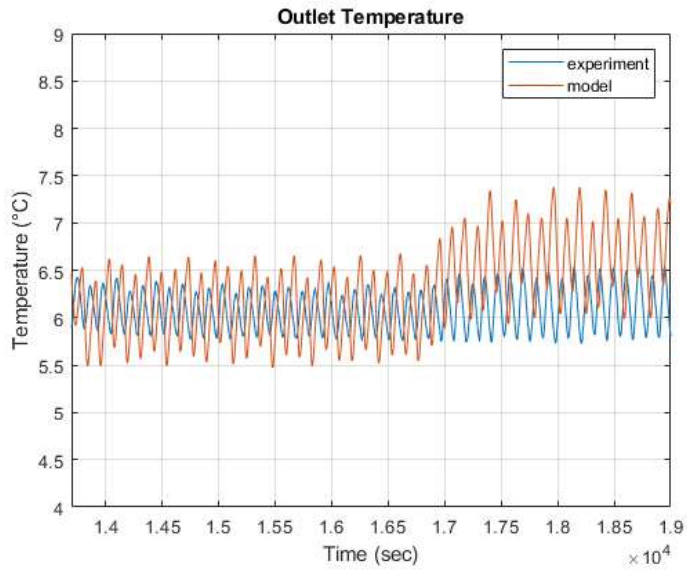

Figure 5.29. Condenser R134a outlet temperature for Step 6-7.

Figure 5.26. – Figure 5.29. show the condenser R134a outlet temperature. In these 4 figures, maximum temperature difference between the model and the experiment is less than 1.3 °C for condenser R134a outlet temperature values. In Figure 5.30, condenser water outlet temperature for Step 1-2 is shown.

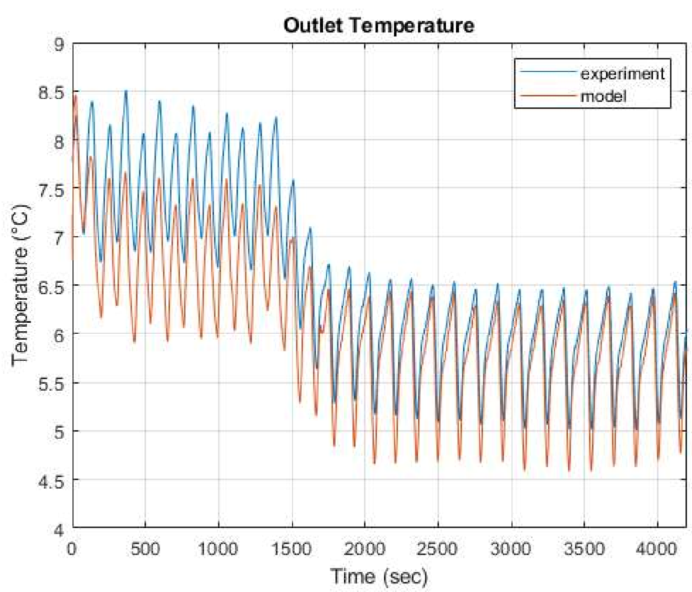

Figure 5.30. Condenser water outlet temperature for Step 1-2.

In Figure 5.31, condenser water outlet temperature for Step 3-4 is shown.

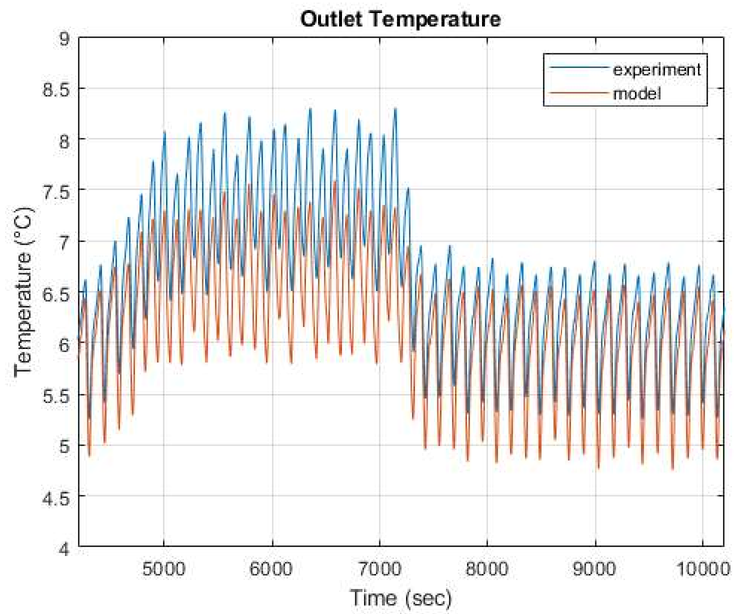

Figure 5.31. Condenser water outlet temperature for Step 3-4.

In Figure 5.32, condenser water outlet temperature for Step 5-6 is shown.

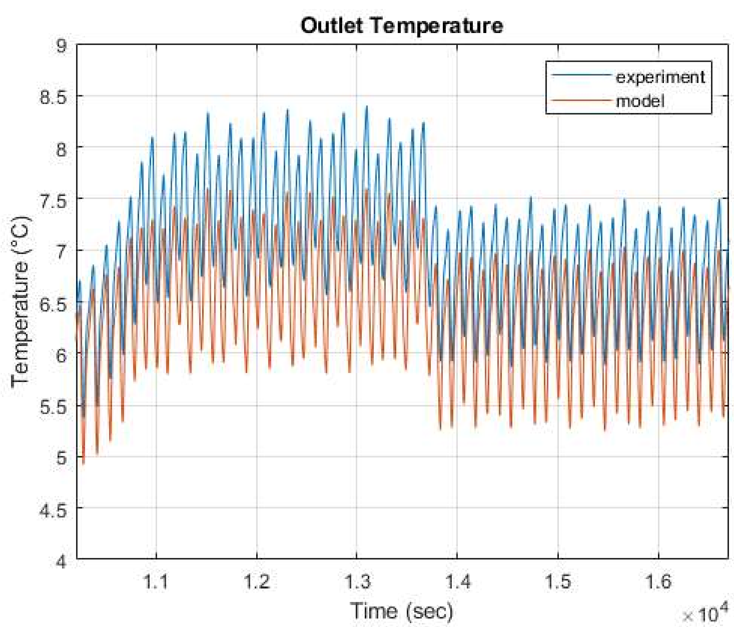

Figure 5.32. Condenser water outlet temperature for Step 5-6.

In Figure 5.33, condenser water outlet temperature for Step 6-7 is shown.

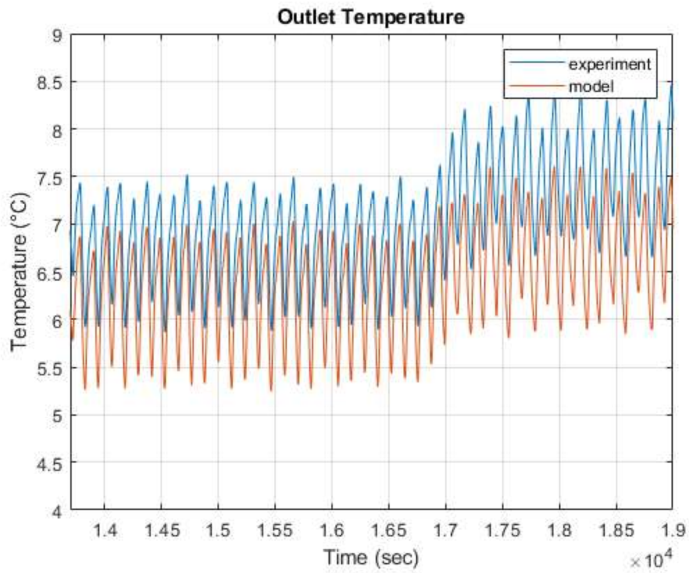

Figure 5.33. Condenser water outlet temperature for Step 6-7.

Figure 5.30. – Figure 5.33. show the condenser water outlet temperature. In these 4 figures, maximum temperature difference between the model and the experiment is less than 0.6 °C for condenser water outlet temperature values. In Figure 5.34, condenser R134a inlet temperature for Step 1-2 is shown.

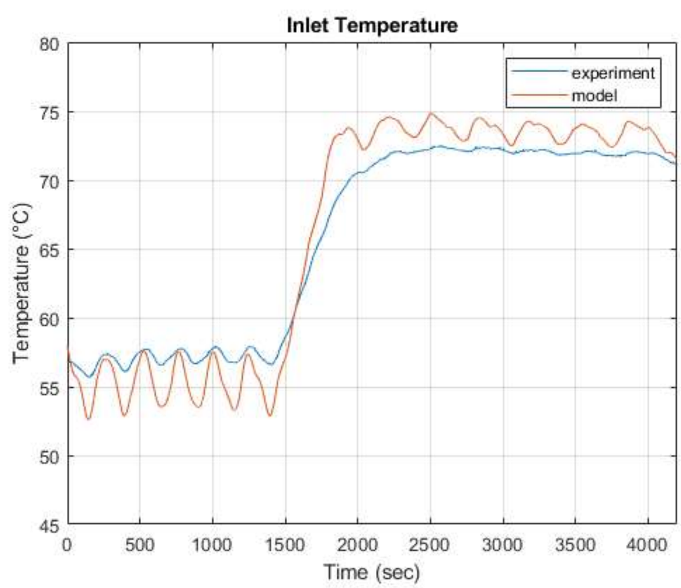

Figure 5.34. Condenser R134a inlet temperature for Step 1-2.

In Figure 5.35, condenser R134a inlet temperature for Step 3-4 is shown.

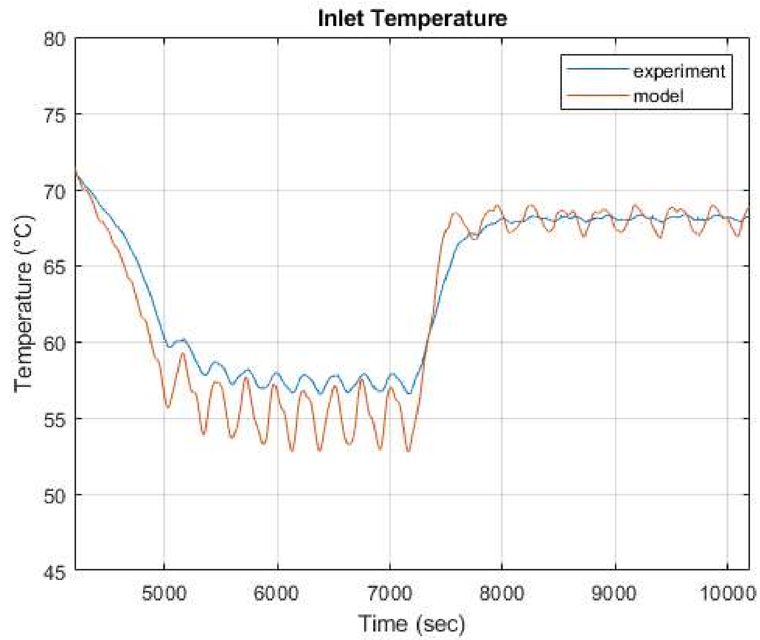

Figure 5.35. Condenser R134a inlet temperature for Step 3-4.

In Figure 5.36, condenser R134a inlet temperature for Step 5-6 is shown.

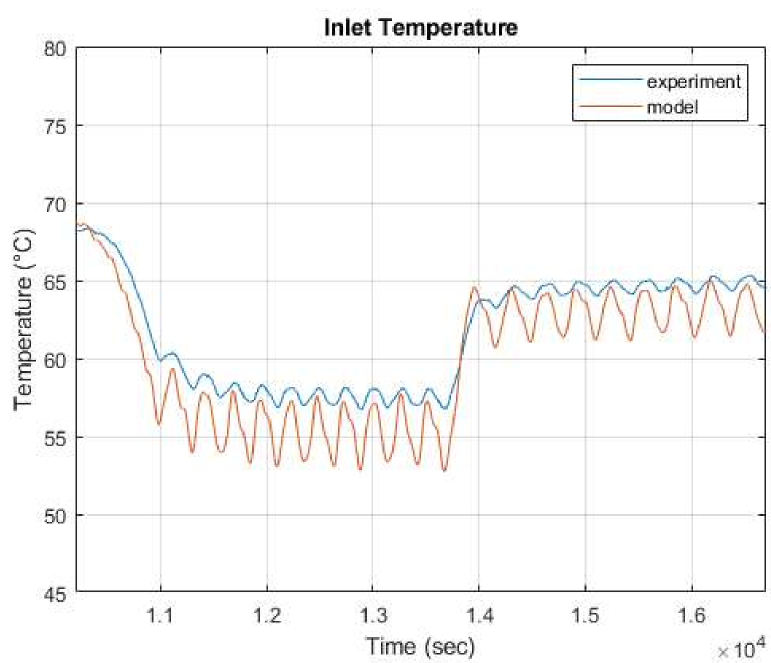

Figure 5.36. Condenser R134a inlet temperature for Step 5-6.

In Figure 5.37, condenser R134a inlet temperature for Step 6-7 is shown.

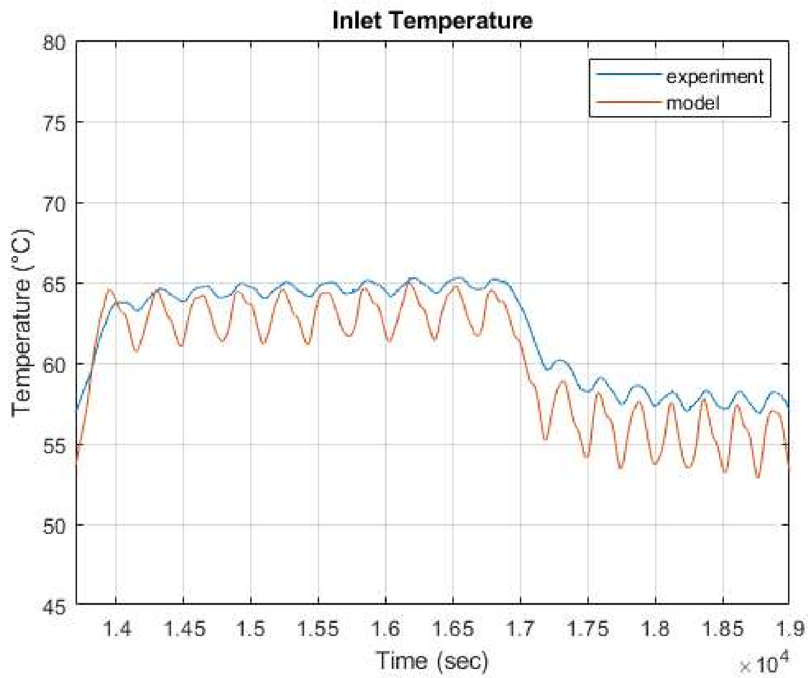

Figure 5.37. Condenser R134a inlet temperature for Step 6-7.

Figure 5.34. – Figure 5.37. show the condenser R134a outlet temperature. In these 4 figures, the maximum temperature difference between the model and the experiment is about 5 ℃ and it is maximum when hot oil temperature is set to 110 ℃. When the hot oil temperature decreases, the temperature difference between the model and experiment decreases. The reason for that is when the hot oil temperature increases, the temperature and pressure values of cycle increase. Also, fluctuations on mass flowrate of working fluid increase. Therefore, calculation sensitivity of model decreases. However, current model vs experiments results are good enough.

In Figure 5.38, condenser R134a outlet pressure for Step 1-2 is shown.

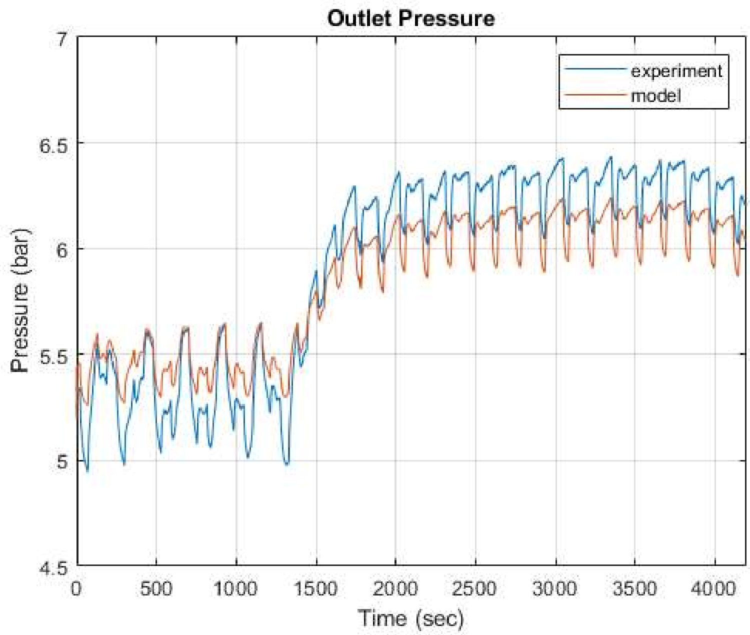

Figure 5.38. Condenser R134a outlet pressure for Step 1-2.

In Figure 5.39, condenser R134a outlet pressure for Step 3-4 is shown.

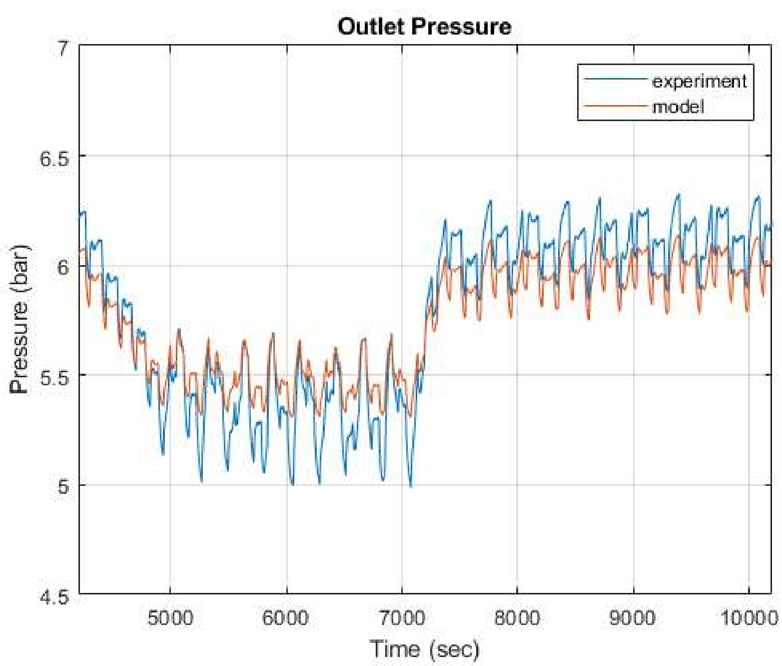

Figure 5.39. Condenser R134a outlet pressure for Step 3-4.

In Figure 5.40, condenser R134a outlet pressure for Step 5-6 is shown.

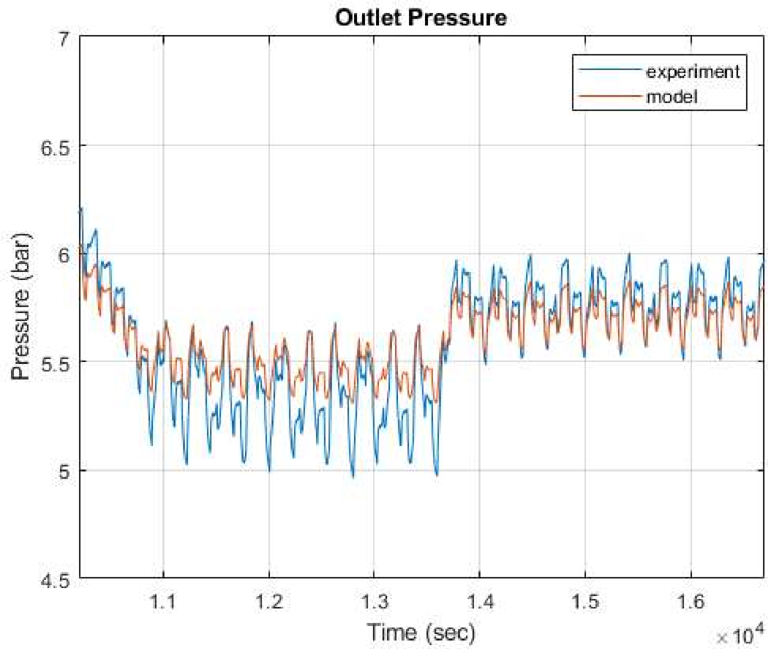

Figure 5.40. Condenser R134a outlet pressure for Step 5-6.

In Figure 5.41, condenser R134a outlet pressure for Step 6-7 is shown.

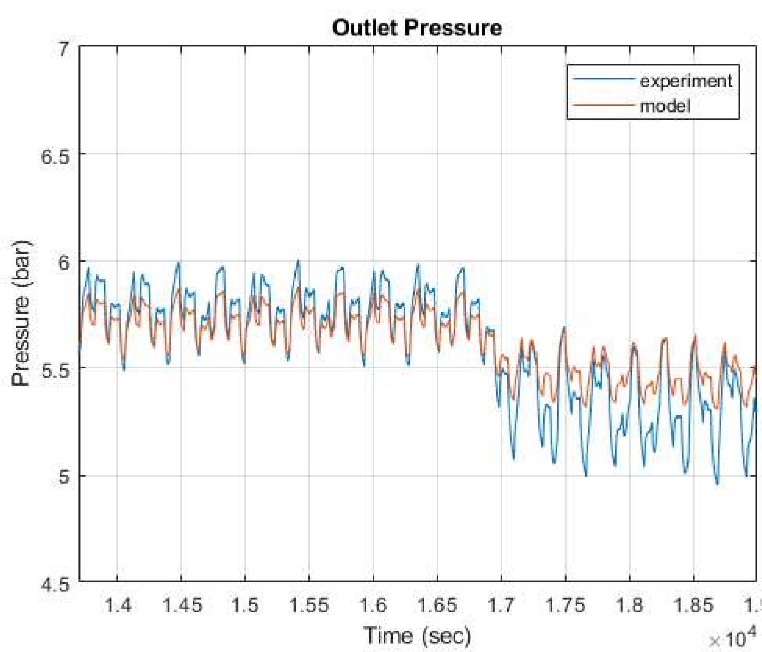

Figure 5.41. Condenser R134a outlet pressure for Step 6-7.

Figure 5.38. – Figure 5.41. show the condenser R134a outlet pressure. In these 4 figures, the maximum pressure difference between the model and the experiment is less than 10 percent. However, pressure difference increases in steps where hot oil temperature is increased. The reason is both pressure and temperature values increase in the system and sensitivity of correlations used in heat transfer and pressure loss decreases.

In Figure 5.42, condenser R134a inlet pressure for Step 1-2 is shown.

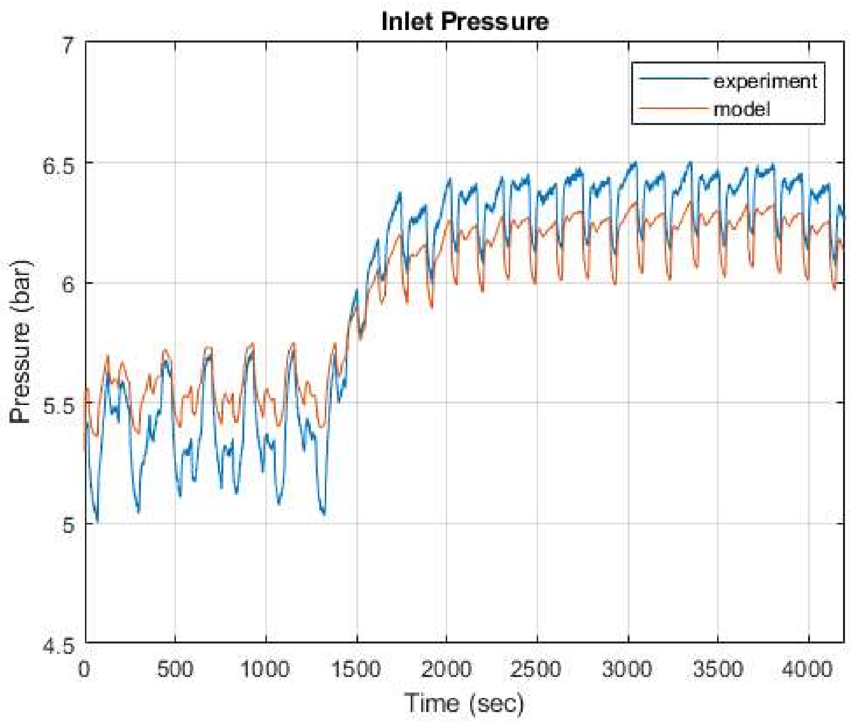

Figure 5.42. Condenser R134a inlet pressure for Step 1-2.

In Figure 5.43, condenser R134a inlet pressure for Step 3-4 is shown.

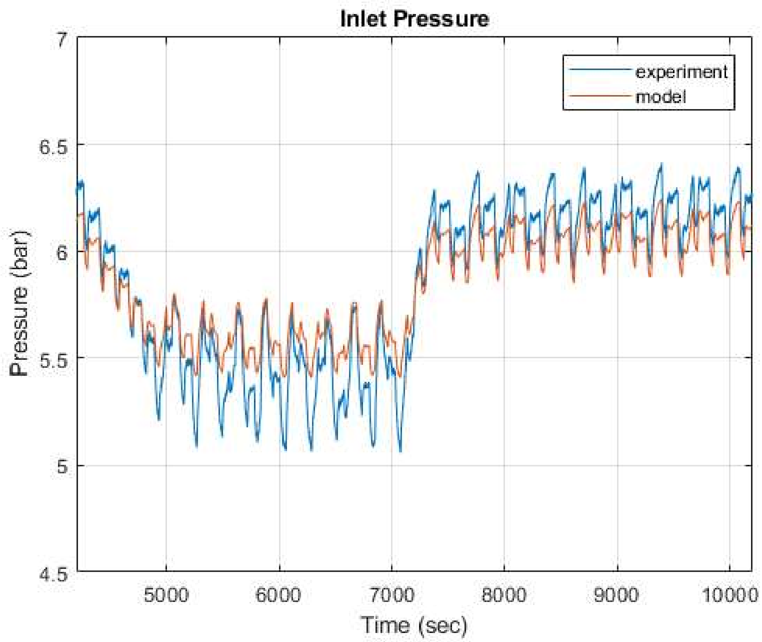

Figure 5.43. Condenser R134a inlet pressure for Step 3-4.

In Figure 5.44, condenser R134a inlet pressure for Step 5-6 is shown.

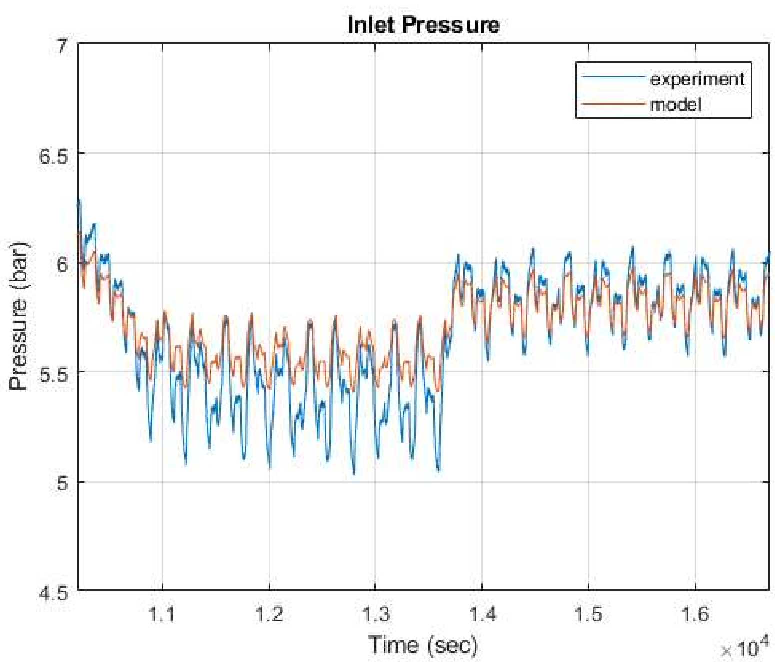

Figure 5.44. Condenser R134a inlet pressure for Step 5-6.

In Figure 5.45, condenser R134a inlet pressure for Step 6-7 is shown.

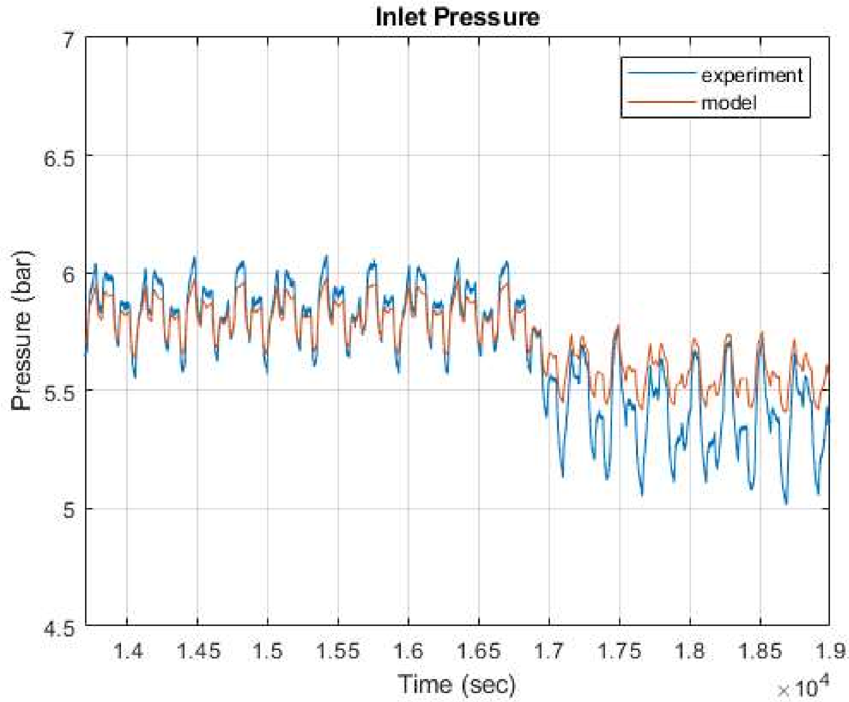

Figure 5.45. Condenser R134a inlet pressure for Step 6-7.

Figure 5.42. – Figure 5.45. show the condenser R134a inlet pressure. In these 4 figures, the maximum pressure difference between the model and the experiment is less than 10 percent. However, pressure difference increases in steps where hot oil temperature is increased. The reason is that, when pressure and temperature values increase in the system, sensitivity of correlations used in heat transfer and pressure loss decrease. However, current model vs experiment results are acceptable compared to literature.

5.3. Throttle Valve Results

Throttle valve outlet pressure is given as an output to the dynamic model. Valve's inlet temperature and pressure come from evaporator's outlet conditions, but the model includes the heat and pressure losses in pipes between evaporator and throttle valve.

There is no temperature sensor right after the throttle valve on the ORC setup. Therefore, the throttle valve outlet temperature cannot be measured directly. However, there is a temperature sensor at the condenser inlet. It is approximately at 6 meters after the throttle valve. The model includes the heat and the pressure losses for the pipe. Although the dynamic model calculates both throttle valve's outlet and condenser inlet temperatures, there is no experimental data for throttle valve outlet temperature. Therefore, the condenser inlet temperature comparison between the model and the experiment is made under Condenser Results section.

Similarly, there are no temperature and pressure sensors at throttle valve inlet on the setup. Therefore, throttle valve inlet temperature and pressure cannot be measured directly. However, there are temperature and pressure sensors at evaporator outlet and the model takes the evaporator outlet temperature and pressure and add the change due to the pipe between the evaporator and the throttle valve. Along the pipe, the temperature and pressure both decrease. Even if model calculates throttle valve inlet temperature and pressure there is no experimental data to compare. Evaporator outlet temperature and pressure comparison is made under Evaporator Results part. Only the throttle valve inlet and outlet enthalpy comparison is given in this part.

As it is mentioned in Dynamic Model chapter, inlet and outlet enthalpy values of throttle valve are the same. In Figure 5.46, throttle valve inlet and outlet enthalpy are shown. Throttle valve model keeps enthalpy constant.

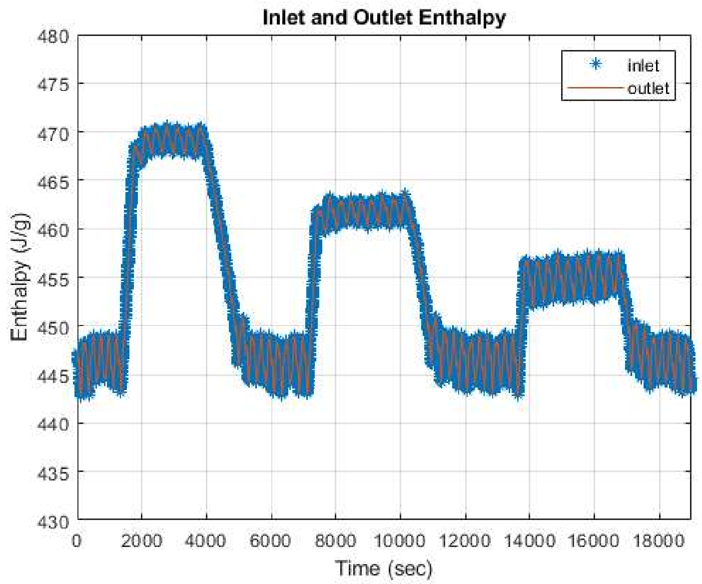

Figure 5.46. Throttle valve's inlet and outlet enthalpy.

5.4. Working Fluid Pump Results

In this part, working fluid pump R134a outlet temperature, inlet temperature, outlet pressure, and inlet pressure for both model and experiment are shown. In Figure 5.47, working fluid pump outlet temperature for Step 1-2 is shown.

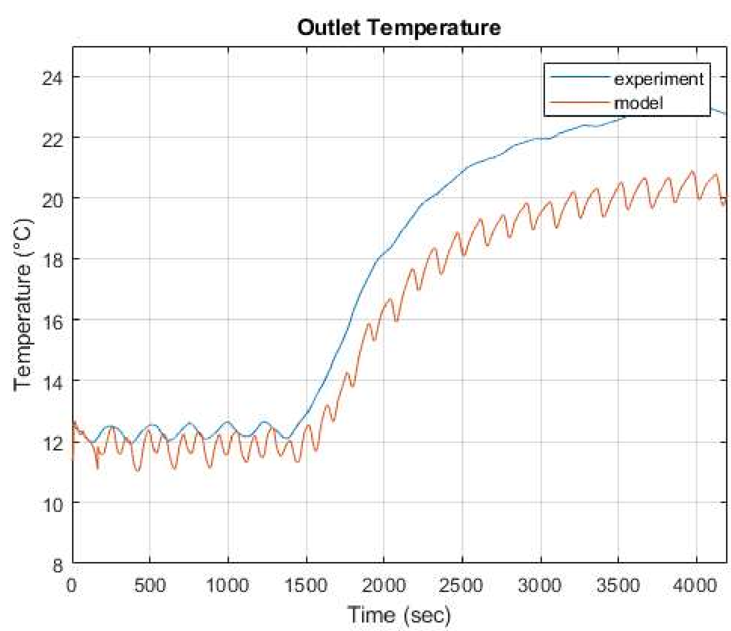

Figure 5.47. Working fluid pump outlet temperature for Step 1-2.

In Figure 5.48, working fluid pump outlet temperature for Step 3-4 is shown.

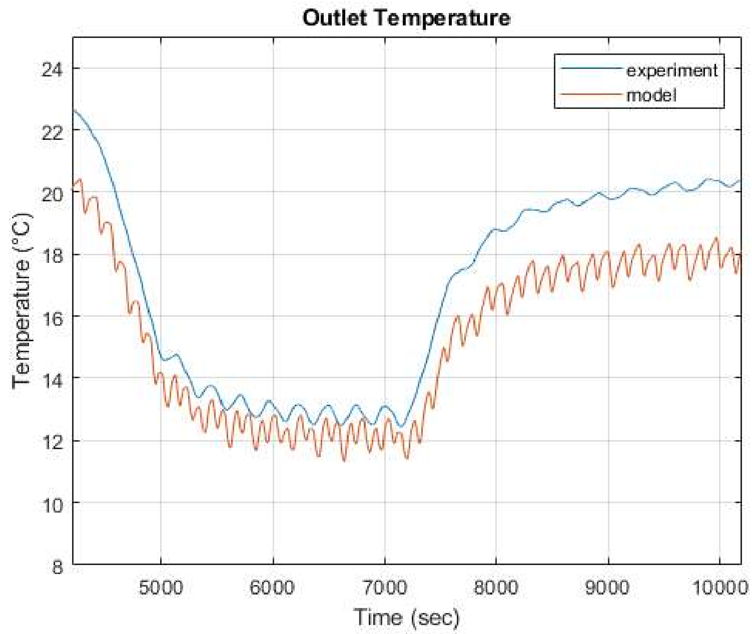

Figure 5.48. Working fluid pump outlet temperature for Step 3-4.

In Figure 5.49, working fluid pump outlet temperature for Step 5-6 is shown.

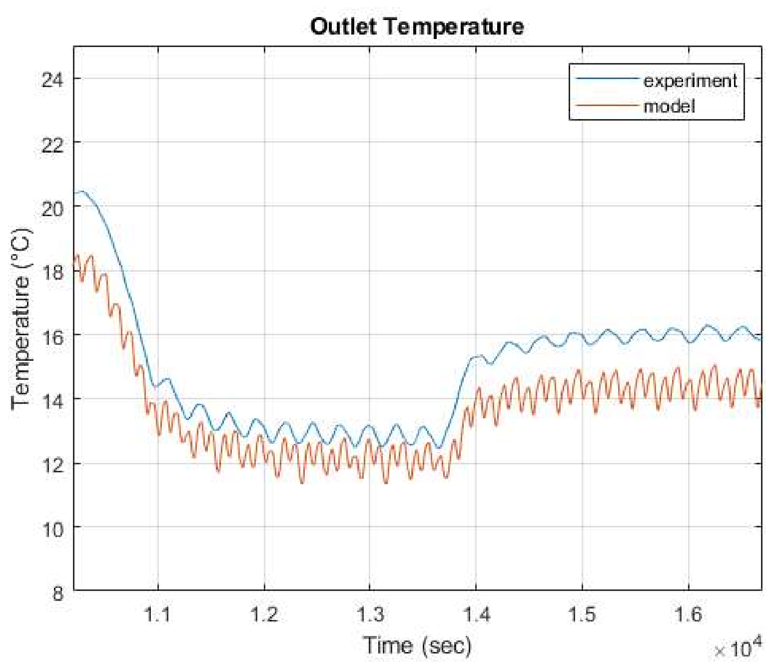

Figure 5.49. Working fluid pump outlet temperature for Step 5-6.

In Figure 5.50, working fluid pump outlet temperature for Step 6-7 is shown.

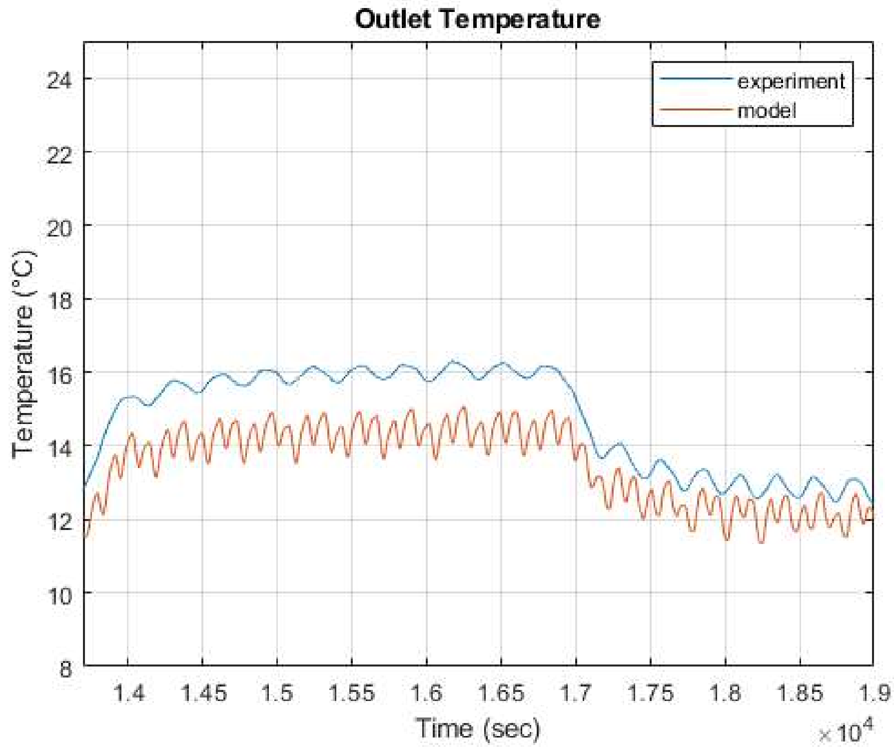

Figure 5.50. Working fluid pump outlet temperature for Step 6-7.

Figure 5.47. – Figure 5.50. show the working fluid pump outlet temperature. In these 4 figures, the maximum temperature difference between the model and the experiment is less than 3.5 °C. Temperature difference between model and experiment increases for the steps that hot oil temperature increases. When cycle temperature and pressure values get higher, difference between model and experiment gets bigger. However, current difference is well enough compared to literature.

In Figure 5.51, working fluid pump inlet temperature for Step 1-2 is shown.

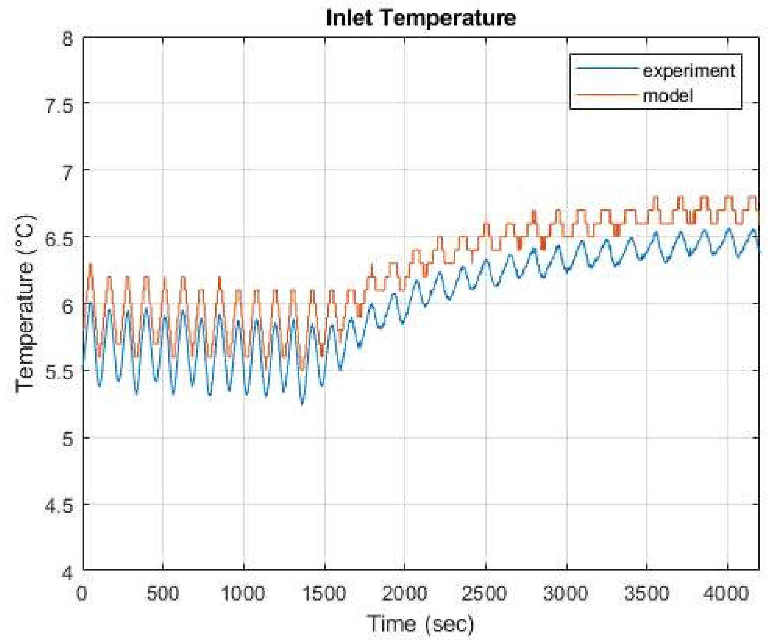

Figure 5.51. Working fluid pump inlet temperature for Step 1-2.

In Figure 5.52, working fluid pump inlet temperature for Step 3-4 is shown.

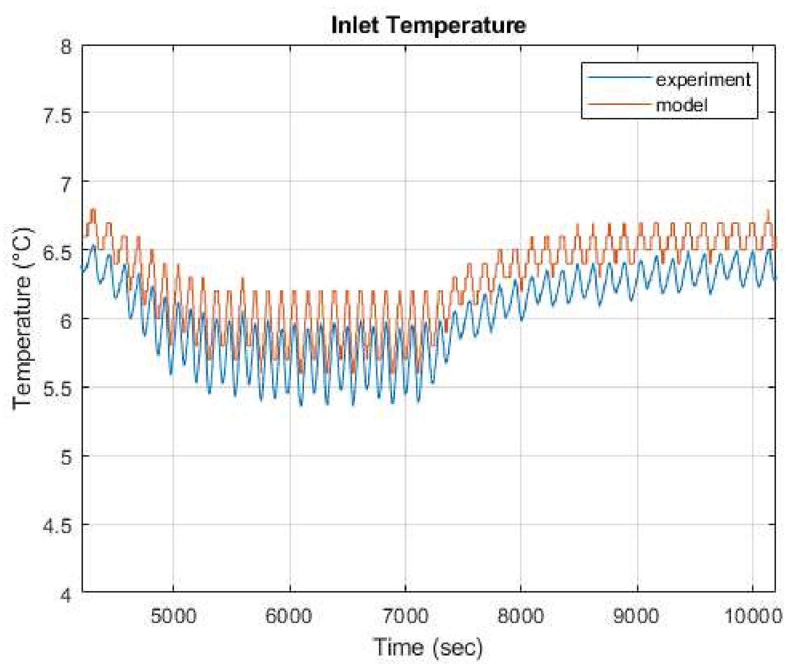

Figure 5.52. Working fluid pump inlet temperature for Step 3-4.

In Figure 5.53, working fluid pump inlet temperature for Step 5-6 is shown.

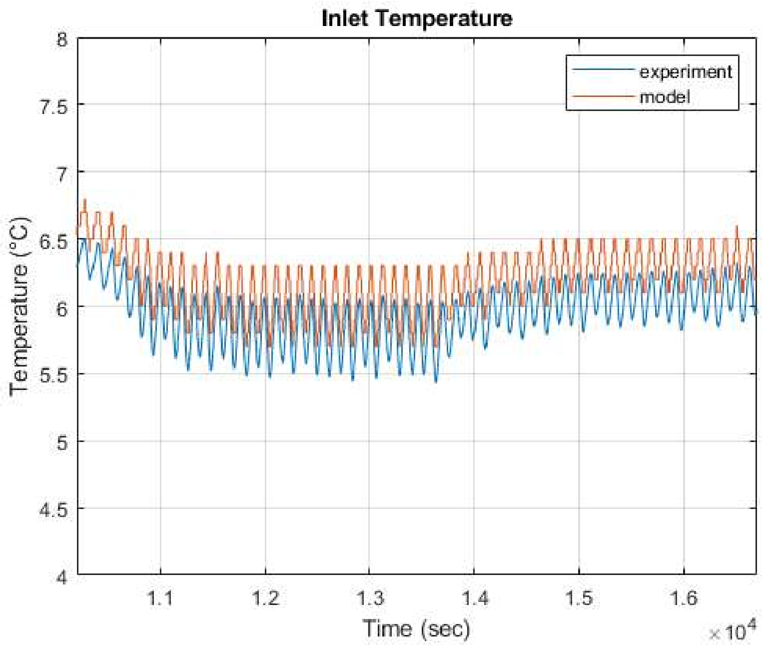

Figure 5.53. Working fluid pump inlet temperature for Step 5-6.

In Figure 5.54, working fluid pump inlet temperature for Step 6-7 is shown.

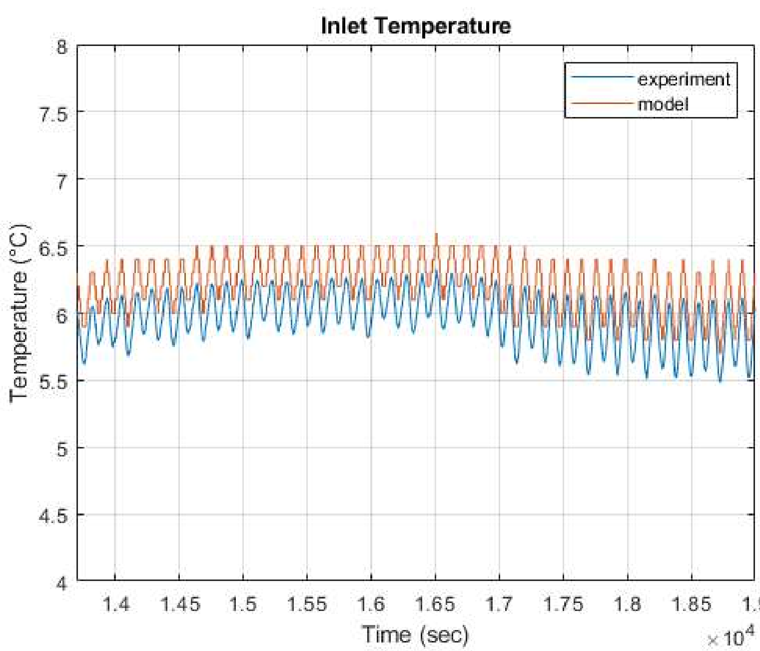

Figure 5.54. Working fluid pump inlet temperature for Step 6-7.

Figure 5.51. – Figure 5.54. show the working fluid pump inlet temperature. In these 4 figures, the maximum temperature difference between the model and the experiment is less than 0.6 ℃.

In Figure 5.55, working fluid pump outlet pressure for Step 1-2 is shown.

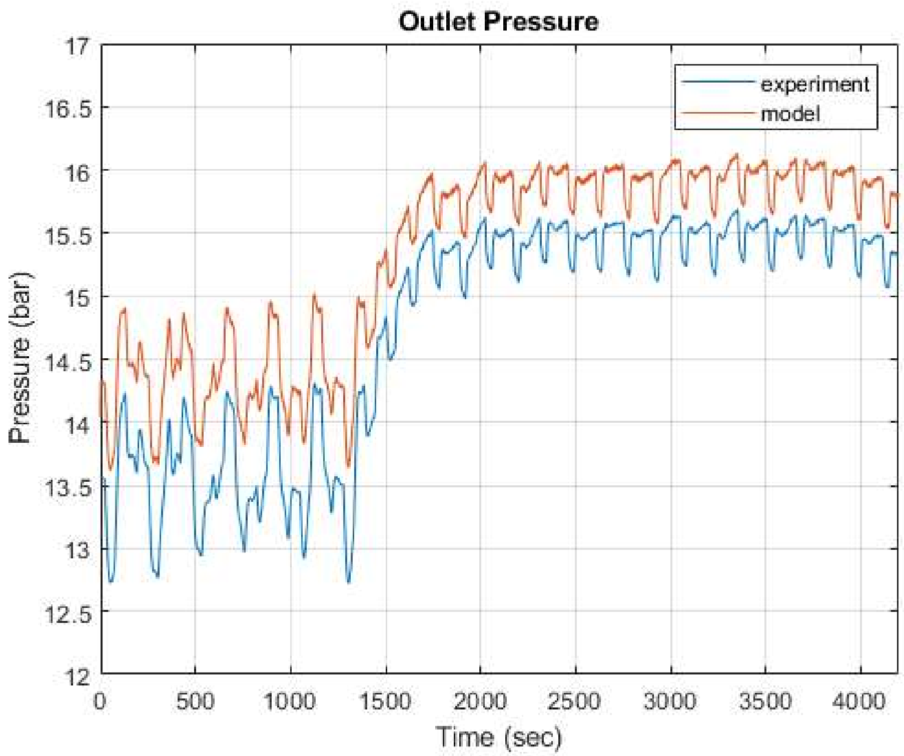

Figure 5.55. Working fluid pump outlet pressure for Step 1-2.

In Figure 5.56, working fluid pump outlet pressure for Step 3-4 is shown.

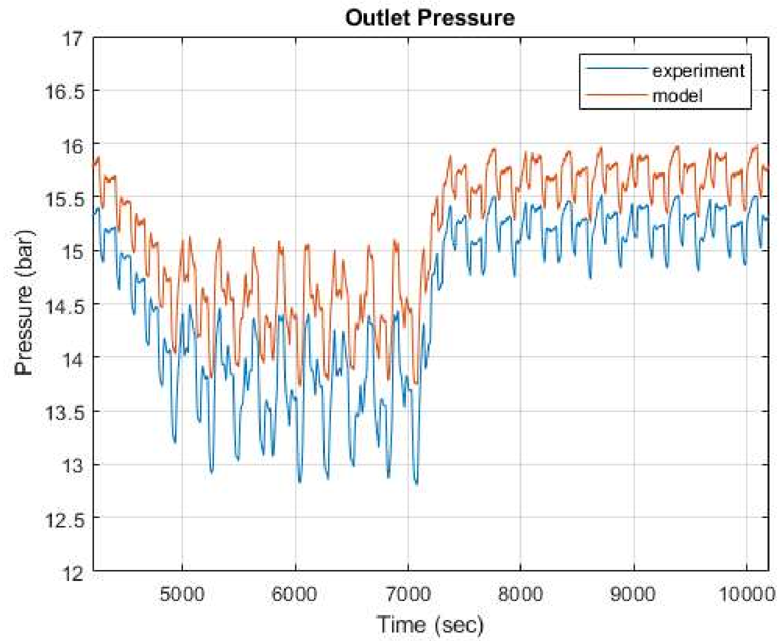

Figure 5.56. Working fluid pump outlet pressure for Step 3-4.

In Figure 5.57, working fluid pump outlet pressure for Step 5-6 is shown.

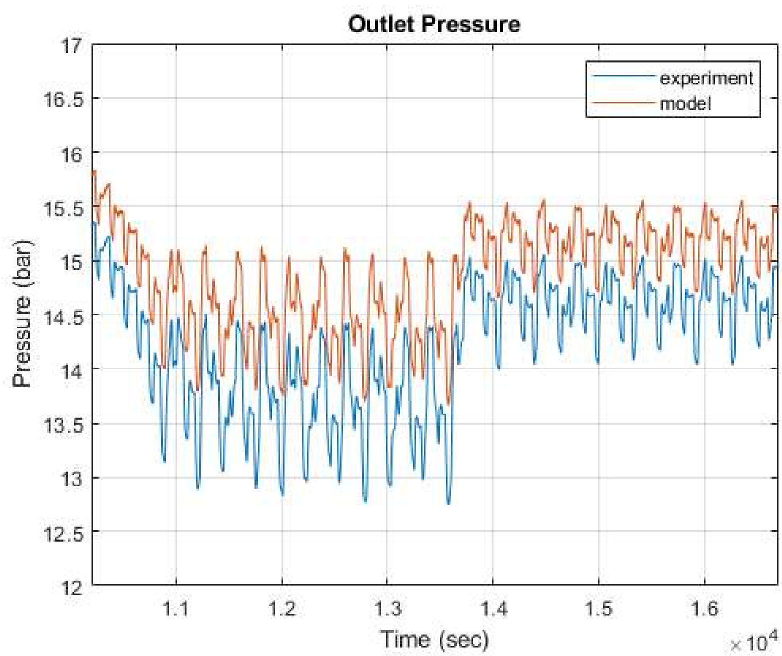

Figure 5.57. Working fluid pump outlet pressure for Step 5-6.

In Figure 5.58, working fluid pump outlet pressure for Step 6-7 is shown.

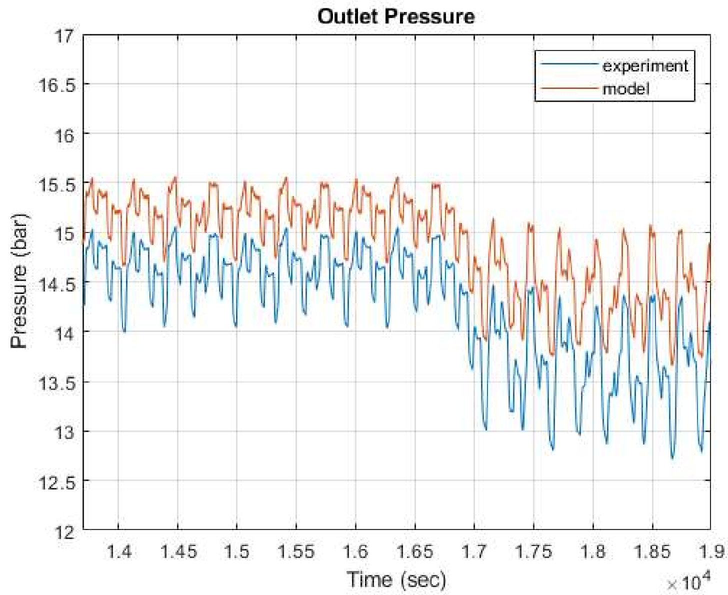

Figure 5.58. Working fluid pump outlet pressure for Step 6-7.

Figure 5.55. – Figure 5.58. show the working fluid pump outlet pressure. In these 4 figures, the maximum pressure difference between the model and the experiment is less than 8 percent. In Figure 5.59, working fluid pump inlet pressure for Step 1-2 is shown.

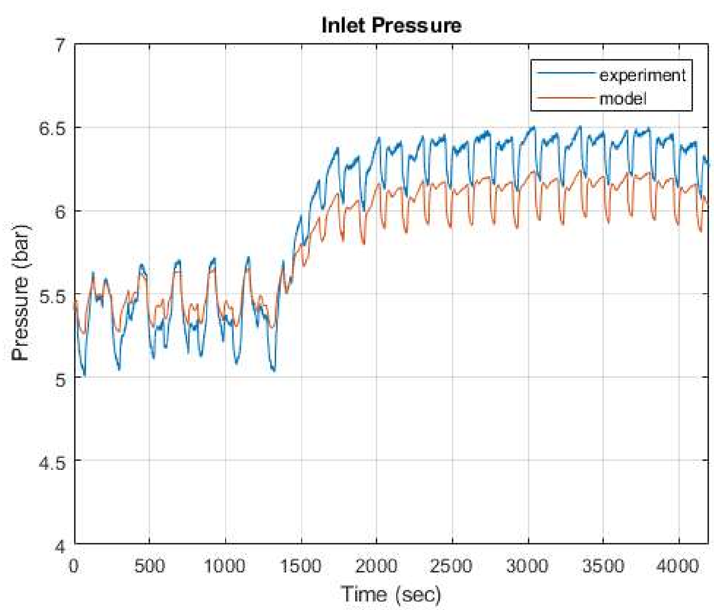

Figure 5.59. Working fluid pump inlet pressure for Step 1-2.

In Figure 5.60, working fluid pump inlet pressure for Step 3-4 is shown.

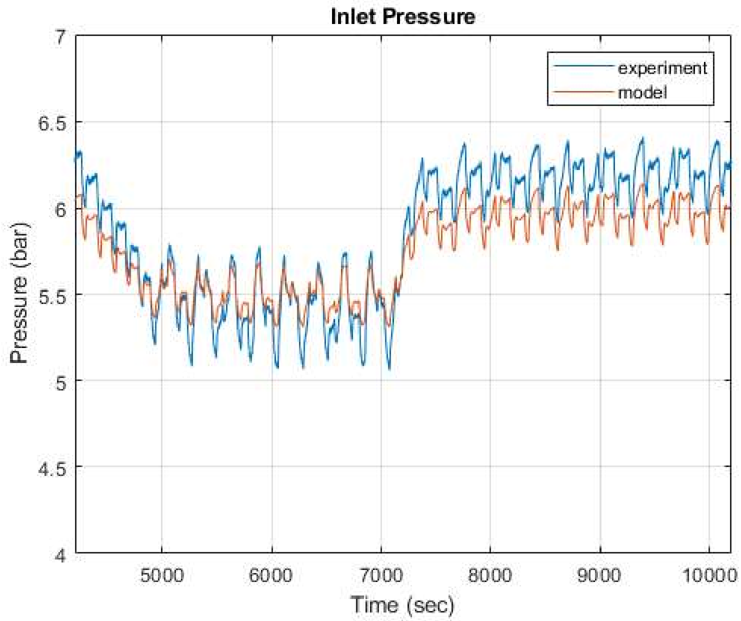

Figure 5.60. Working fluid pump inlet pressure for Step 3-4.

In Figure 5.61, working fluid pump inlet pressure for Step 5-6 is shown.

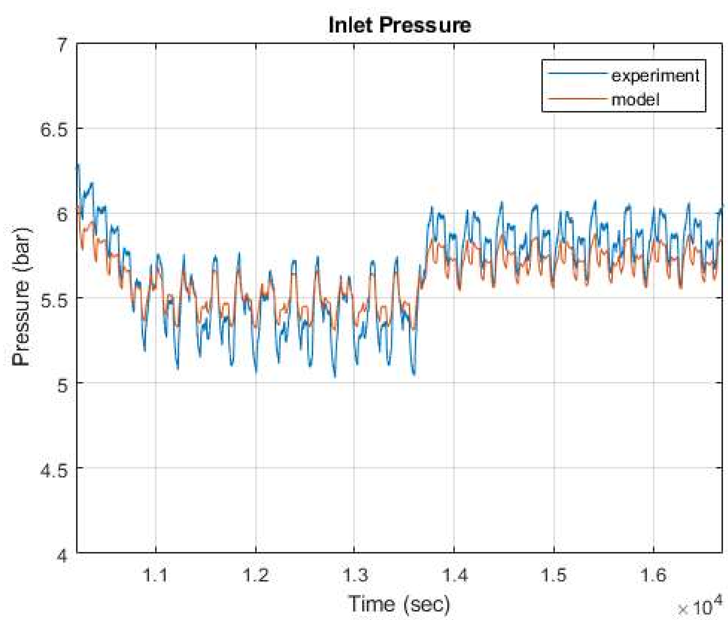

Figure 5.61. Working fluid pump inlet pressure for Step 5-6.

In Figure 5.62, working fluid pump inlet pressure for Step 6-7 is shown.

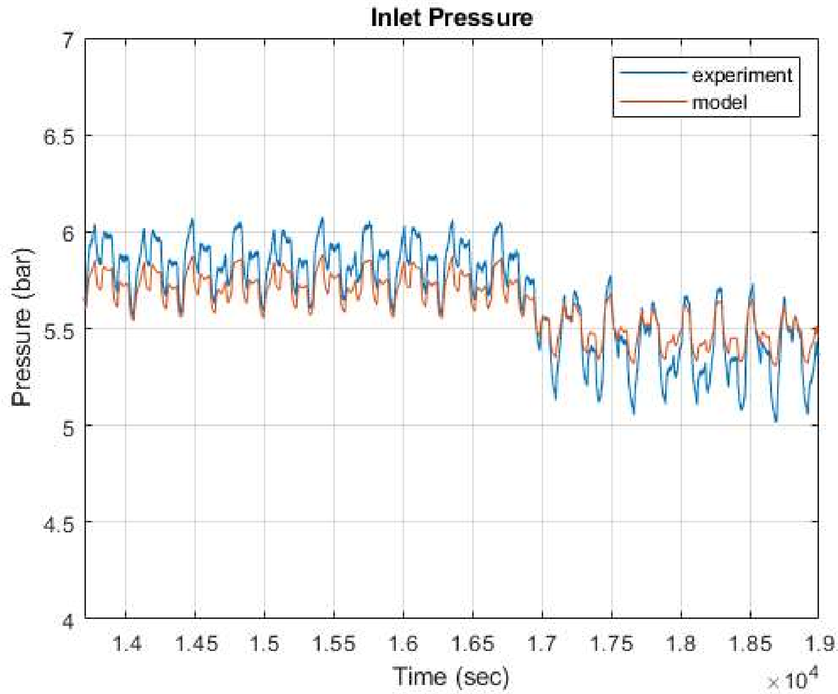

Figure 5.62. Working fluid pump inlet pressure for Step 6-7.

Figure 5.59. – Figure 5.62. show the working fluid pump inlet pressure. In these 4 figures, the maximum difference between the model and the experiment is less than 10 percent.

5.5. Working Fluid Mass Flowrate Results

In this part, working fluid mass flowrate for model and experiment is compared. In previous results, R134a mass flowrate fluctuation was mentioned many times. In this part, fluctuations on R134a mass flowrate are shown clearly.

In Figure 5.63, working fluid mass flowrate for Step 1-2 is shown.

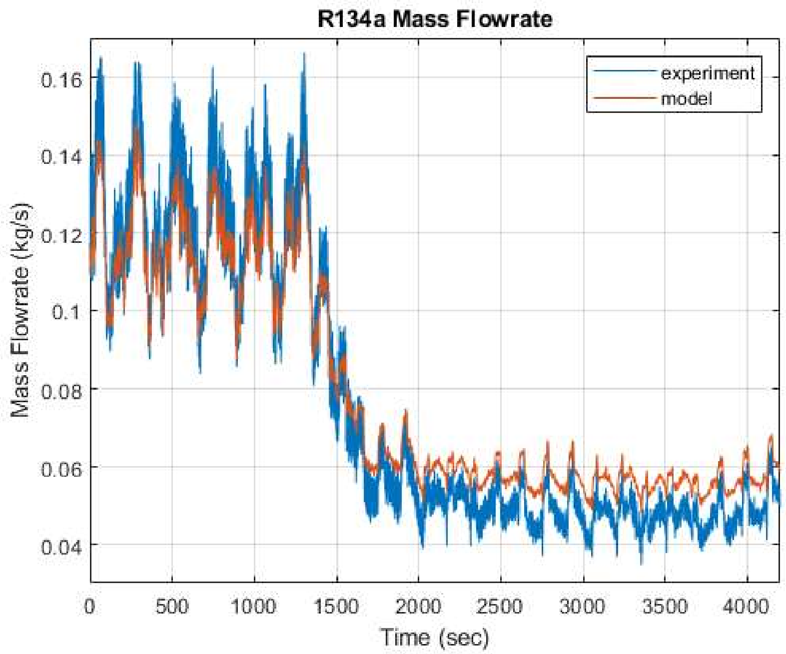

Figure 5.63. Working fluid mass flowrate for Step 1-2.

In Figure 5.64, working fluid mass flowrate for Step 3-4 is shown.

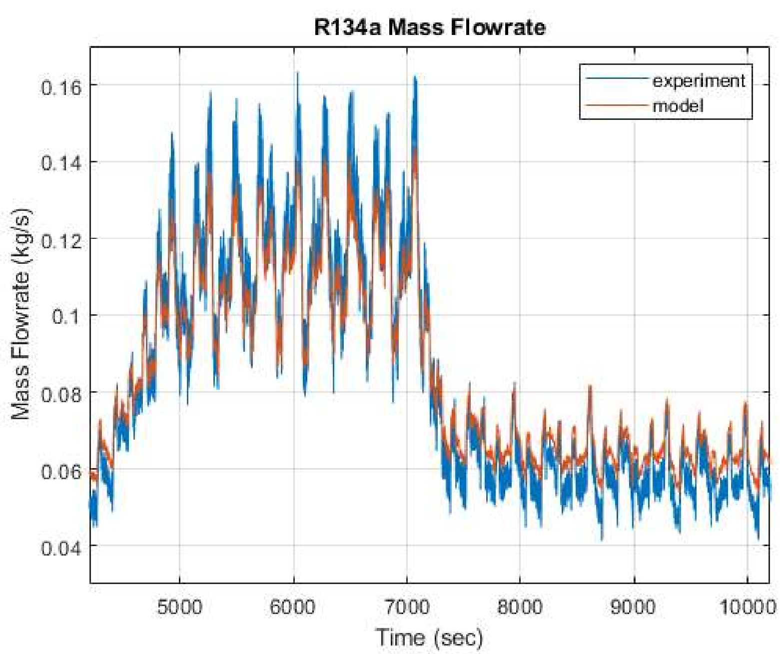

Figure 5.64. Working fluid mass flowrate for Step 3-4.

In Figure 5.65, working fluid mass flowrate for Step 5-6 is shown.

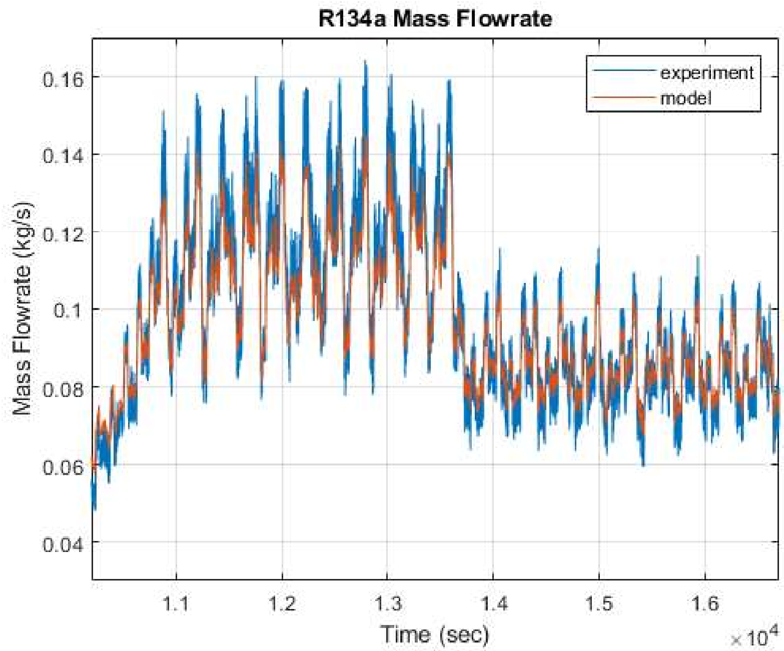

Figure 5.65. Working fluid mass flowrate for Step 5-6.

In Figure 5.66, working fluid mass flowrate for Step 6-7 is shown.

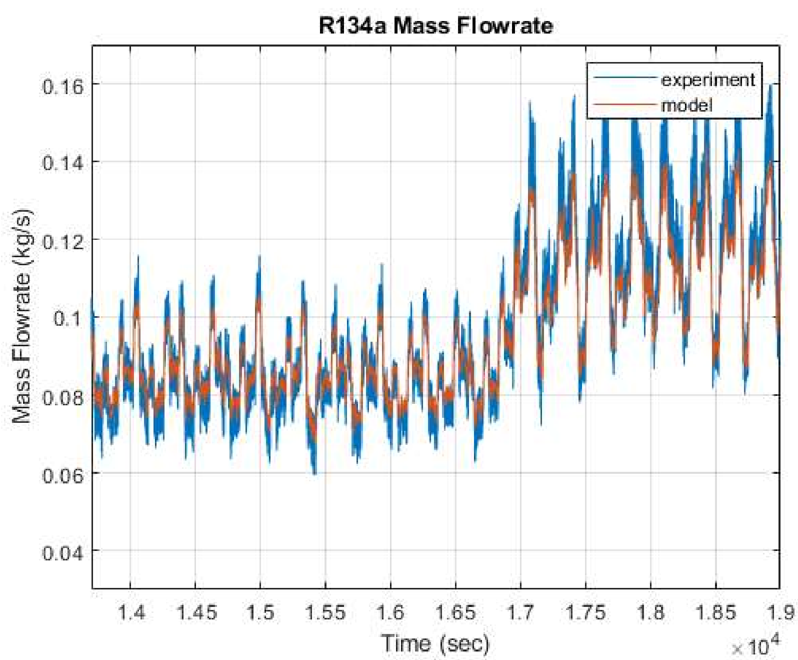

Figure 5.66. Working fluid mass flowrate for Step 6-7.

Figure 5.63. – Figure 5.66. show the working fluid pump mass flowrate. In these 4 figures, the maximum difference between the model and the experiment is less than 19 percent.

5.6. TS Diagrams for Experiment

Four different hot oil set temperatures are used in the experiment. Oil inlet set temperatures are 80 °C, 90 °C, 100 °C, and 110 °C. For each value, data are recorded. In the following figures, TS diagrams for ORC setup at BURET laboratory different hot oil set temperatures are given. Average of experimental data is used to create TS diagrams. In Figure 5.67, TS diagram for the ORC setup for 80 °C oil set temperature is shown.

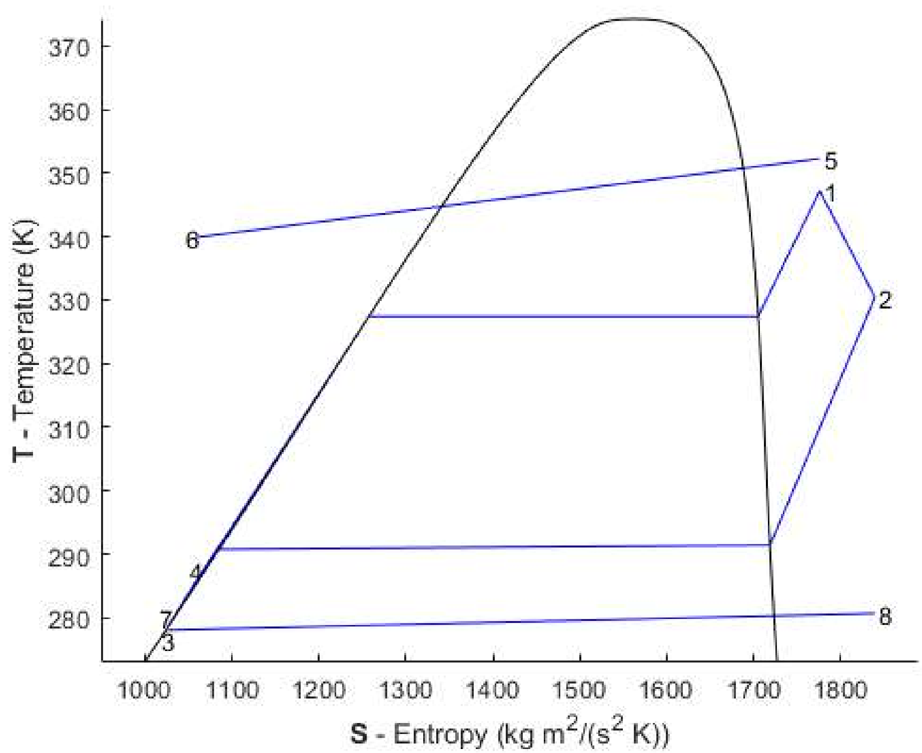

Figure 5.67. TS diagram for the ORC setup for 80 °C oil set temperature.

In Figure 5.68, TS diagram for the ORC setup for 90 °C oil set temperature is shown.

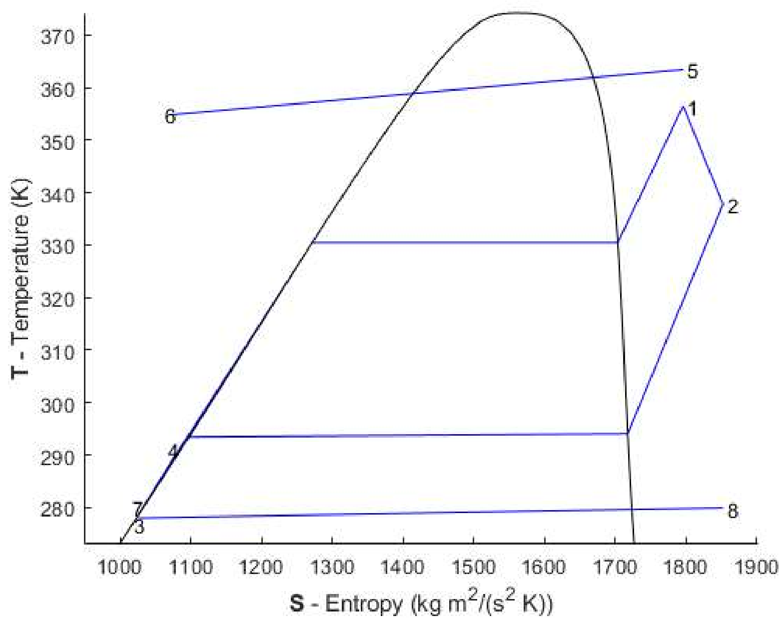

Figure 5.68. TS diagram for the ORC setup for 90 °C oil set temperature.

In Figure 5.69, TS diagram for the ORC setup for 100 °C oil set temperature is shown.

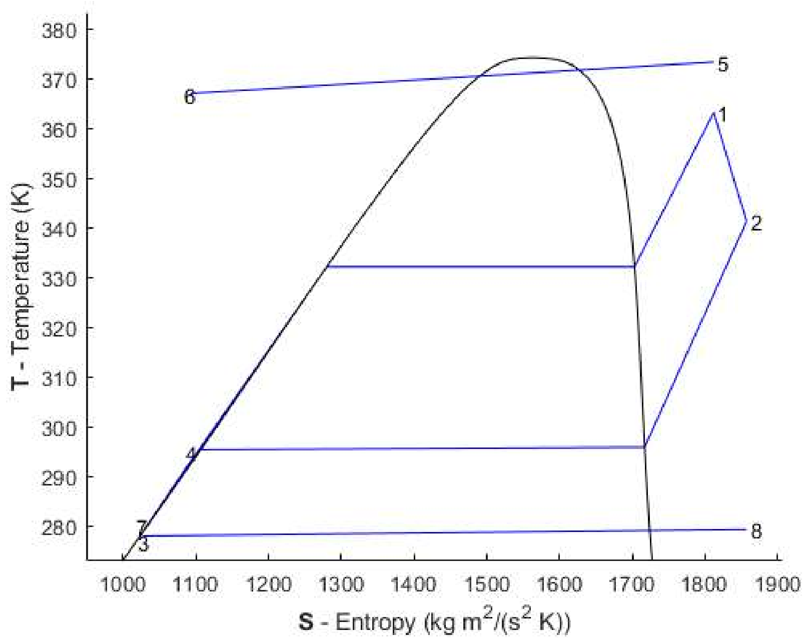

Figure 5.69. TS diagram for the ORC setup for 100 °C oil set temperature.

In Figure 5.70, TS diagram for the ORC setup for 110 °C oil set temperature is shown.

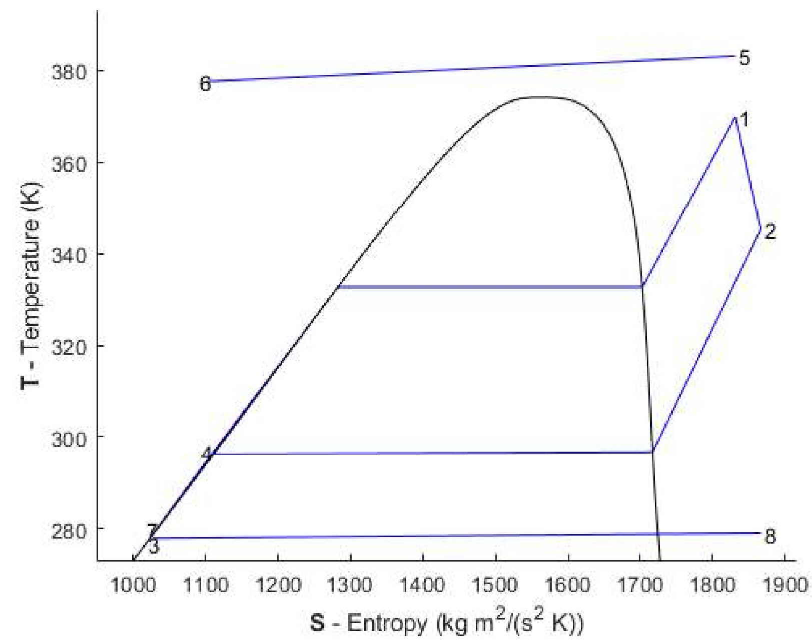

Figure 5.70. TS diagram for the ORC setup for 110 °C oil set temperature.

From Figures 5.67-5.70, it is seen that experiments are carried out at reasonable conditions. 1-2-3-4 shows the working fluid line, 5-6 shows the heat transfer oil line, and 7-8 shows the cooling water line.

5.7. Results for a Virtual Experimental Input

In this part, a virtual cold water inlet temperature similar to real one is created and given as input to the condenser tester and results are shown. The average value of virtual cold water input is 5 °C, the maximum value is 7 °C, and the minimum value is 3 °C. Frequency of the wave input is 1/110 second and it is like a sinus wave. In Figure 5.71, real and virtual cold water inlet temperatures are shown.

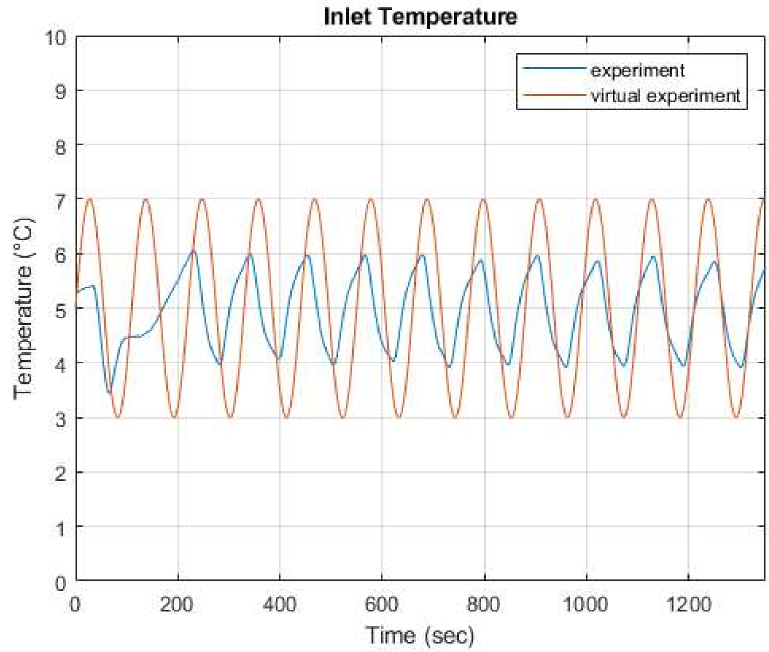

Figure 5.71. Real and virtual cold water inlet temperature.

In Figure 5.72, condenser R134a outlet temperature for experiment, model, and virtual experiment is shown.

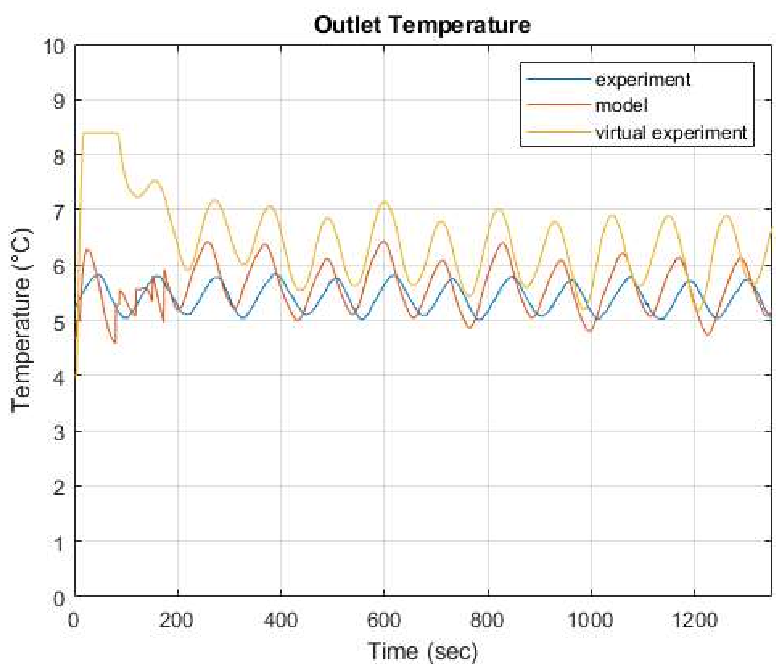

Figure 5.72. Condenser R134a outlet temperature for experiment, model, and virtual experiment.

In Figure 5.73, condenser water outlet temperature for experiment, model, and virtual experiment is shown.

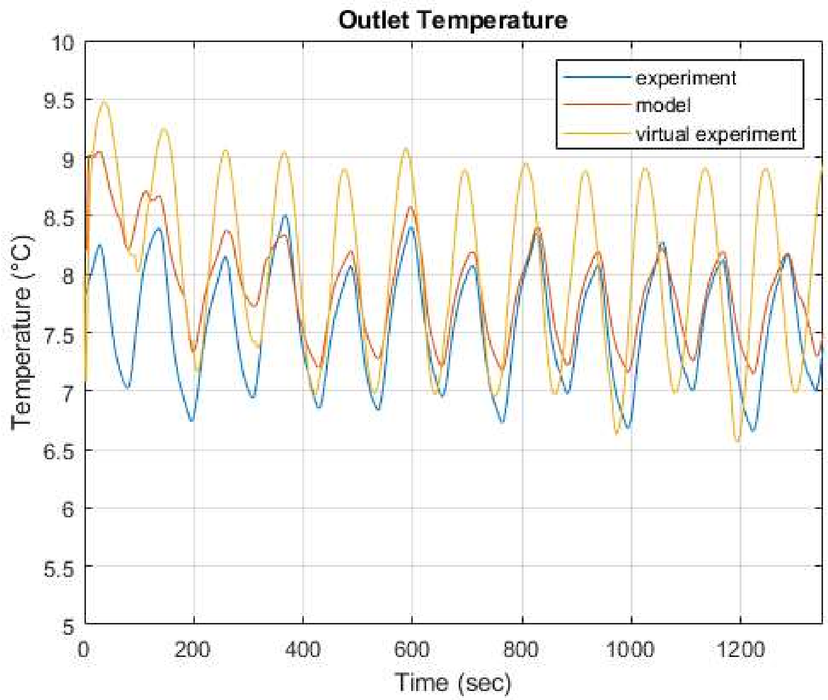

Figure 5.73. Condenser water outlet temperature for experiment, model, and virtual experiment.

In Figures 5.71-5.73, it is observed that a virtual input can be created without making an experiment. When the dynamic model uses the virtual input, it gives results close to both previous model with real inputs and experiments.

5.8. General Evaluation for Results

Outlet temperature, inlet temperature, outlet pressure, and inlet pressure values for both model and experiment are compared for each component of the ORC.

When temperature and pressure values get bigger, differences between model and experiment increase. There are two main reasons for this: The first reason is, when temperature and pressure values get larger, sensitivity and accuracy of correlations used in heat transfer and pressure drop gets less because Longo correlations are less accurate for higher temperatures as it is mentioned in the corresponding paper. The second reason is that, fluctuations in the working fluid mass flowrate gets bigger when temperature and pressure values increase. Therefore, when temperature and pressure values are higher, difference between model and experiment gets bigger. However, even differences get bigger when temperature and pressure values get higher, differences between model and experiment are acceptable and they are better than most studies in literature.

Especially in the throttle valve results, direct comparisons between the model and the experiment cannot be made because there are no temperature sensors at the inlet and outlet of the valve and there is no pressure sensor at the inlet of the valve. Therefore, there are no experimental results for those sensor locations. Thus, comparisons between the model and the experiment are made for the evaporator outlet and the condenser inlet that are the previous and the next components to the throttle valve. To have direct comparison for the throttle valve results between the model and the experiment, some sensors may be added to the inlet and the outlet of the valve.

Working fluid mass flowrate is not smoot like temperature or pressure data. Calibration of the flowmeter and data acquisition system may be improved.

6. SUMMARY AND CONCLUSIONS

In this study, the ORC test setup at BURET laboratory is modified to do proper experiments without leakage, and major heat and pressure losses in pipes. After the setup's preparation several experiments are carried out and experimental data are recorded by using the data acquisition system. Then a dynamic ORC model to simulate whole the ORC setup including heat losses and pressure losses in pipes is created by using Dymola software which is a Modelica language based dynamic simulation program. After all experimental and dynamic model simulation studies are completed, ORC setup's parameters such as temperature and pressure for both experiment and dynamic model are compared.

To include heat losses and pressure losses in pipes in the dynamic model for the ORC setup is the contribution of this study to literature.

Comparison between the dynamic model and the experiment shows that, dynamic model studied in this thesis successfully simulates the ORC setup at BURET laboratory.

With this dynamic modeling, experiments at BURET laboratory can be carried out on a virtual environment. If experiment conditions need to be changed, this could be done and tested on computer. Also, this dynamic simulation will prevent waste of time for the experimental input determination process.

One other outcome of this study is, when researcher give experimental inputs to the model, the model will show the pressure and temperature levels in the cycle, so researcher can see whether the pressure or temperature limits of the system are exceeded or not. Therefore, unsafe experimental conditions can be eliminated, and they will not be applied to the system.

6.1. Future Work

The main objective of an ORC is to generate electricity from a low temperature heat source. Therefore, a simple ORC has a turbine attached to a generator to generate electricity. As mentioned in the previous chapters, instead of a turbine a throttle valve is used to simulate the expander. As a future work, first, the available scroll turbine in the laboratory will be added to the system.

Secondly, there is a pre-cooler and additional heat exchanger in the test setup. When the turbine is added to the cycle, these heat exchangers will also be used. Dynamic model will be re-created to simulate the latest version of the ORC at BURET laboratory.

Thirdly, R134a mass flowrate data are not smooth like temperature or pressure data. Data acquisition system and working fluid coriolis flow meter will be checked to determine if these fluctuations are due to noise in the system or actual characteristics of the flow.

Fourthly, some sensors will be added to the system. A temperature sensor will be added to the throttle valve's outlet. A temperature sensor and a pressure sensor will be added to the throttle valve's inlet. Therefore, researchers in BURET laboratory can measure the throttle valve inlet and outlet temperatures and pressures and compare data with the dynamic model easily.

Lastly, other correlations for heat transfer and pressure drop will be investigated to improve accuracy of predictions at high evaporator temperature and pressure operating conditions.

REFERENCES

1. Rahbar, K., S. Mahmoud, R. K. Al-Dalah, N. Moazami and S. A. Mirhadizadeh, “Review of Organic Rankine Cycle for Small-Scale Applications”, *Energy Conversion and Management*, Vol. 134, pp. 135-155, 2016.

2. World Energy Council, “Global Electricity Initiative: 2014 Report”, 2014, https://www.worldenergy.org/wpcontent/uploads/2014/12/Global_Electricity_Initiative_WEB.pdf, accessed on October 20, 2019.

3. International Energy Agency, “I. Energy Technology Perspectives-ETP 2017”, 2017, https://www.iea.org/reports/energy-technology-perspectives-2017, accessed on October 27, 2020.

4. European Union, “The Paris Protocol - A Blueprint for Tackling Global Climate Change Beyond 2020”, 2015, https://ec.europa.eu/info/publications/paris-protocol-blueprint-tackling-global-climate-change-beyond-2020_en, accessed on November 22, 2020.

5. Lecompte, S., H. Huisseune, M. V. D. Broek, B. Vanslambrouck and M. De Paepe, “Review of Organic Rankine Cycle (ORC) Architectures for Waste Heat Recovery”, *Renewable and Sustainable Energy Reviews*, Vol.47, pp. 448-461, 2015.

6. Hung, T. C., “Waste Heat Recovery of Organic Rankine Cycle Using Dry Fluids’’, *Energy Conversion and Management*, Vol. 42, pp 539-553, 2001.

7. Nguyen, B. K, D. Thornhill D and J. I. Chowdhury, “Dynamic Model of Supercritical Organic Rankine Cylce Waste Heat Recovery System for Internal Combustion Engine”, *International Journal of Automotive Engineering Technology*, Vol. 18, pp. 589-601, 2017.

8. Campana, F., M. Bianchi, L. Branchini, A. De Pascale, A. Peretto, M. Baresi, A. Fermi, N. Rossetti, and R. Vescovo, "ORC Waste Heat Recovery in European Energy Intensive Industries: Energy and GHG Savings", *Energy Conversion and Management*, Vol. 76, pp. 244-252, 2013.

9. Feng, Y., T. Hung, K. Greg, Y. Zhang, B. Li and J. Yang, "Thermoeconomic Comparison Between Pure and Mixture Working Fluids of Organic Rankine Cycles (ORCs) for Low Temperature Waste Heat Recovery", *Energy Conversion and Management*, Vol. 106, pp. 859-872, 2015.

10. Liu, C., C. He, H. Gao and X. Xu, "The Optimal Evaporation Temperature of Subcritical ORC Based on Second Law Efficiency for Waste Heat Recovery", *Entropy*, Vol. 14, pp. 491–504, 2012.

11. Marchionni, M., G. Bianchi, A. Karvountzis-Kontakiotis, A. Pesiridis and S.A. Tassou, "Dynamic Modeling and Optimization of an ORC Unit Equipped with Plate Heat Exchangers and Turbomachines", *Energy Procedia*, Vol. 129, pp. 224–231, 2017.

12. Wei, D., X. Lu, Z. Lu and J. Gu, "Dynamic Modeling and Simulation of an Organic Rankine Cycle (ORC) System for Waste Heat Recovery", *Applied Thermal Engineering*, Vol. 28, pp. 1216–1224, 2008.

13. Carraro, G., S. Rech, A. Lazzaretto, G. Toniato, and P. Danieli, "Dynamic Simulation and Experiments of a Low-Cost Small ORC Unit for Market Applications", *Energy Conversion and Management*, Vol. 197, p. 111863, 2019.

14. Tong, L., W. Enhua, M. Fanxiao and Z. Xu, "Dynamic Simulation of an ICE-ORC Combined System Under Various Working Conditions", *IFAC-PapersOnLine*, Vol. 51, pp. 29–34, 2018.

15. Zhang, Y., S. Deng, L. Zhao, S. Lin, M. Bai, W. Wang and D. Zhao, "Dynamic Test and Verification of Model-Guided ORC System", *Energy Conversion and Management*, Vol. 186, pp. 349–367, 2019.

16. Quoilin, S., A. Desideri, J. Wronski, I. Bell, and V. Lemort, "ThermoCycle: A Modelica Library for the Simulation of Thermodynamic Systems", in *Proceedings of the 10th International Modelica Conference*, Lund, Vol. 96, pp. 683–692, 2014.

17. Dymola User Manual 1A: Introduction, Getting Started, and Installation, Dassault Systèmes, 2019.

18. Petzold, L. R., "A Description of DASSL: A Differantial/Algebraic System Solver", paper presented at the *10th IMACS World Congress*, Montreal, 1982.

19. Fernandes, C. S., R.P. Dias, J. M. Nobrega and J. M. Maia, "Laminar Flow in Chevron-Type Plate Heat Exchangers: CFD Analysis of Tortuosity, Shape Factor and Friction Factor", *Chemical Engineering and Processing: Process Intensification*, Vol. 46, No. 9, pp. 825–833, 2007.

20. Indiamart, "Stainless Steel Back and Front Ferrule Sets", https://www.indiamart.com/proddetail/stainless-steel-back-and-front-ferrule-sets-15281132630.html, accessed on December 13, 2021.

21. Borsen Boru, "Let-Lok Fittings, Let-Lok Genel Ürün Bilgisi – Katalog", https://borsenboru.com/catalog/let-lok-tup-fittingleri-tanitimi, accessed on December 10, 2021.

22. TLV Co. Ltd., "Bypass Valves", https://www.tlv.com/global/ME/steam-theory/bypass-valves.html, accessed on December 15, 2021.

23. Plate Type Heat Exchangers: Operation & Maintenance Manual, Sondex, Louisville, 2011.

24. Longo, G. A., S. Mancin, G. Righetti and C. Zilio, “A New Model for Refrigerant Boiling Inside Brazed Plate Heat Exchangers (BPHEs)”, *International Journal of Heat and Mass Transfer*, Vol. 91, pp. 144–149, 2015.

25. Longo, G. A., G. Righetti and C. Zilio, “A New Computational Procedure for Refrigerant Condensation inside Herringbone-Type Brazed Plate Heat Exchangers”, *International Journal of Heat and Mass Transfer*, Vol. 82, pp. 530–536, 2015.

26. Konakov, P. K., “A New Correlation for the Friction Coefficient in Smooth Tubes”, *Berichte der Akademie der Wissenschaften der UdSSR*, Vol. 51, pp. 503–506, 1946.